GMe Gesellschaft für Mikroelektronik

The Society for Microelectronics

Annual Report

1999

Vienna, May 2000

GMe Gesellschaft für Mikroelektronik

The Society for Microelectronics

Annual Report

1999

Gesellschaft für Mikroelektronik
c/o Technische Universität Wien
Institut für Industrielle Elektronik und Materialwissenschaften
Gußhausstraße 27-29/366, A-1040 Wien

Vienna, May 2000

Editor: Karl Riedling

Layout: Claudia Benedela
Karl Riedling

The Society for Microelectronics (GMe — Gesellschaft für Mikroelektronik)

G. Bauer, K. Riedling

Gesellschaft für Mikroelektronik,
c/o Institut für Industrielle Elektronik und Materialwissenschaften,
TU Wien
Gußhausstraße 27 – 29, A-1040 Wien

1. Goals of the Society for Microelectronics

The Society for Microelectronics (GMe) was founded in 1985 with the aim to "*support microelectronics technology and its applications*" in Austria. The GMe defines its tasks as follows:

- Support of university-based "high-tech" research in the areas of microelectronics, semiconductor technology, sensors, and opto-electronics;
- Operation of research facilities;
- Support and consulting for industry, in particular, for small and medium enterprises, within the area of microelectronics.

The central task of the GMe is to provide an internationally competitive *infra-structure* in the area of microelectronics technology. The GMe allocates funds to maintain research projects in the fields of semiconductor technology, sensors, opto-electronics, and ASIC design. Thus the infra-structure support generates a base for research projects that are funded by other funding agencies.

2. Activities of the Society

The present focal point activities of the GMe are:

- Operation of university-based laboratories for microelectronics technology;
- Design of application specific integrated circuits (ASICs) —TMOe.

The GMe currently supports mainly the first focal point activity but also coordinates the Austria-wide activities of the TMOe program.

The main task of the GMe in the area of microelectronics technology is the operation of the cleanroom laboratories in Vienna and Linz. The GMe has coordinated the construction of the Microstructure Center (MISZ — Mikrostrukturzentrum) in Vienna; the funds were supplied by the Austrian Federal Ministry of Science and Research. The GMe now finances a significant part of the operation costs for the cleanroom laboratories in Vienna and Linz.

2.1 Microelectronics Technology — Cleanroom Vienna

The following university institutes receive support within this focal point activity:

- TU Wien:
  - Institut für Festkörperelektronik
  - Institut für Industrielle Elektronik und Materialwissenschaften

2.2 Microelectronics Technology — Cleanroom Linz

The following university institutes receive support within this focal point activity:

- Johannes Kepler Universität Linz:
  - Institut für Halbleiter- und Festkörperphysik
  - Institut für Mikroelektronik

3. Other Activities of the Society

One of the declared tasks of the GMe is to provide information on current Austrian academic activities in the field of microelectronics to industry, in particular to Austrian small- and medium enterprises (SMEs). This will improve the transfer of "know-how" between Austrian universities and industry. As an example, the GMe supplied editorial articles to an Austrian publishing house that targets its magazines on the management and technical staff of Austrian industrial enterprises. The articles presented some of those projects supported by the GMe that had a direct impact on Austrian industry.

To enhance the distribution of the results of the research work done with GMe support, the GMe has put the contents of its previous annual reports — 1995 through 1998 — on its Web server; this will also happen for this report. Although we did not explicitly advertise on a larger scale the existence of this server and its contents, it has apparently been fairly well accepted by the international community. Access statistics show an average access of 3 counts per day; however, an amazingly large percentage of these accesses — close to 50 per cent — originates from net domains outside Austria. About one quarter of the visitors of the GMe's web site visited it more than once. The GMe Web server is available under the URL:

http://www.iaee.tuwien.ac.at/gme/

Finally, the GMe prepared and carried out the biennial seminar "*Aktuelle Entwicklungen der Mikroelektronik*" in Bad Hofgastein, Salzburg, which took place in March 1999. The predecessor of this seminar has first been held in 1977 in Großarl; since 1987, the GMe contributes financial support, and since 1993, the Society acts as its main organizer. The seminar presented thirteen invited lectures given by international experts, and 25 oral and poster contributions which resulted from work supported by the GMe. For the first time, greater emphasis was put into making the seminar more attractive to an industrial audience, thus intending an enhanced knowledge transfer between universities and industry.

4. Changes to the Society's Managing Committee

As required by the Society's statutes, Erich GORNIK who had been the Society's president for six years stepped down by the end of 1999. His successor is Günther BAUER, head of the Institut für Halbleiterphysik at the Johannes Kepler University in Linz, and in charge of the cleanroom laboratories at his university. Wolfgang ATTWENGER, formerly with ÖFZ Seibersdorf, retired from the Society's board, while Emmerich BERTAGNOLLI and Rainer URANSCHEK newly joined the board as representatives of the Institut für Festkörperelektronik of the TU Vienna and of the Forschungs- und Prüfzentrum Arsenal in Vienna, respectively.

5. The Annual Report for 1999 of the Society for Microelectronics

The GMe is currently supporting the microelectronics technology activities of the cleanroom laboratories in Vienna and Linz.

All projects described in this report were carried out in the cleanrooms in Vienna and Linz, respectively. They are *not* specific projects of the GMe but were funded by a variety of other sources. They all have in common that they use the infra-structure provided by the GMe. It would therefore not have been possible to carry out these projects without the support by the GMe.

Contents

Microelectronics Technology — Cleanroom Vienna

Cleanroom Vienna

G. Strasser

Institut für Festkörperelektronik, Technische Universität Wien, Floragasse 7, A-1040 Vienna, Austria

This report is a summary of the 1999 main activities of the MISZ TU Wien (microstructure center). The available technologies for the production of optoelectronic and microelectronic prototype devices are: state of the art growth of III-V nanostructures, standard contact lithography, the production of patterned masks to be used in standard lithography, various structuring techniques like dry etching and plasma enhanced chemical vapor deposition, electron beam writing, focused ion beam etching and depositing, and various metallization techniques. An additional molecular beam system was brought into the cleanroom end 1999 and will be set up within the ongoing year. State of the art silicon processing began in 1998 and may need further support to mature. In 1999 the installation of various oxidation and diffusion furnaces to be used in silicon processes started. In this report, a short description of research projects with a high need of technological input, using the equipment in the cleanroom and the cleanroom environment, is given.

1. Introduction

The present main research areas of the solid state electronics institute taking advantage of the fully equipped cleanroom of the MISZ are: transport studies in low dimensional semiconductor nanostructures, scanning probe spectroscopy, realization of new and improved optoelectronic devices, quantum cascade lasers, THz sources, and the characterization of microelectronic devices.

To satisfy this variety of topics, state of the art growth of semiconductor nanostructures is needed as well as a complete process line including structure definition (lithography), structure transfer (RIE, FIB, ion milling, wet chemical etching techniques) and coating with metals and/or dielectrics (PE-CVD, sputtering, electron gun evaporation, FIB deposition). All the equipment necessary for the above mentioned technologies needs the cleanroom environment (cooling, filtered air, constant temperature and humidity, high quality water, various inert gases) as well as periodic maintenance of the equipment and the cleanroom itself, e.g. pumping systems (rotary pumps, turbo pumps), exhaust filtering, liquid nitrogen, and cleaning and repair. Testing of the cleanroom quality and adjustment (laminar air flow, filters, cooling, humidity, temperature) is done periodically.

In 1999, the following additional equipment was installed :

- an wet bench for chemical processes;
- a furnace for wet and dry oxidation and annealing;
- a chemical vapor deposition system for amorphous silicon, silicon nitride, and aluminum oxide coatings;
- a solid source molecular beam epitaxy system.

In the following, the main research activities making use of the cleanroom itself or using samples grown, structured, and tested in the MISZ are described. These activities are not the only projects running in the MISZ, but are intended to show a representative overview of the basic research as well as applied projects which need the cleanroom infrastructure. For a more general overview the listed projects and the attached publication list may give more insides on the broad range of activities.

Project Information

Project Manager

Dr. Gottfried STRASSER

Institut für Festkörperelektronik, Technische Universität Wien

Project Group

Last Name	First Name	Status	Employer
Bertagnolli	Emmerich	Full Prof.	TU Wien
Boxleitner	Winfried	Post Doc	EC (HQ Sonate)
Bratschitsch	Rudolf	dissertation	FWF (Start)
Finger	Norman	dissertation	TU/VW
Fischler	Wolfgang	dissertation	FWF/Nationalbank
Fuchshuber	Michael	student	
Fürböck	Christoph	dissertation	Infineon
Gianordoli	Stefan	dissertation	EC (Unisel)
Goebel	Bernd	dissertation	Infineon/fke
Gornik	Erich	Full Prof.	TU Wien
Harasek	Stefan	dissertation	**GMe**
Heer	Rudolf	dissertation	TU Wien
Hirner	Heimo	student	
Hobler	Gerhard	Assistant Prof.	TU Wien
Hoffmann	Rainer	student	
Hvozdara	Lubos	dissertation	EC (Unisel)
Kast	Michael	student	fke
Kellermann	Peer Oliver	dissertation	VW
Kersting	Roland	Post Doc	EC (Interact)
Kostner	Hannes	student	
Kröll	Peter	technician	TU Wien
Langfischer	Helmut	dissertation	**GMe**
Lampacher	Peter	student	
Langmann	Gottfried	technician	TU Wien
Litzenberger	Martin	dissertation	Infineon/fke
Lugstein	Alois	assistant	TU Wien
Maier	Thomas	dissertation	TU Wien/fke

Last Name	**First Name**	**Status**	**Employer**
Pacher	Christoph	student	**GMe**
Patz	Sybille	student	
Ploner	Guido	dissertation	FWF (Wittgenstein)
Pogany	Dionyz	guest scientist	Infineon/fke
Prinzinger	Johannes	technician	TU Wien
Rainer	Alexander	secretary	**GMe**
Rakoczy	Doris	dissertation	FWF
Rauch	Christoph	dissertation	TU Wien
Riegler	Erich	technician	TU Wien
Schinnerl	Markus	technician	TU Wien
Schenold	Helmut	technician	TU Wien
Schrenk	Werner	dissertation	EC (Unisel)
Smoliner	Jürgen	Assistant Prof.	TU Wien
Stöckl	Herbert	technician	TU Wien
Strasser	Gottfried	Assistant Prof.	TU Wien
Thaller	Edwin	student	
Ulrich	Jochen	dissertation	FWF (Wittgenstein)
Unterrainer	Karl	Assistant Prof.	TU Wien
Wanzenböck	Heinz	assistant	TU Wien
Zobl	Reinhard	dissertation	FWF (Start)

Publications in Reviewed Journals

1. R. Heer, J. Smoliner, G. Strasser, E. Gornik: "*Temperature dependent studies of InAs base layers for Ballistic Electron Emission Microscopy*"; Phys. Rev. B **59**, 4618 (1999)
2. J. Smoliner, R. Heer, G. Strasser: "*Biased GaAs-AlGaAs superlattices employed as energy filter for Ballistic Electron Emission Microscopy*"; Surface and Interface Analysis **27**, 542 (1999)
3. R.Heer, J.Smoliner, G.Strasser E.Gornik: "*A highly transmittive semiconductor base for Ballistic Electron Emission Microscopy*"; Surface and Interface Analysis **27**, 517 (1999)
4. C. Rauch, G. Strasser, E. Gornik: "*Current Spectroscopy of Superlattice Bandstructure and Transport*"; Microelectronic Engineering **47**, 59 (1999)
5. J. Smoliner, R. Heer, G. Strasser: "*Ballistic Electron Emission Microscopy on buried GaAs-AlGaAs superlattices*"; Microelectronic Engineering **47**, 69 (1999)
6. O. Gauthier-Lafaye, F.H. Julien, S. Cabaret, J.-M. Lourtioz, G. Strasser, E. Gornik, M. Helm, P. Bois: "*High-power GaAs/AlGaAs Quantum Fountain Laser emitting at 14.5 µm with 2.5% tunability*"; Appl. Phys. Lett. **74**, 1537 (1999)

7. K. Kempa, P. Bakshi, C. Du, G. Feng, A. Scorupsky, G. Strasser, C. Rauch, K. Unterrainer, E. Gornik: "*Towards stimulated generation of coherent plasmons in nanostructures*"; Journ. of Appl. Phys. **85**, 3708 (1999)
8. M. Helm, W. Hilber, G. Strasser, R. De Meester, F.M. Peeters, A. Wacker: "*Continuum Wannier-Stark ladders strongly interacting by Zener resonances in semiconductor superlattices*"; Phys. Rev. Lett. **82**, 3120 (1999)
9. G. Ploner, H. Hirner, T. Maier, G. Strasser, J. Smoliner, E. Gornik: "*A novel device layout for tunneling spectroscopy of barrier separated electron systems with electrically tunable dimensionality*"; Appl. Phys. Lett. **74**, 1758 (1999)
10. A. Wacker, S. Bose, C. Rauch, G. Strasser, E. Gornik: "*Transmission through Superlattices with Interface Roughness*"; Superlattices and Microstructures **25**, 43 (1999)
11. C. Rauch, G. Strasser, M. Kast, E. Gornik: "*Mean Free Path of Ballistic Electrons in GaAs/AlGaAs superlattices*"; Superlattices and Microstructures **25**, 45 (1999)
12. J. Ulrich, R. Zobl, K. Unterrainer, G. Strasser, E. Gornik, K.D. Maranowski, A.C. Gossard: "*Temperature dependence of far-infrared electroluminescence in parabolic quantum wells*"; Appl. Phys. Lett. **74**, 3158 (1999)
13. N.E. Hecker, R.A. Höpfel, N. Sawaki, T. Maier, G. Strasser: "*Surface plasmon enhanced photoluminescence from a single quantum well*"; Appl. Phys. Lett. **75**, 1577 (1999)
14. N. Finger and E. Gornik: "*Analysis of Metallized-Grating Coupled Twin-Waveguide Structures*", IEEE J. Quantum Electron. **35**, No. 5, May 1999
15. P.O. Kellermann, N. Finger, W. Schrenk, E. Gornik, R. Winterhoff, H. Schweizer and F. Scholz: "*Wavelength adjustable surface-emitting single-mode laser diodes with contradirectional surface-mode coupling*"; Appl. Phys. Lett. **75**, 3748 (1999)
16. G. Strasser, L. Hvozdara, S. Gianordoli, K. Unterrainer, E. Gornik, P. Kruck, M. Helm: "*GaAs/AlGaAs Quantum Cascade Intersubband and Interminiband Emitter*"; Journal of Crystal Growth **201/202**, 919-922 (1999)
17. R. Kersting, R. Bratschitsch, E. Thaller, G. Strasser, K. Unterrainer, and J.N. Heyman: "*Excitation of intersubband transitions by THz pulses*", CLEO/QELS ´99 Technical Digest, p 219, Baltimore, 23.-28. Mai 1999
18. R. Bratschitsch, R. Kersting, G. Strasser, K. Unterrainer, W. Fischler, and R.A. Höpfel: "*THz emission of coherent plasmons in semiconductor superlattices*", CLEO/QELS ´99 Technical Digest, p 221, Baltimore, 23.-28. Mai 1999
19. S. Gianordoli, L. Hvozdara, G.Strasser, W. Schrenk, K. Unterrainer, and E. Gornik: "*GaAs/AlGaAs-based microcylinder lasers emitting at 10 µm*", Appl. Phys. Lett. **75**, 1045 (1999)
20. J.Smoliner, R.Heer, G.Strasser: "$k_{||}$*=0 filtering in resonant tunneling processes between materials of different effective electron mass*"; Phys. Rev. B **60**, 5137 (1999)
21. G. Strasser, S. Gianordoli, L. Hvozdara, W. Schrenk, K. Unterrainer, E. Gornik: "*GaAs/AlGaAs superlattice quantum cascade lasers at 13 microns*"; Appl. Phys. Lett. **75**, 1345 (1999)

22. O. Gauthier-Lafaye, B. Seguin-Roa, F.H. Julien, G. Strasser, P. Collot, C. Sirtori, J-Y. Duboz: "*Long-wavelength High-power Quantum Fountain Unipolar Lasers in GaAs/AlGaAs Quantum Wells*"; in THz Spectroscopy and Applications II, J.M. Chamberlain, Editor, Proc. of SPIE **3828**, 6 (1999)
23. L. Hvozdara, S Gianordoli, W. Schrenk, G. Strasser, K. Unterrainer, E. Gornik: "*GaAs/AlGaAs Intersubband MIR Lasers*"; in THz Spectroscopy and Applications II, J.M. Chamberlain, Editor, Proc. of SPIE **3828**, 32 (1999)
24. K. Kempa, P. Bakshi, M. Ciftan, E. Gornik, K. Unterrainer, G. Strasser, C. Rauch: "*Plasmon Based Terahertz Laser Without Population Inversion*"; in THz Spectroscopy and Applications II, J.M. Chamberlain, Editor, Proc. of SPIE **3828**, 151 (1999)
25. G. Strasser, L. Hvozdara, S. Gianordoli, W. Schrenk, K.Unterrainer, E. Gornik, M. Helm: "*Intersubband and interminiband GaAs/AlGaAs quantum cascade lasers at 10 micrometers*"; accepted for publication in Physica E
26. K. Unterrainer, R. Kersting, R. Bratschitsch, G. Strasser, and J. N. Heyman: "*Few-Cycle THz Spectroscopy of Nanostructures*"; accepted in Physica E
27. J. Smoliner, R. Heer, G. Strasser: "*Wave Vector Filtering and Incoherent Transport through Low Dimensional States and Areas of Different Effective Mass*"; accepted for publication in Physica E
28. G. Ploner, H. Hirner, T. Maier, G. Strasser, J. Smoliner and E.Gornik: "*A novel device layout for tunneling spectroscopy of low-dimensional electron systems*", accepted for publication in Physica E
29. L. Hvozdara, S. Gianordoli, G. Strasser, W. Schrenk, K.Unterrainer, E. Gornik: "*GaAs/AlGaAs unipolar mid-infrared quantum cascade lasers*", Proc. 26th International Symposium on Compound Semiconductors, Berlin, Germany 22-26 August 1999
30. S. Gianordoli, L. Hvozdara, G. Strasser, W. Schrenk, K. Unterrainer, E. Gornik: "*GaAs/AlGaAs Interminiband Unipolar Semiconductor Laser at 13 µm*"; Proc. 29th European Solid-State Device Research Conference ESSDERC 99; Leuven, Belgium, 13-15.9.1999
31. G. Strasser, G. Ploner, C. Rauch and E. Gornik: "*Transport Spectroscopy of Quantum Wires and Superlattices*"; Proc. of MBE-GPT, Warsaw, Poland, 1999, accepted for publication in Thin solid Films
32. A. Ertl, P.O. Kellermann, M. Zehetmayer, A. Schoggl, P. Kindl und A.H. Maitz: "*A novel 675.2 nm diode laser densitometer for use with GafChromic films*" Medical-Physics **26**, 834 (1999)
33. R.Heer, J. Smoliner, G. Strasser: "$k_{//}=0$ *filtering effects in ballistic electron transport through sub-surface resonant tunneling diodes*"; Physica B **272**, 187-189 (1999)
34. J.Smoliner, R. Heer, G.Ploner and G. Strasser: "$k_{//}=0$ *filtering effects in ballistic electron transport through sub-surface GaAs-AlGaAs double barrier resonant tunneling structures*", Proc. EP2DS, (Ottawa 1999), accepted for publication in Physica E

35. P. Bakshi, K. Kempa, A. Scorupsky, C.G. Du, G. Feng, R. Zobl, G. Strasser, C. Rauch, C. Pacher, K. Unterrainer, E. Gornik: "*Plasmon-based terahertz emission from quantum well structures*"; Appl. Phys. Lett. **75**, 1685 (1999)
36. S. Gianordoli, L. Hvozdara, G.Strasser, T. Maier, N. Finger, K. Unterrainer, E. Gornik: "*GaAs/AlGaAs microresonator quantum cascade lasers*"; accepted for publication in Physica E
37. L. Hvozdara, S. Giaordoli, G.Strasser, W. Schrenk, K. Unterrainer, E. Gornik, V. Pustogow, C.S.S.S. Murthy, M. Kraft, B. Mizaikoff: "*GaAs/AlGaAs Quantum Cascade Laser – a Source for Gas Absorption Spectroscopy*"; accepted for publication in Physica E
38. G. Strasser, S. Gianordoli, L. Hvozdara, W. Schrenk, E. Gornik: "*Intersubband and interminiband GaAs/AlGaAs quantum cascade lasers*"; accepted for publication in Physica E
39. O. Gauthier-Lafaye, B. Seguin-Roa, F.H. Julien, P. Collot, C. Sirtori, J.Y. Duboz, G. Strasser: "*High power tunable quantum fountain unipolar lasers*"; accepted for publication in Physica E
40. J. Ulrich, R. Zobl, N. Finger,K. Unterrainer, G. Strasser, E. Gornik: "*Terahertz electroluminescence in a quantum cascade structure*"; Physica B **272**, 216-218 (1999)
41. R.Heer, D.Rakoczy, G.Ploner, G.Strasser, E.Gornik and J.Smoliner: "*A metal-insulator-metal injector for ballistic electron spectroscopy*", Appl. Phys. Lett. **75**, 4007-4009 (1999)
42. R. Bratschitsch, R. Kersting, T. Müller, G. Strasser, K. Unterrainer, W. Fischler, R.A. Höpfel: "*Coherent THz plasmons in GaAs/AlGaAs superlattices*"; Physica B **272**, 375-377 (1999)
43. C. Fürböck, R. Thalhammer, M. Litzenberger, N. Seliger, D. Pogany, E. Gornik and G. Wachutka: "*A differential backside laserprobing technique for the investigation of the lateral temperature distribution in power devices*", Proc. 11th International Symposium on Power Semiconductor Devices and ICs, Toronto, 193-196 (1999).
44. C. Fürböck, M. Litzenberger, D. Pogany, E. Gornik, T. Müller-Lynch, H. Goßner, M. Stecher and W. Werner: "*Study of bipolar transistor action during ESD stress in Smart Power ESD protection devices using interferometric temperature mapping*", Proc. of the 29th European Solid-State Device Research Conference, Editions Frontieres, ISBN 2-86332-245-1, 596-599 (1999).
45. C. Fürböck, D. Pogany, M. Litzenberger, E. Gornik, N. Seliger, H. Goßner, T. Müller-Lynch, M. Stecher, and W. Werner: "*Interferometric temperature mapping during ESD stress and failure analysis of Smart Power technology ESD protection devices*", Proc. EOS/ESD Symposium, Orlando,.241-250 (1999)
46. C. Fürböck, M. Litzenberger, D. Pogany, E. Gornik, N. Seliger, T. Müller-Lynch, M. Stecher, H. Goßner and W. Werner: "*Laser interferometric methode for ns-time scale thermal mapping of Smart Power ESD protection devices during ESD stress*", Microel. Reliab. **39**, 925-930 (1999).

47. R. Zobl, K. Unterrainer, G. Strasser, E. Gornik: "*Magneto-optical terahertz emission from plasmons in parabolic quantum wells*", accepted for publication in Semiconductor Science and Technology

48. G.Ploner and E.Gornik: "*Tunneling spectroscopy of voltage tunable quantum wires*", Proc. SIMD´99 (Hawaii 1999), accepted for publication in Superlattices and Microstructures

49. S. Gianordoli, L. Hvozdara, G.Strasser, W. Schrenk, K. Unterrainer, and E. Gornik: "*GaAs/AlGaAs based micro lasers emitting at 10 µm and 13 µm*", IEEE Lasers and Electro-Optics Society, Conf. Proc. LEOS '99, ISBN 0-7803-5634-9, 9 (1999)

50. T. Maier, G. Strasser, E. Gornik, M. Moser, R. Hoevel: "*Integrated vertical-cavity laser diodes and resonant photodetectors with hybrid Si_3N_4/SiO_2 top Bragg mirrors*", IEEE Lasers and Electro-Optics Society, Conf. Proc. LEOS '99, ISBN 0-7803-5634-9, 677 (1999)

51. C. Rauch, G. Strasser, K. Unterrainer, A. Wacker, E. Gornik: "*Scattering and Bloch oscillation in semiconductor superlattices*"; Physica B **272**, 175-179 (1999)

52. M. Helm, W. Hilber, G. Strasser, R. DeMeester, F.M. Peeters, A. Wacker: "*Simultaneous investigation of vertical transport and intersubband absorption in a superlattice: continuum Wannier-Stark ladders and next-nearest neighbor tunneling*"; Physica B **272**, 194-197 (1999)

53. M. Helm, W. Hilber, G. Strasser, R. DeMeester, F. M Peeters: "*Minibands and Wannier-Strak Ladders in Semiconductor Superlattices studied by infrared spectroscopy*"; Braz. J. Physics **29**, 652-660 (1999)

54. D. Pogany, G. Guillot: "*Random telegraph signal noise instabilities in lattice-mismatched InGaAs/InP photodiodes*", Microel. Reliab **39**, 341-345 (1999)

55. S. Pierunek, D. Pogany, J.L. Autran, B. Leroy: "*Study of hot carrier degradation in dram cells combining random telegraph signal and charge pumping measurements*", J. Noncryst. Solids **245**, 59-66 (1999)

56. D.Pogany, N. Seliger, M. Litzenberger, H. Gossner, M. Stecher, T. Müller-lynch, W. Werner, E. Gornik: "*Damage analysis in smart-power technology electrostatic discharge (ESD) protection devices*", Microel. Reliab. **39**, 1143-1148 (1999)

57. D.Pogany, J. A Chroboczek, G. Ghibaudo: "*Investigation of RTS noise mechanisms in reverse base current of stressed submicron bipolar transistors*", Proc. Int. Conf. On Noise in Phys. Systems and 1/f Fluctuations, Hong Kong, 22-27 August 1999, pp.348-351.

58. D.Pogany, E. Gornik, M. Stecher, W. Werner: "*Study of random telegraph noise in smart power technology DMOS devices*", Proc. Int. Conf. On Noise in Phys. Systems and 1/f Fluctuations, Hong Kong, 22-27 August 1999, pp. 88-91.

59. D.Pogany, C. Fürböck, M. Litzenberger, E. Gornik, H.Gossner, K. Esmark, J. Otto, G. Sölkner: "*Stress evolution of low frequency (RTS) noise and leakage current in grounded-gate nMOSFET ESD protection devices*", Proc. ESSDERC'99, Leuven, Belgium 11-13. Sept. 1999, pp. 604-607.

60. C. Fürböck, K. Esmark, M. Litzenberger, G. Groos, D. Pogany, H. Goßner, M. Stecher, R. Zelsacher, and E. Gornik: "*Backside interferometric thermal mapping of*

ESD protection devices during high current stress", IEEE Electron Dev. Lett. (submitted).

Non-refereed reports:

1. J. Ulrich, R. Zobl, K. Unterrainer, G. Strasser, E. Gornik, K.D. Maranowski, A.C. Gossard: "*Far-Infrared Electroluminescence in Parabolic Quantum Wells*"; Current developments of microelectronics, ISBN 3-901578-04-8 (1999).
2. C. Fürböck, R. Thalhammer, M. Litzenberger, N. Seliger, G. Wachutka and E. Gornik: "*Internal Characterization of IGBTs Using the Backside Laserprobing Technique*", Current developments of miroelectronics; ISBN 3-901578-04-8, 39 (1999).
3. R. Heer, J. Smoliner, G. Strasser, E. Gornik: "*Enhanced Energy Resolution in Ballistic Electron Emission Microscopy through InAs Base Layers*"; Current developments of mircoelectronics, ISBN 3-901578-04-8, 181 (1999)
4. C. Rauch, G. Strasser, E. Gornik: "*Onset of Scattering Induced Miniband Transport*"; Current developments of mircoelectronics, ISBN 3-901578-04-8, 185 (1999)

Presentations

1. R. Kersting, K. Unterrainer, G. Strasser (invited talk): "*Plasma oscillations: emission and modulation of THz pulses*", PHOTONICS West (Terahertz Spectroscopy and Applications), 27-29 January 1999, San Jose, California.
2. J.N. Heyman, K. Unterrainer, R. Kersting, G. Strasser: "*THz time-domain spectroscopy of wide quantum wells*", PHOTONICS West (Terahertz Spectroscopy and Applications), 27-29 January 1999, San Jose, California.
3. K. Unterrainer, R. Kersting, J.N. Heyman, G. Strasser, E. Gornik, K.M. Maranowski, A.C. Gossard (invited talk): "*Coherent THz emission from plasmons in semiconductors*", PHOTONICS West (Ultrafast Phenomena in Semiconductors III), 27-29 January 1999, San Jose, California.
4. Karl Unterrainer (invited talk): "*Few-Cycle THz Spectroscopy of Semiconductor Quantum Structures*", 1999 Centennial Meetting of the APS, March 20-26, 1999, Atlanta, Georgia.
5. E. Gornik (invited talk): "*THz emission from low dimensional electron systems*", 1999 Centennial Meetting of the APS, March 20-26, 1999, Atlanta, Georgia.
6. C. Rauch: "*Coherent and Incoherent Electron Transport in Superlattices*", 1999 Centennial Meeting of the APS, March 20-26, 1999, Atlanta, Georgia.
7. N. Finger, P.O. Kellermann, W. Schrenk and E. Gornik: "*Analysis of surface mode-coupled semiconductor laser structures with adjustable emission wavelength*", PHOTONICS West (Physics and Simulation of Optoelectronic Devices VII), 27-29 January 1999, San Jose, California.
8. C. Fürböck, R. Thalhammer, M. Litzenberger, N. Seliger, D. Pogany, E. Gornik and G. Wachutka: "*A differential backside laserprobing technique for the investigation*

of the lateral temperature distribution in power devices", ISPSD'99, 25-28 May 1999, Toronto, Canada.

9. C. Fürböck, M. Litzenberger, D. Pogany, E. Gornik, T. Müller-Lynch, H. Goßner, M. Stecher and W. Werner: "*Study of bipolar transistor action during ESD stress in Smart Power ESD protection devices using interferometric temperature mapping*", ESSDERC'99 – 29th European Solid-State Device Research Conference, 13-15 September 1999, Leuven, Belgium.
10. C. Fürböck, D. Pogany, M. Litzenberger, E. Gornik, N. Seliger, H. Goßner, T. Müller-Lynch, M. Stecher, and W. Werner: "*Interferometric temperature mapping during ESD stress and failure analysis of Smart Power technology ESD protection devices*", EOS/ESD Symposium, 27-30 September 1999, Orlando, Florida.
11. C. Fürböck, M. Litzenberger, D. Pogany, E. Gornik, N. Seliger, T. Müller-Lynch, M. Stecher, H. Goßner and W. Werner: "*Laser interferometric methode for ns-time scale thermal mapping of Smart Power ESD protection devices during ESD stress*", ESREF'99 – Xth European Symposium Reliability of Electron Devices, Failure Physics and Analysis, 5-8 October 1999, Bordeaux, France.
12. R. Bratschitsch, R. Kersting, J.N. Heyman, G. Strasser, and K. Unterrainer: "*Visible Pump and THz spectroscopy of semiconductor nanostructures*", SPIE meeting "Conference on Terahertz Spectroscopy and Applications" , München, 16.-18. Juni 1999.
13. R. Kersting, R. Bratschitsch, J.N. Heyman, G. Strasser, and K. Unterrainer: "*Few-cycle THz spectroscopy of semiconductor nanostructures*", SPIE meeting "Conference on Terahertz Spectroscopy and Applications" , München, 16.-18. Juni 1999.
14. R. Bratschitsch, R. Kersting, G. Strasser, K. Unterrainer, W. Fischler, and R.A. Höpfel: "*THz emission of coherent plasmons in semiconductor superlattices*", Conference on Lasers and Electro-Optics/Quantum Electronics and Laser Science Conference, CLEO/QELS ´99, Baltimore, 23.-28. Mai 1999.
15. R. Kersting, R. Bratschitsch, E. Thaller, G. Strasser, K. Unterrainer, and J.N. Heyman: "*Excitation of intersubband transitions by THz pulses*", Conference on Lasers and Electro-Optics/Quantum Electronics and Laser Science Conference, CLEO/QELS ´99, Baltimore, 23.-28. Mai 1999.
16. R. Bratschitsch, R. Kersting, E. Thaller, J.N. Heyman, G. Strasser, and K. Unterrainer: "*Few-cycle THz spectroscopy of semiconductor quantum structures*", DPG Frühjahrstagung, Münster, 22.-26. März 1999.
17. F.H. Julien, O. Gauthier-Lafaye, G. Strasser (invited): "*Long-wavelength high-power quantum fountain unipolar lasers in GaAs/AlGaAs quantum wells*"; SPIE meeting "Conference on Terahertz Spectroscopy and Applications" , München, June 16-18, 1999
18. K. Unterrainer, R. Kersting, R. Bratschitsch, G. Strasser, and J. N. Heyman (invited): "*Few-Cycle THz Spectroscopy of Nanostructures*"; 9th International Conference on Modulated Semiconductor Structures (MSS9), Fukuoka, Japan, July 12-16, 1999

19. C. Rauch, G.Strasser, K.Unterrainer, A.Wacker, E.Gornik (invited): “*Scattering and Bloch oscillation in semiconductor superlattices*”; 11th International Conference on Nonequilibrium Carrier Dynamics in Semiconductors (HCIS-11); Kyoto, Japan, July 19-23, 1999

20. T. Maier, G. Strasser and E. Gornik: “*Vertical-cavity surface emitting laser diodes and their integration with resonant-cavity enhanced photodetectors*”, Mauterndorfer Laserseminar, March 22-25, 1999, Mauterndorf, Austria

21. L. Hvozdara, S. Gianordoli, G. Strasser, K. Unterrainer, E. Gornik: “*AlGaAs/GaAs quantum cascade intersubband emitters and lasers*”; SPIE meeting “Conference on Terahertz Spectroscopy and Applications” , München, 16.-18. Juni 1999.

22. M. Helm, W. Hilber, G. Strasser, R. DeMeester, F.M. Peeters: “*MIR-infrared spectrocopy of biased superlattices*”; SPIE meeting “Conference on Terahertz Spectroscopy and Applications” , München, 16.-18. Juni 1999.

23. R. Zobl, J. Ulrich, K. Unterrainer, G. Strasser, E. Gornik: “*THz emission from plasmons and magnetoplasmons in parabolic quantum wells*”; SPIE meeting “Conference on Terahertz Spectroscopy and Applications” , München, 16.-18. Juni 1999.

24. K. Kempa, P. Bakshi, M. Ciftan, E. Gornik, K. Unterrainer, G. Strasser, C. Rauch: “*Plasmon based Terahertz laser without population inversion*”; SPIE meeting “Conference on Terahertz Spectroscopy and Applications” , München, 16.-18. Juni 1999.

25. G. Strasser, S. Gianordoli, L. Hvozdara, W. Schrenk, K.Unterrainer, E. Gornik, M. Helm: “*Intersubband and interminiband GaAs/AlGaAs quantum cascade lasers at 10 micrometers*”; 9th International Conference on Modulated Semiconductor Structures (MSS9), Fukuoka, Japan, 12-16 July 1999

26. J. Smoliner, R. Heer, G. Strasser: “*Wave Vector Filtering and Incoherent Transport through Low Dimensional States and Areas of Different Effective Mass*”; 9th International Conference on Modulated Semiconductor Structures (MSS9), Fukuoka, Japan, 12-16 July 1999

27. D. Rakoczy, R. Heer, G. Strasser, J. Smoliner: “*Coherent and sequential tunneling processes in Ballistic Electron Emission Microscopy on GaAs-AlGaAs superlattices*”; 10th International Conference on Scanning Tunneling Microscopy (STM ‘99); Seoul, Korea, 18-23 July 1999

28. J. Smoliner, D. Rakoczy, R. Heer, G. Strasser: “$k_{||}=0$ *filtering effects in Ballistic Electron Emission Microscopy (BEEM) on sub surface double barrier resonant tunneling diodes*”; 10th International Conference on Scanning Tunneling Microscopy (STM ‘99); Seoul, Korea, 18-23 July 1999

29. J. Ulrich, R. Zobl, K. Unterrainer, G. Strasser, E. Gornik: “*THz-electroluminescence in parabolic quantum wells and in quantum cascade structures*”; 11th International Conference on Nonequilibrium Carrier Dynamics in Semiconductors (HCIS-11); Kyoto, Japan, July 19-23, 1999

30. R. Heer, J. Smoliner and G. Strasser: “$k_{//}=0$ *filtering effects in ballistic electron transport through sub-surface resonant tunneling diodes*“; 11th International

Conference on Nonequilibrium Carrier Dynamics in Semiconductors (HCIS-11); Kyoto, Japan, July 19-23, 1999

31. M. Helm, W. Hilber, G. Strasser, R.De Meester, F.M. Peeters, A. Wacker: "*Simultaneous investigation of vertical transport and intersubband absorption in a superlattice: continuum Wannier-Stark ladders and next-nearest neighbor tunneling*"; 11th International Conference on Nonequilibrium Carrier Dynamics in Semiconductors (HCIS-11); Kyoto, Japan, July 19-23, 1999
32. L. Hvozdara, S. Gianordoli, G. Strasser, K. Unterrainer, E. Gornik: "*GaAs/AlGaAs Based Intersubband and Interminiband Mid-Infrared Emitters*"; Current developments of miroelectronics; Society of Microelectronics; Bad Hofgastein, Austria, 3.-6.3.1999
33. T. Maier, G. Strasser, E. Gornik: "*GaAs VCSELs with dielectric Si_3N_4/SiO_2 mirrors*"; Current developments of miroelectronics; Society of Microelectronics; Bad Hofgastein, Austria, 3.-6.3.1999
34. P.O. Kellermann, N. Finger, W. Schrenk, E. Gornik, H.-P. Gauggel, R. Winterhoff und M.H. Pilkuhn: "*Wavelength adjustable surface emitting single mode laser diodes with contradirectional surface mode coupling*"; Current developments of mircoelectronics; Society of Microelectronics; Bad Hofgastein, Austria, 3.-6.3.1999
35. P.O. Kellermann, N. Finger, W. Schrenk, E. Gornik, H. Schweizer und F. Scholz: "*Wellenlängenadjustierbare monomodige Laserdioden mit Oberflächenmodenkopplung*"; Frühjahrstagung 1999 der Deutschen Physikalischen Gesellschaft, Münster 1999
36. W. Schrenk, N. Finger, T Maier, P.O. Kellermann, G. Strasser, E. Gornik: "*GaAs/AlGaAs/InGaAs bandgap lasers — from DH Lasers to VCSELs*"; Current developments of miroelectronics; Society of Microelectronics; Bad Hofgastein, Austria, 3.-6.3.1999
37. J. Ulrich, R. Zobl, K. Unterrainer, G. Strasser, E. Gornik, K.D. Maranowski, A.C. Gossard: "*Far-Infrared Electroluminescence in Parabolic Quantum Wells*", Current developments of miroelectronics; Society of Microelectronics; Bad Hofgastein, Austria, 3.-6.3.1999
38. R. Heer, J. Smoliner, G. Strasser, E. Gornik: "*Enhanced Energy Resolution in Ballistic Electron Emission Microscopy through InAs Base Layers*", Current developments of miroelectronics; Society of Microelectronics; Bad Hofgastein, Austria, 3.-6.3.1999
39. C. Fürböck, R. Thalhammer, M. Litzenberger, N. Seliger, G. Wachutka and E. Gornik: "*Internal Characterization of IGBTs Using the Backside Laserprobing Technique*", Current developments of microelectronics; Society of Microelectronics; Bad Hofgastein, Austria, 3.-6.3.1999
40. C. Rauch, G. Strasser, E. Gornik: "*Onset of Scattering Induced Miniband Transport*"; Current developments of miroelectronics; Society of Microelectronics; Bad Hofgastein, Austria, 3.-6.3.1999
41. S. Gianordoli, L Hvozdara, G. Strasser, K. Unterrainer, T. Maier, E. Gornik: "*Diskstrukturen für unipolare GaAs/AlGaAs Quantenkaskadenemitter im mittleren Infrarot*"; DPG Frühjahrstagung, Münster, Deutschland, 22.-26.3.1999

42. L. Hvozdara, S. Gianordoli, G. Strasser, W. Schrenk, K. Unterrainer, E. Gornik: "*Novel Unipolar GaAs/AlGaAs Lasers*"; 7-th Austrian Hungarian international conference on vibrational spectroscopy; Balatonfüred, Hungary 7.-9.4. 1999
43. R. Bratschitsch, R. Kersting, E. Thaller, T. Mueller, G. Strasser, K. Unterrainer, J.N. Heyman: "*Time resolved THz spectroscopy of intersubband transitions*", 11th International Conference on Nonequilibrium Carrier Dynamics in Semiconductors (HCIS-11); Kyoto, Japan, July 19-23, 1999.
44. J. Ulrich, R. Zobl, K. Unterrainer, G. Strasser, E. Gornik: "*Terahertz electroluminescence in parabolic quantum wells and quantum cascade structures*", DPG Frühjahrstagung, Münster, Deutschland, 22.-26.3.1999
45. J. Ulrich, R. Zobl, K. Unterrainer, G. Strasser, E. Gornik: "*Parabolic quantum wells and quantum cascade structures as electrically driven THz-sources*", 5th International Conference on Intersubband Transitions in Quantum Wells (ITQW'99), Bad Ischl, Österreich, 7.-11.9.1999.
46. R. Bratschitsch, R. Kersting, T. Müller, G. Strasser, K. Unterrainer, W. Fischler, J. N. Heyman: "*Time-resolved intersubband spectroscopy of semiconductor nanostructures*", 5th International Conference on Intersubband Transitions in Quantum Wells (ITQW'99), Bad Ischl, Österreich, 7.-11.9.1999.
47. J. Ulrich, R. Zobl, K. Unterrainer, G. Strasser, E. Gornik: "*Terahertz emission from electrically driven parabolic quantum wells*", Workshop on Quantum Heterostructures and Superlattices, Regensburg, Deutschland, 21.1.1999.
48. D.Pogany, N. Seliger, M. Litzenberger, H. Gossner, M. Stecher, T. Müller-lynch, W. Werner, E. Gornik: "*Damage analysis in smart-power technology electrostatic discharge (ESD) protection devices*", Microel. Reliab. **39**, 1143-1148 (1999). Proc. Xth European Symposium on Reliability of Electron Devices, Failure Physics and Analysis, Bordeaux, France, 5-8 Oct. 1999.
49. D.Pogany, J. A Chroboczek, G. Ghibaudo: "*Investigation of RTS noise mechanisms in reverse base current of stressed submicron bipolar transistors*", Proc. Int. Conf. On Noise in Phys. Systems and 1/f Fluctuations, Hong Kong, 22-27 August 1999, pp.348-351.
50. D.Pogany, E. Gornik, M. Stecher, W. Werner: "*Study of random telegraph noise in smart power technology DMOS devices*", Proc. Int. Conf. On Noise in Phys. Systems and 1/f Fluctuations, Hong Kong, 22-27 August 1999, pp. 88-91.
51. D.Pogany, C. Fürböck, M. Litzenberger, E. Gornik, H.Gossner, K. Esmark, J. Otto, G. Sölkner: "*Stress evolution of low frequency (RTS) noise and leakage current in grounded-gate nMOSFET ESD protection devices*", Proc. ESSDERC'99, Leuven, Belgium 11-13. Sept. 1999, pp. 604-607.
52. G. Strasser, S. Gianordoli, L. Hvozdara, W. Schrenk, K.Unterrainer, E. Gornik (invited): "*Intersubband and interminiband GaAs/AlGaAs quantum cascade lasers*"; 5th International Conference on Intersubband Transitions in Quantum Wells ITQW'99; Bad Ischl, Austria, 7-11.9.1999
53. O. Gauthier-Lafaye, B. Seguin-Roa, F.H. Julien, P. Collot, C. Sirtori, J.Y. Duboz, G. Strasser: "*High power tunable quantum fountain unipolar lasers*"; 5th International

Conference on Intersubband Transitions in Quantum Wells ITQW'99; Bad Ischl, Austria, 7-11.9.1999

54. G. Ploner, H. Hirner, T. Maier, G. Strasser, J. Smoliner, E. Gornik: "*A novel device layout for tunneling spectroscopy of low-dimensional electron systems*"; 13th Int. Conf. on the Electronic Properties of 2D Systems (EP2DSXIII), Ottawa, Canada, August 1-7, 1999
55. J.Smoliner, R. Heer, G.Ploner and G. Strasser: "*$k_{//}=0$ filtering effects in ballistic electron transport through sub-surface GaAs-AlGaAs double barrier resonant tunneling structures*"; 13th Int. Conf. Electronic Properties of 2D Systems (EP2DSXIII), Ottawa, Canada, 1-7 August 1999
56. L. Hvozdara, S. Gianordoli, G. Strasser, W. Schrenk, K.Unterrainer, E. Gornik: "*GaAs/AlGaAs unipolar mid-infrared quantum cascade lasers*"; 26th International Symposium on Compound Semiconductors, Berlin, Germany, August 22-26, 1999
57. M. Helm, W. Hilber, G. Strasser, R. DeMeester, F.M. Peeters, A. Wacker: "*Interminiband spectroscopy of biased superlattices*"; 5th International Conference on Intersubband Transitions in Quantum Wells ITQW'99; Bad Ischl, Austria, 7-11.9.1999
58. A. Lugstein, H.D. Wanzenboeck, E. Bertagnolli: "*Focused Ion Beam Technology – A New Approach for the sub 100nm Microfabrication Regime*", GMe-Tagung (Bad Hofgastein) March 1999
59. H. Langfischer, B. Goebel, A. Lugstein, H.D. Wanzenboeck, E. Bertagnolli: "*Charakterisierung der Grenzflächenzustände von MOS-Transistoren der 0.25 μm Technologie nach Focused Ion Beam Implantation von Ga*", Austrian Physics Society (ÖPG '99) – Innsbruck 20 - 25 September 1999
60. G. Hobler and C.S. Rafferty: "*Modeling of {311} Defects*", Materials Research Society 1999 Spring Meeting (San Francisco) April 1999 (invited).
61. G. Hobler, L. Pelaz, and C.S. Rafferty: "*Dose, energy, and ion species dependence of the effective plusfactor for transient enhanced diffusion*", 5th Intl. Symp. Process Physics and Modeling in Semiconductor Technology, 195th Meeting of The Electrochemical Society (Seattle) May 1999.
62. R. Heer, J. Smoliner, G. Strasser, E. Gornik: "*Ballistic Electron Emission Microscopy, eine Erweiterung des STM zur Charakterisierung von vergrabenen Halbleiterstrukturen*", Jahrestagung der Österreichischen Physikalischen Gesellschaft1999, Fachtagung Festkörperphysik, Innsbruck, Austria, 21.09.1999
63. S. Gianordoli, L. Hvozdara, G. Strasser, T. Maier, N. Finger, K. Unterrainer, E. Gornik: "*GaAs/AlGaAs microresonator quantum cascade lasers*"; 5th International Conference on Intersubband Transitions in Quantum Wells ITQW'99 Bad Ischl, Austria, 7-11.9.1999
64. L. Hvozdara, S. Gianordoli, G. Strasser, W. Schrenk, K.Unterrainer, E. Gornik; V. Pustogow, C.S.S.S. Murthy, M. Kraft, B. Mizaikoff: "*GaAs/AlGaAs quantum cascade laser – a source for gas absorption spectroscopy*"; 5th International Conference on Intersubband Transitions in Quantum Wells ITQW'99; Bad Ischl, Austria, 7-11.9.1999

Doctor’s Theses

1. Christina Messner: “*Generierung von gepulster, durchstimmbarer THz-Strahlung zur zeitaufgelösten THz-Spektroskopie an Halbleitern*”.

Diploma Theses

1. Michael Fuchshuber: “*Elektrisch gepumpte Intersubband THz-Emitter*”.
2. Rainer Hoffmann: “*Ultrakurze THz-Pulse von Halbleiter-Heterostrukturen*”.
3. Michael Kast: “*Charakterisierung von Halbleiter-Heterostrukturen*”.
4. Peter Lampacher: “*DRAM-Leseverstärker mit Mismatchkompensation der Entscheidertransistoren*”.
5. Christoph Pacher: “*Untersuchung von Übergittertransport für THz-Quellen*”.
6. Ban Bishnu: “*Ultrasensitive laser measurement system using an all-electronic noise canceller*”.
7. Hannes Kostner: “*Zeitaufgelöste THz-Spektroskopie an strahlengeschädigtem InP*”.
8. Edwin Thaller: “*Intersubband Spectroscopy of Semiconductor Quantum Wells*”.
9. Martin Litzenberger: “*Thermal Characterization of Smart Power Electrostatic Discharge Protection Devices by Backside Laserprobing*”.

Cooperations

- Universität Innsbruck, Inst. F. Experimentalphysik, Mag. Fischler, Dr. J. Schmiedmayer
- Universität Linz, AO. Prof. M. Helm, Dr. W. Heiss, Prof. F. Schäffler, Prof. H. Thiem, AO. Prof. L. Palmetshofer
- AMS-Unterpremstätten, Dr. F. Noll, Dr. M. Schatzmayr
- Philips Consumer Electronics, DI E. Kaun
- Siemens AG: Prof. E. Wolfgang, Dr. G. Sölkner, Dr. W. Maurer
- Infineon: Dr. Stecher, Dr.M. Stoisiek, Dr. D. Schuhmann, Dr. J. Willer, Dr. R. Zelsacher
- Plansee AG, Reutte, Dr. Willhartitz
- Walter Schottky Institut, TU-München, Dr. W. Wegscheider, Germany
- TU München, Lehrstuhl für Techn. Elektrophysik, Prof. G. Wachutka, Germany
- LMU München, Lehrstuhl Photonik und Optoelektronik, Dr. N. Hecker, Germany
- Technische Universität Berlin, Dr. A. Wacker, Germany,
- Universität Bremen, Inst. für Festkörperphysik, Prof. Dr. D. Hommel, Germany
- Universität Stuttgart, 4. Physikalisches Institut, Prof. Dr. M.H. Pilkuhn, Germany
- RWTH Aachen, Inst. f. Halbleiterelektronik, Prof. H. Kurz, Germany

- Mütek Infrared Laser Systems, Dr. H. Wachernig, Germany
- Centre National de la Recherche Scientific, Laboratoire de Microstructures et de Microelectronique, B.Etienne, Cedex, France
- Thomson-CSF LCR, Orsay , Dr. Sirtori, Dr. Corbin, France
- Universite Paris Sud, Prof. F. Julien, France
- Institute National des Sciences Appliques de Lyon, VilleUrbanne, France
- Interuniversity Microelectronics Center (IMEC), Leuven, Belgien
- Ioffe Physico-Technical Institute, St. Petersburg, Prof. Y. Ivanov, Russia
- Sub-Micron Center, Weizmann Institute, Rehovot, Prof. M. Heiblum, Israel
- Univ. of California, Lawrence Berkeley Laboratories, Prof. E. E. Haller , USA
- University of California, Santa Barbara, Free-Electron-Laser, Prof. J. Allen, Prof. A. Gossard, USA
- Boston College, Dep. of Physics, Boston, Massachusetts, Prof. K.Kempa, USA
- EPI MBE Components, St. Paul, Minnesota, USA
- Pontificia Universidade Catolica de Rio de Janeiro, Prof. de Souza, Brasil
- Herriot Watt University, Edinburgh, Prof. C. Pidgeon, Scotland
- Univ. Nottingham, Prof. M. Chamberlain, England
- INFM-SNS Pisa, Prof. F. Beltram, Italy
- Technische Universität Delft, Faculty of Applied Physics, Prof. Wenckebach, Netherlands
- University Neuchatel, Prof. J. Faist, Switzerland
- Orbisphere Semiconductor Lasers, Switzerland
- Institute of Electrical Engineering, Slovak Academy of Sciences, Bratislava, Slowakia

Nanostructures:

- TU Wien:
  Institut für Angewandte Elektronik und Quantenelektronik; Prof. F. Krausz
- Universität Wien:
  Institut für Physikalische Chemie; Prof. Kauffmann
- Universität Linz:
  Institut für Halbleiterphysik; AO. Prof. Manfred Helm
- Universität Leoben:
  Institut für Physik; Prof. Kuchar
- LMU München:
  Lehrstuhl Photonik und Optoelektronik; Dr. N. Hecker

- Thomson-CSF, F
  Laboratoire Central de Recherches, Orsay; Dr. Sirtori, Dr. Kruck
- Universite Paris Sud, F
  Prof. F. Julien
- University of Surrey, UK:
  Physics Department; Dr. B.N.Murdin
- Herriot Watt University, Edinburgh, UK
  Prof. C. Pidgeon
- Boston College, Boston, Massachusetts, USA
  Dep. of Physics; Prof. K.Kempa. Prof. P. Bakshi

Electronic Transport

E. Gornik, M. Kast, C. Pacher, G. Ploner, C. Rauch, G. Strasser, J. Ulrich, K. Unterrainer

Institut für Festkörperelektronik, Technische Universität Wien, Floragasse 7, A-1040 Vienna, Austria

A. Neubauer, S. Kaufmann, D. Pum, U. Sleytr
Vienna University of Agriculture

1. Quantum wire photoconductive FIR detectors

(G. Ploner, J. Ulrich, G. Strasser, E. Gornik)

Quasi one-dimensional (1D) conductors or quantum wires are promising devices for photoconductive detection in the far-infrared spectral range. The energetic spacing of their 1D sublevels is typically in the range between 1 – 10 meV, which can be exploited to detect radiation in the corresponding frequency range. One possibility to do this is to investigate the frequency-dependent changes of the wire conductance under FIR radiation. The device principle currently under investigation is shown in Fig. 1.

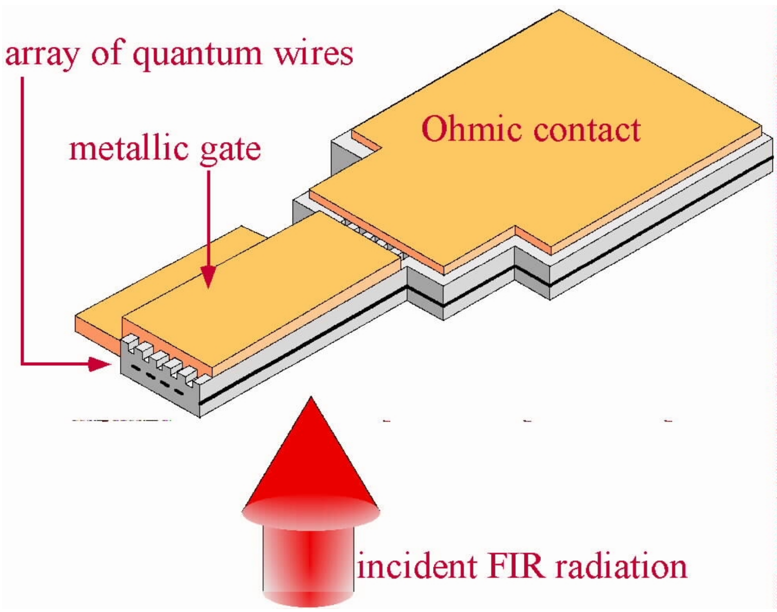

Fig. 1: Quantum wire FIR detector. The metallic top gate used to vary the strength of the lateral 1D confinement potential necessitates that the radiation is coupled into the device from the back side, as indicated by the red solid arrow.

Since previous investigations with side gated single wires have shown that in order to obtain a measurable photoconductive signal it is necessary to have relatively large areas covered with a wire array, we adopt the sample layout indicated in Fig. 1. The wire array is fabricated by shallow etching of 100 – 200 nm wide channels into the surface of the semiconductor and subsequently covered by a metallic gate. The gate gives the possibility to vary the confinement strength and thus to tune the frequency position of the expected photoconductive signal. Transport measurements show that the sublevel energies of these devices, when fabricated from standard heterostructure material, is in the range of 1 – 2 meV. An alternative, currently implemented approach for wire fabrication consists in structuring some insulating material (e.g. polyimide) into an array of narrow stripes, again followed by covering the resulting structure with a tuning gate.

Figure 2 shows an STM topograph of a typical shallow etched wire array. The roughness of the surface seen in the picture is due to the granularity of a thin Au film deposited on top of the sample prior to the STM imaging.

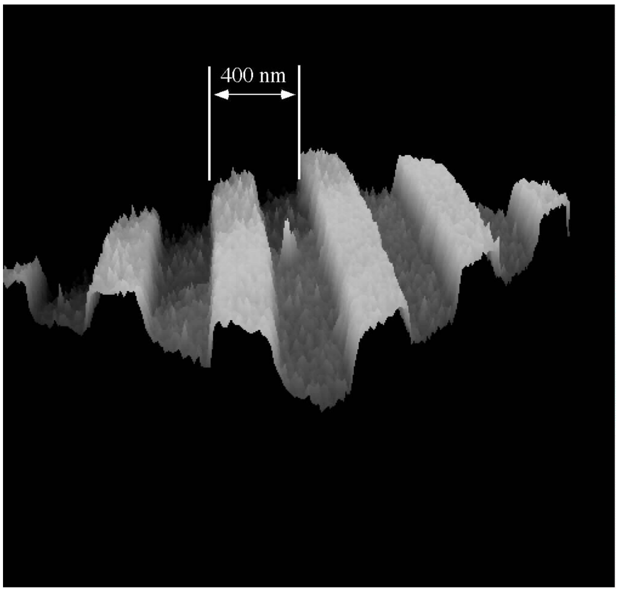

Fig. 2: STM topograph of a shallow etched wire array with 400 nm period.

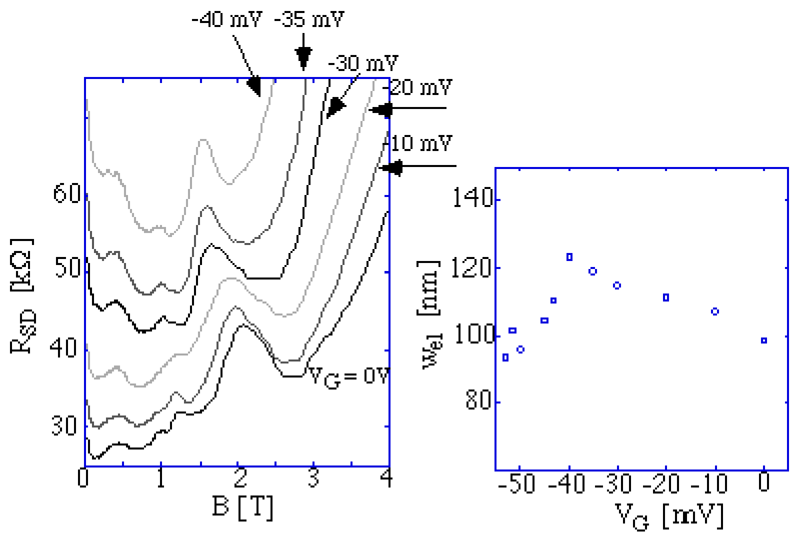

Fig. 3: Magnetotransport data of a gated wire array (left); Variation of the wire width as a function of the top gate voltage VG (right).

Figure 3 shows some typical magnetotransport data for a sample similar to the one depicted in Fig. 1. The magnetoresistance displayed on the left hand side shows the characteristic features of 1D transport. From these curves an estimate for the effective wire width is obtained (right hand side of Fig. 3) along with its dependence on the top gate voltage. Since the wire width is an indirect measure of the subband energies this shows the tuning capability of the gated wire array.

2. Fabrication of 2D lateral superlattices by deposition of bacterial crystalline surface (s-) layers on top of a GaAs-AlGaAs heterojunction

(G. Ploner, E.Gornik; A. Neubauer, S. Kaufmann, D. Pum, U. Sleytr)

In cooperation with the Center of Ultrastructure Research of the Vienna University of Agriculture an attempt is made to use crystalline layers of bio-molecules as templates for nanolithographic processes. These so-called s-layers form, when recrystallized on a semiconductor surface, large arrays of regularly arranged nanopores. The diameter of these pores can be as small as 3 nm; the period of the crystalline arrangement is typically of the order 10 nm. It has been shown that it is possible to deposit metal clusters within these pores. When transferred to the surface of a semiconductor heterostructure, the resulting regular array of metal clusters could be used to induce a weak potential modulation in a nearby two-dimensional electron gas (2DEG), thereby forming a lateral superlattice (SL). We currently investigate the possibility to induce artificial band-structure in a 2DEG via a grating of Pt/C metal clusters on top of a GaAs-AlGaAs heterostructure that has been arranged into a lateral SL via an s-layer (see the schematics in Fig. 4).

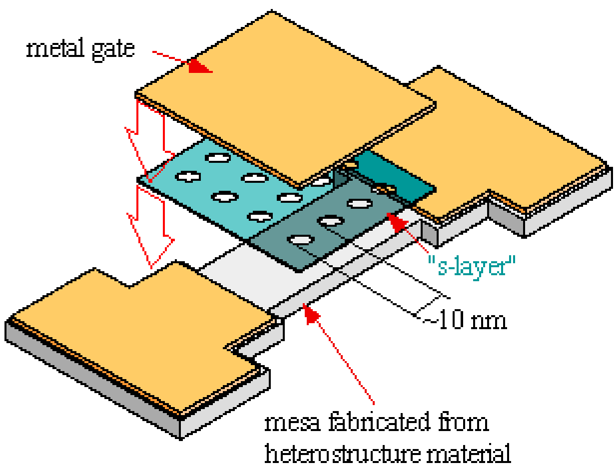

Fig. 4: Schematics of the use of biomolecular s-layers as template for nanofabrication.

We have shown that the required combination of standard lithography with s-layer processing is possible and recently succeeded in depositing a nanocrystalline s-layer on top of a GaAs semiconductor sample. Figure 5 shows an AFM image of the s-layer, which has been deposited on the surface of a GaAs sample within a 4 µm wide photoresist window. The s-layer is seen to form nano-crystals with an average grain size of 100 nm.

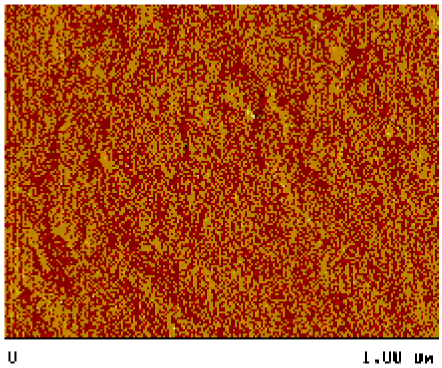

Fig. 5: Contact mode AFM image of an s-layer, deposited on top of a GaAs wafer.

The use of high-mobility material situated close to the sample surface as a substrate for the s-layer superlattice will possibly allow the investigation of band structure effects on the magnetotransport properties or an extensive study of ballistic weak localization effects. These subjects are not easily accessible when the surface superlattice is fabricated by standard lithographic methods, since the currently accessible superlattice periods are in the range of 100 nm. Using s-layers for nanofabrication the SL period could be reduced by an order of magnitude, which would facilitate the experimental investigation.

3. Current spectroscopy of novel GaAs/AlGaAs-heterostructures with three-terminal device technology

(C. Pacher, C. Rauch, M. Kast, K. Unterrainer, G. Strasser, E. Gornik)

Lately we used the three-terminal device technology to demonstrate the transition between coherent and incoherent transport in undoped GaAs/AlGaAs-superlattice minibands. Furthermore we could estimate the coherence length of electrons in this type of superlattice to be approximately 150 nm.

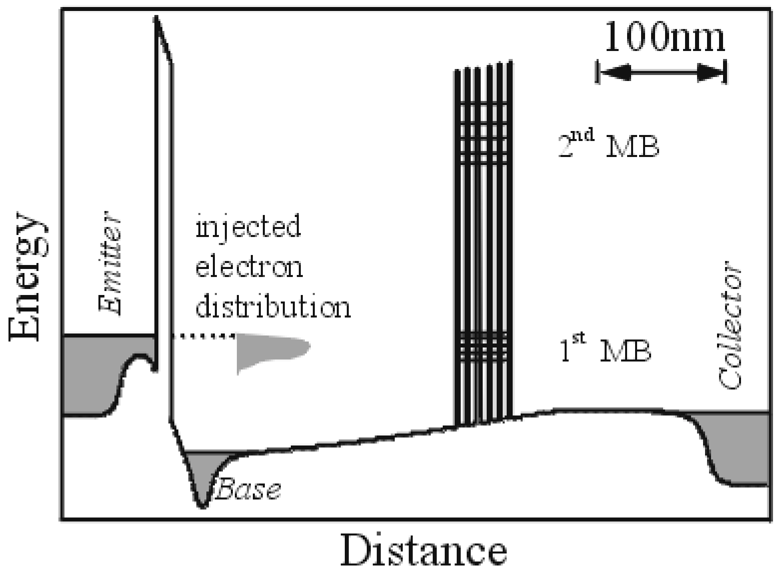

Fig. 6: Band structure of a Three-Terminal Device (5-period superlattice)

The technology of three-terminal devices (3TD) provides the necessary flexibility to study the transmission in dependence of both incident energy and applied electric field across the superlattice. The incident energy can be controlled through the emitter voltage; the collector voltage defines the electric field across the superlattice. The drift region in front of the superlattice reduces resonance effects, which come from the quantum well consisting of the injector barrier and the first barrier of the superlattice.

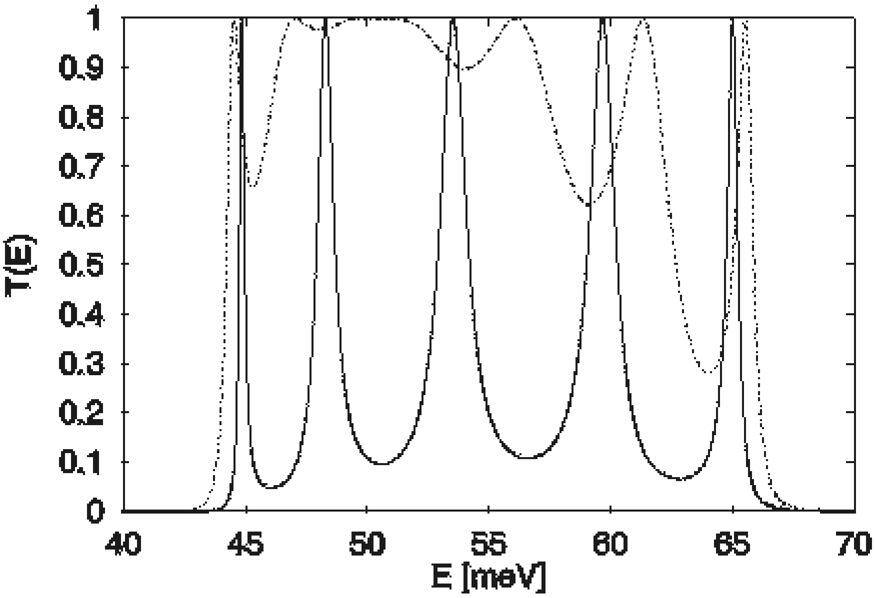

Fig. 7: Transfer-matrix based calculation of transmission through 5-period superlattice (first miniband) with anti-reflection coating (ARC) (dotted line) and without ARC (solid line). (calculations by F. Elsholz, TU Berlin)

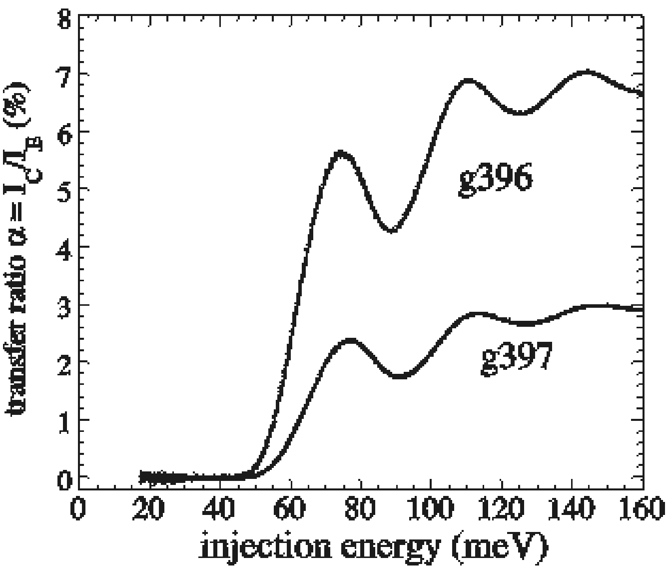

Fig. 8: Experimental data from two 3TDs: 5-period superlattice with (sample g396) and without (g397) anti-reflection coating. The multiple resonances have their origin in ballistic electrons which emitted one or more LO phonons.

The 3TD-technology can also be used to study ballistic transport through (nearly) arbitrary GaAs/AlGaAs heterostructures within a length of the order of 150 nm. We demonstrated the effect of an anti-reflection coating (ARC) for superlattices: an additional barrier with half the width of the superlattice barriers both in front of and after the superlattice increases the integrated transmission through the first miniband by a factor of about 2.5 in very good agreement with a simple transfer matrix calculation.

4. Observation of electron transport in GaAs/AlGaAs superlattices in the presence of crossed electric and magnetic fields

(M. Kast, C. Rauch, G. Strasser, E. Gornik)

In this work we present a study about the influence of crossed electric and magnetic fields on the electron transport in superlattice minibands. A three terminal device is used to probe the transmittance of undoped GaAs/GaAlAs superlattices in crossed electric and magnetic fields. An energy tunable electron beam is generated by a tunneling barrier and passes the superlattice after traversing a thin highly doped base layer and an undoped drift region. The transfer ratio ($=I_c/I_e$) reflects the probability of an injected electron to be transmitted through the superlattice. Electric field is applied across the superlattice and magnetic field perpendicular to the growth direction. Applying an in-plane magnetic field causes a deflection of the electron beam due to the Lorentz force. While the electric field leads to the localization of the electron wave function, the magnetic field increases the total effective electron path in the superlattice. As a result, incoherent transport is observed at positive superlattice bias conditions. The increase of the transfer ratios, at positive superlattice bias, with increasing magnetic field is shown in Fig. 9. We have taken the total miniband transmission, which is defined as twice the area of the lower energy side of the first transfer ratio peak, as a measure for the average current through the first miniband at given bias conditions. The change in the asymmetric behavior of the miniband-transmission, due to the increase of the total effective electron path in the superlattice, is shown in Fig. 10.

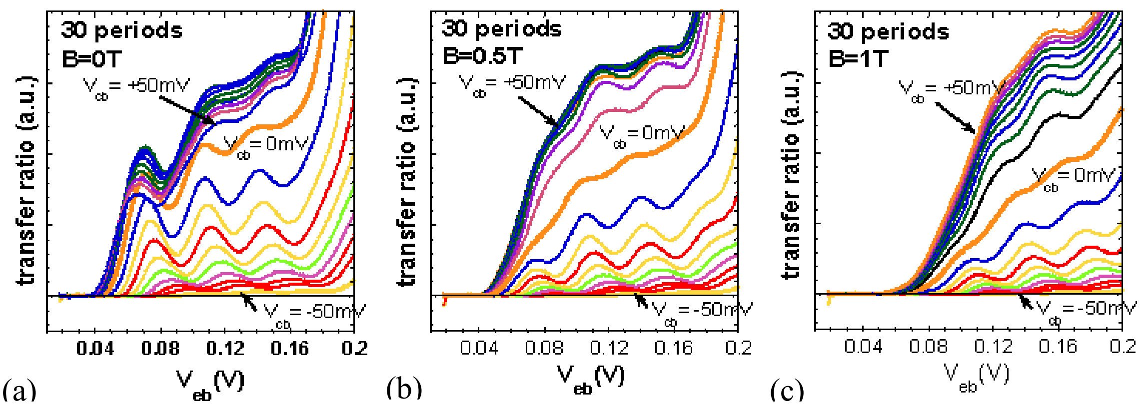

Fig. 9: Transfer ratios of a 30 periods superlattice at B = 0 T (a), B = 0.5 T (b) and B = 1 T (c).

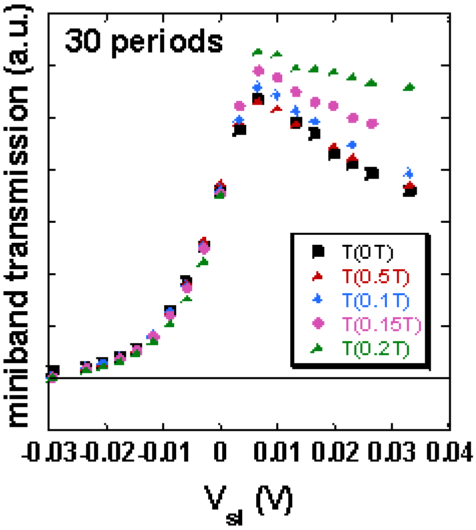

Fig. 10: Miniband transmission at various magnetic fields

Scanning Probe Spectroscopy

R. Heer, G. Ploner, D. Rakoczy, J. Smoliner, G. Strasser

Institut für Festkörperelektronik, Technische Universität Wien, Floragasse 7, A-1040 Vienna, Austria

1. Magnetic field effects in $k_{//}=0$ filtering structures for BEEM experiments

(J. Smoliner, R. Heer, G. Strasser)

Until now, only little attention was paid to the situation where electrons are transferred between areas of different effective mass, since it seems to need a combination of locally varying effective mass and low dimensional states in order to observe some interesting physical effects. A field of research where electron transfer between areas of different effective mass plays an especially important role is Ballistic Electron Emission Microscopy (BEEM). BEEM is a three terminal extension of conventional scanning tunneling microscopy (STM), where ballistic electrons are injected from a STM tip into a semiconductor (GaAs, $m^*=0.067m_0$) via a thin metal base layer ($m^*=m_0$) evaporated onto the sample.

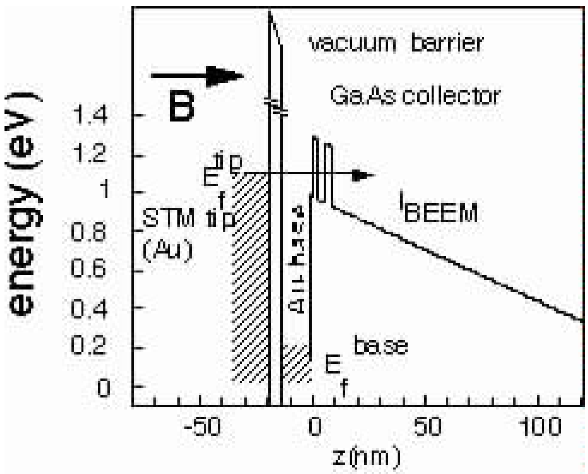

Fig. 1: Setup of the experiment.

As we have shown earlier, GaAs-AlGaAs double barrier resonant tunneling structures directly grown below the sample surface exhibit characteristic step-like features in the BEEM spectrum. Qualitatively, this effect is due to electron "refraction" at the Au-GaAs interface in combination with the resonant tunneling process through the states inside the double barrier structures. To describe the observed effect in a quantitative way, an extended Transfer Matrix Method (TMM) was introduced. We have found, that at interfaces between regions of different effective mass, the transmission coefficient for ballistic electrons becomes a function both of $E_\perp$ and $k_{//}$ and that sub surface resonant tunneling structures act as $k_{//}$ filters for electrons close to $k_{//} = 0$. In this way, the typical steplike behavior of the BEEM spectrum can be explained. To investigate the $k_{//}$ filtering behavior in more detail, BEEM measurements were carried out in magnetic fields applied perpendicular to the sample. As one can see, the BEEM spectrum is strongly influenced by the magnetic field. The step can be quenched and even double steps can occur at certain fields. If the bias is fixed and the magnetic field is varied, it becomes obvious that the ballistic current oscillates independently for each value of V_t.

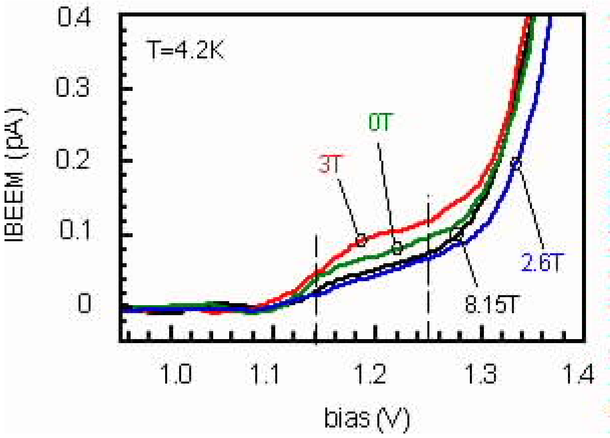

Fig. 2: Typical BEEM spectrum obtained on sub-surface resonant tunneling diodes for various magnetic fields. The measurement was carried out in liquid helium.

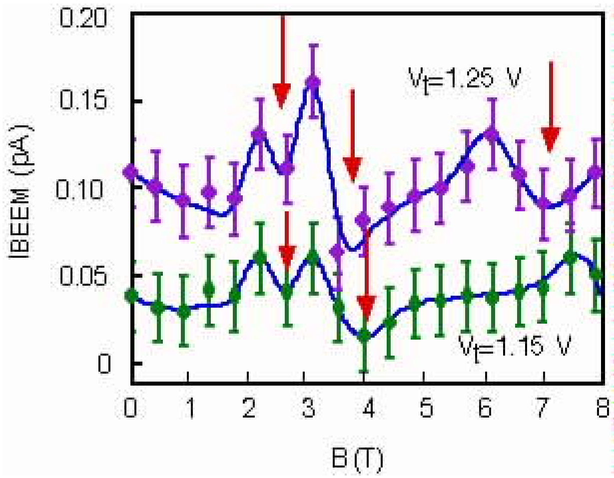

Fig. 3: BEEM current as a function of magnetic field and tunneling bias.

This behavior comes clear if the $k_{//}$ filtering effect is taken into account. If our structure really acts as filter for electrons close to $k_{//} = 0$ or $E_{//} = 0$, the oscillatory behavior can be explained in analogy to the Shubnikov de-Haas effect in two-dimensional electron gas systems: In magnetic fields, Landau level will exist inside the resonant tunneling diode. If the field is increased, the level spacing increases, too, and the number of levels inside the allowed $E_{//}$ range will decrease. As each allowed Landau level carries a part of the BEEM current, a minimum in the BEEM current an be expected each time a Landau level is shifted outside the allowed energy range.

2. GaAs cap layers in ballistic electron transport through GaAs-AlGaAs RTD's

(R. Heer, J. Smoliner, G. Ploner, G. Strasser)

Until now, only little attention was paid to the situation where electrons are transferred between areas of different effective mass, since it seems to need a combination of locally varying effective mass and low dimensional states in order to observe some interesting physical effects. On InAs-AlSb resonant tunneling diodes, e.g., this is the case and it was found that the calculated current voltage characteristics differs qualitatively from the experimental data because the longitudinal and transversal components of the electron wave vectors are coupled on these samples.

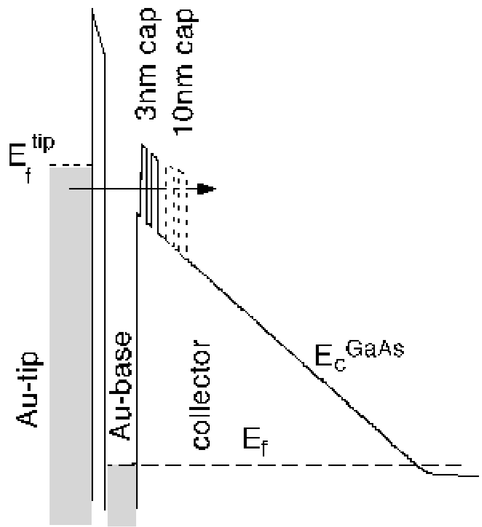

Fig. 4: Schematic setup, the thickness of the cap layer is modulated by wire etching.

A field of research where electron transfer between areas of different effective mass plays an especially important role is Ballistic Electron Emission Microscopy (BEEM). BEEM is a three terminal extension of conventional scanning tunneling microscopy (STM), where ballistic electrons are injected from a STM tip into a semiconductor (GaAs, $m^* = 0.067\ m_0$) via a thin metal base layer ($m^* = m_0$) evaporated onto the sample. In our group, the energetic distribution of ballistic electrons in GaAs is studied employing buried GaAs-AlGaAs resonant tunneling structures as energy filter in BEEM experiments. The conduction band diagram is shown in Fig. 4 in the configuration of the 10 nm cap layer.

Due to the large difference in electron mass in the Au base electrode and the GaAs collector, we found that parallel momentum conservation leads to considerable electron refraction at the Au-GaAs interface, and as a consequence, an almost linear behavior of the BEEM spectrum is observed in the energetic regime below the AlGaAs barrier height, as shown in Fig. 5 curve (A). Buried GaAs-AlGaAs resonant tunneling structures acts as an energy filter in BEEM experiments for $E_\perp$. GaAs-AlGaAs double barrier resonant tunneling structures grown directly below the sample surface exhibit characteristic step-like features in the BEEM spectrum and act as parallel momentum filter for ballistic electrons at $k_{//} = 0$, as shown in Fig. 5 curve (B).

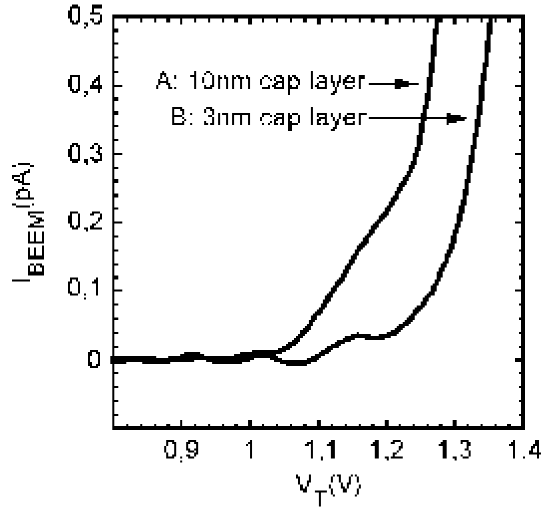

Fig. 5: BEES data obtained on top of the wire (A) and in the valley (B) @ 4,2K. Curve (A) shows a linear behavior, curve (B) shows a step-like feature in the region of the RTD barriers, respectively. Since the tunneling current in curve (A) was 5 nA and in curve (B) was 2 nA, the step-like feature is somehow less pronounced.

Qualitatively, this effect is due to electron refraction at the Au-GaAs interface in combination with the resonant tunneling process through the states inside the double barrier structures. To describe the observed effect in a quantitative way, an extended Transfer Matrix Method (TMM) is used. It shows that at interfaces between regions of different effective mass, the transmission coefficient for ballistic electrons becomes a function both of $E_{\perp}$ and $k_{//}$ and that $k_{//}$ filtering is a natural consequence of the situation, where an electron tunnels through a resonant state while its effective mass is changed. The filter characteristic of the GaAs-AlGaAs double barrier resonant tunneling structure is tremendously influenced by the thickness of the covering GaAs cap layer. The spectra shown in Fig. 5 are taken at the same sample at the positions A and B, as shown in Fig. 6.

By variation of the etch depth the transition between the steplike, $k_{//} = 0$, filter characteristic and the linear, $k_{//} >> 0$, filter characteristic can be investigated.

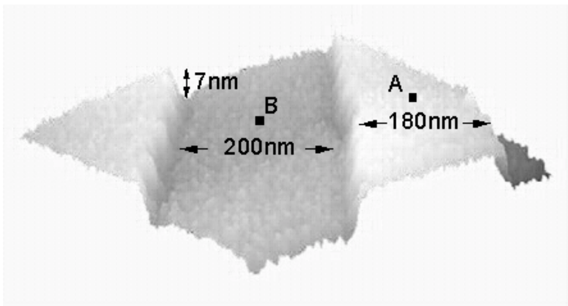

Fig. 6: STM based topographic image of the sample @ 4,2K. In the etched regions 3 nm GaAs, whereas in the unetched regions the initial 10 nm GaAs cap layer is remaining. The BEES data shown above are taken at point A on the wire and at point B in the valley.

3. A metal-insulator-metal injector for ballistic electron emission spectroscopy

(D. Rakoczy, R. Heer, G. Strasser, J. Smoliner)

As a supplement to STM (Scanning Tunneling Microscope) based BEES (Ballistic Electron Emission Spectroscopy) we have developed a solid-state version of BEES using a MIM (metal-insulator-metal) injector structure that replaces the tip of the STM. Our aim was to make an easy-to-fabricate, versatile and robust emitter for ballistic electrons.

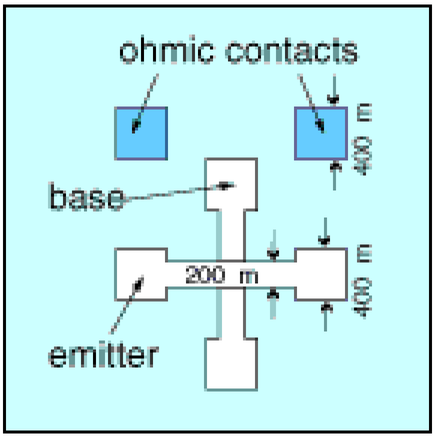

Fig. 7: Layout of the device.

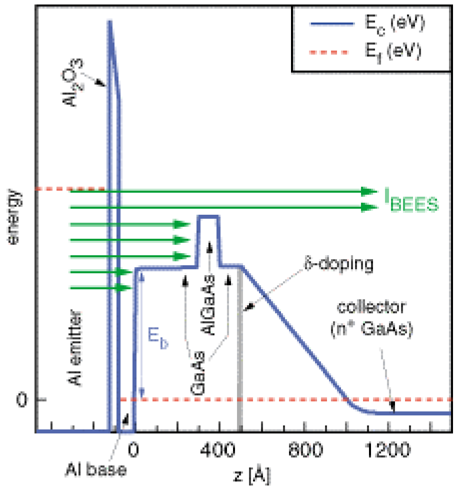

Fig. 8: MIM-Injector on a GaAs-AlGaAs-single barrier heterostructure: Schematic view of the conduction band profile and principle of ballistic electron injection.

The injector itself is realized by an Al-Al_2O_3-Al tunnel junction which is deposited on the structure under investigation. Up to now we concentrated our work on GaAs-AlGaAs heterostructures only, but of course the principle of a MIM injector for BEES can also be used for the investigation of other semiconductors. The size of a typical tunnel junction is 200 µm x 200 µm, but we did also some measurements using smaller emitters. The design of our device allows an easy access to emitter, base, and collector and therefore is ideal for the simultaneous measurement of tunnel and BEES current with a quite simple setup. Moreover we can apply a bias voltage V_c (which is independent of the emitter voltage V_t used to provide the ballistic electrons) between base and collector and therefore "tilt" the band structure in the GaAs-AlGaAs.

To test our new emitter concept we investigated two different types of MBE grown GaAs-AlGaAs samples. The first (g218) consisted of GaAs only, while the other one (g232) had a single, 10 nm thick AlGaAs barrier 30 nm below the surface (the cap layer consisted of nominally undoped GaAs). Both samples were grown with a very thin region (just some atomic layers thick) of highly p-doped GaAs ("delta-doping") in the otherwise nominally undoped GaAs to provide a "flatband" condition at the surface.

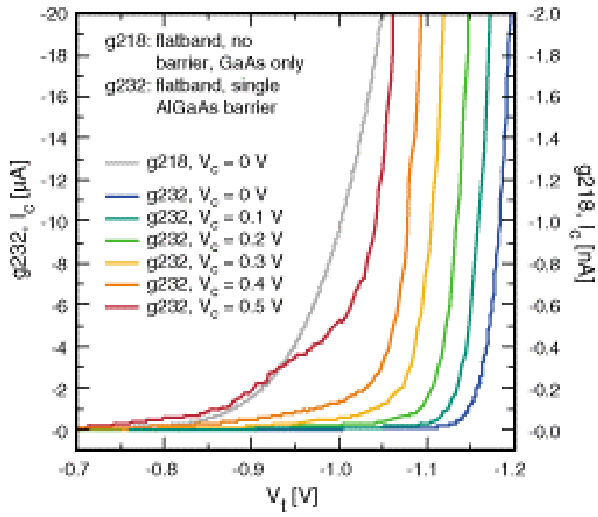

Fig. 9: Measured collector currents (Ic) on sample g232 for various collector voltages. The onset of the collector currents shifts in dependence of V_c. For higher collector voltages some leakage effects can be seen. For comparison also the (V_c = 0 V) collector current for sample g218 is shown.

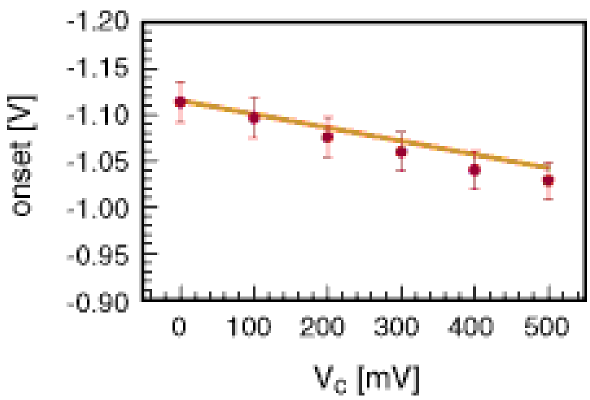

Fig. 10: Onset voltages of the collector current as a function of the applied collector voltage (V_c) for sample g232. The dots are experimental values extracted from the measured BEES spectra, the line shows the calculated behavior.

The measured onset voltages agree very well with the values expected from the band profile parameters. For $V_c = 0$ V we obtain a $V_{onset} = -0.803$ V for sample g218 and $V_{onset} = -1.113$ V for sample g232, respectively. The measured height of the AlGaAs barrier of g232 is thus 310 meV, in good agreement with the results obtained earlier on the same samples by STM-based BEES measurements. The shape of the BEES curves and the values of the onset voltages were reproduced on several samples and also agree excellently with the calculated results. On the other hand the total amount of the ballistic electron current shows large deviations when measured on different samples. This seems to originate in variations of the properties of the injector structures, i.e. especially the quality of the aluminum oxide barrier.

Applying a positive bias voltage to the collector electrode shifts the onset to smaller absolute values in V_t. This is exactly what is expected from the behavior of the band profile: $V_c > 0$ V means a lowering of the collector Fermi level which leads to a tilt of the band profile and therefore reduces the effective height of the AlGaAs barrier. The measured decrease in V_{onset} agrees quite well with results from self-consistent calculations. For higher collector bias values we observe some leakage effects.

4. Temperature dependent studies of InAs base layers for ballistic electron emission microscopy

(R. Heer, G. Strasser, J. Smoliner)

InAs is a promising new base material for ballistic electron emission microscopy (BEEM) since in this material, the attenuation length of ballistic electrons is more than one order of magnitude larger than for metal base layers and the corresponding transmission factor for ballistic electrons is strongly enhanced. Figure 11 shows a typical band diagram of a InAs-GaAs heterostructure with 240 nm thick InAs base layer.

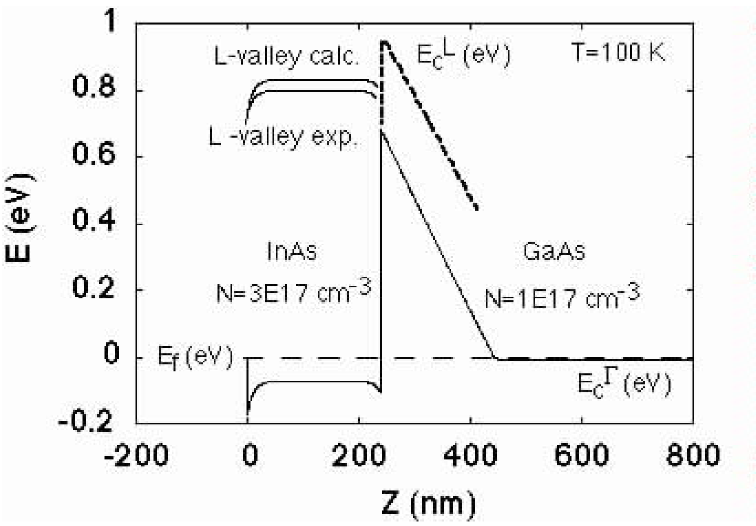

Fig. 11: Self consistently calculated band diagram of our InAs-GaAs heterostructure.

Unlike than other semiconductors, InAs has a surface accumulation layer of electrons and using the results of earlier magnetocapacitance and magnetotransport experiments, the Fermi level pinning at the surface is found to be 160 meV above the conduction band. Figure 12 shows typical BEEM data of such a sample measured at temperatures of T = 100 K and T = 25 K, respectively. Obviously, the BEEM spectra are shifted to higher voltages with decreasing temperature.

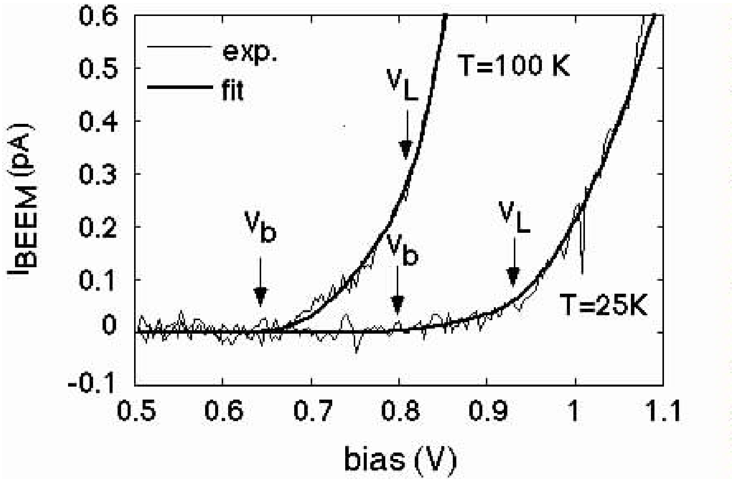

Fig. 12: Measured and calculated BEEM spectra at temperatures of T = 100 K and T = 25 K, respectively. The tunneling current was 1 nA, the InAs film thickness, 240 nm.

As shown previously, two different onset voltages can be identified in these BEEM spectra. The lower onset voltage, V_b, is the threshold voltage for ballistic electrons crossing the barrier at the InAs-GaAs interface in the Γ–valley. The second threshold at higher bias, V_L , corresponds to the onset of ballistic electron transport through the L-valley of the InAs film. The onset of ballistic electron transport through the X-valley of the InAs film would be expected 1 eV above the threshold for L-valley transport, which is outside the range of our measurement. To determine the onset voltages V_b and V_L and also the transmission factors for electrons traveling through the Γ and L valley, $t_Γ$ and t_L, a modified Bell-Kaiser model was applied.

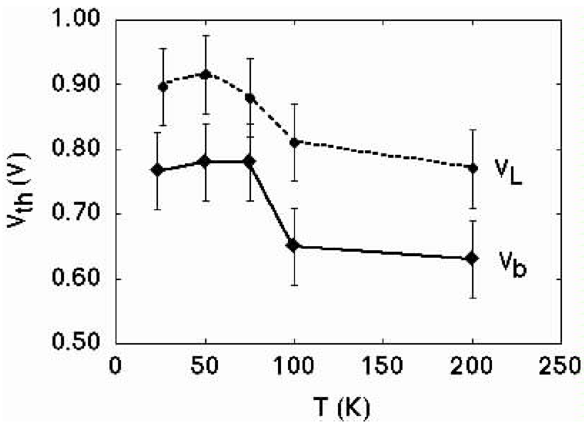

Fig. 13: Threshold voltages V_{th} as a function of temperature. V_b is the threshold voltage for the Γ valley, V_L the threshold for the L-valley. The variation of the threshold voltages determined on various sample positions was ± 0.06 V.

We now discuss the temperature behavior of the onset voltages V_b and V_L.

In Fig. 13, V_b and V_L are plotted as a function of temperature. Within the experimental errors, V_b and V_L increase equally with decreasing temperature. In addition, a steplike feature is revealed in the temperature curves around T = 100 K. Quantitatively, V_b and V_L increase by 160 meV in the temperature range between T = 200 K and T = 25 K. At T = 200 K and also when extrapolated to room temperature, the (Γ) barrier height at the InAs-GaAs interface on our samples agrees well with the data reported in the literature. A possible explanation for the large threshold shift around T = 100 K is a temperature dependent Fermi level pinning at the InAs-GaAs interface, however, we have no proof for this.

Our second major finding is somewhat surprising: With decreasing temperature, we find a decreasing base transmission for our InAs-GaAs heterostructures and InAs-GaAs heterostructures and we have verified this behavior on many different samples and also on different wafers. In Fig. 14 (a) we have plotted the temperature dependence of the transmission factors t_Γ and t_L for a 240 nm thick InAs film. Remarkably, the transmission decreases significantly with decreasing temperature. For the Γ valley, it decreases from 1.8% at T = 200 K to 0.35%, at T = 25 K. For the L valley, it decreases from 7% down to 1.5%. To get some information on the origin of this behavior, we have also made an Arrhenius plot of our data, which is shown in Fig. 14 (b). As one can see, the transmission shows a linear behavior when plotted on logarithmic scale as a function of (1/T). This behavior suggests a temperature activated transmission process, with an activation energy E_A^{Γ}= 4.9 ± 1 meV for the Γ and E_A^{L}= 5.3 ± 1 meV for the L-valley, respectively. The origin of this behavior is not understood at the moment, but we think that either temperature dependent scattering processes in the InAs and at the InAs-GaAs interface or traps can be made responsible for the observed effects.

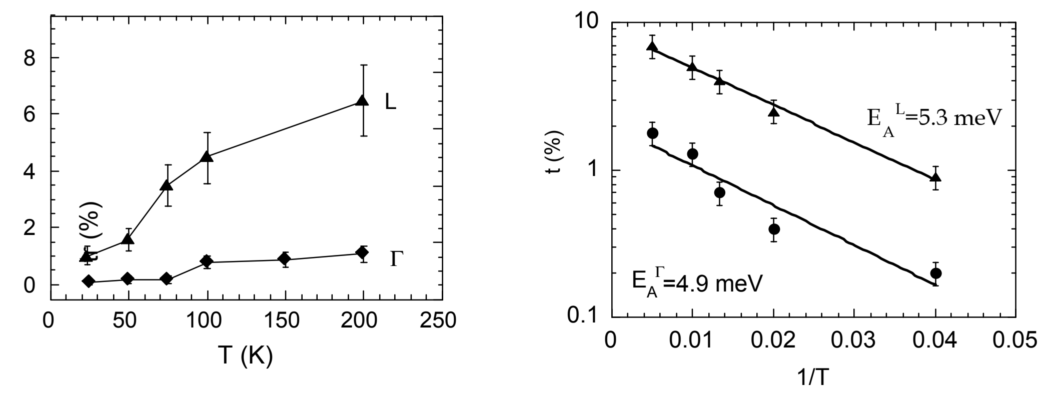

(a) (b)

Fig. 14: (a): Experimentally measured transmission factors for the Γ- and L-valley (t_Γ, t_L) as a function of temperature. Typically, the transmission factors varied by ≈18% across a sample. (b): Same data as a function of (1/T) plotted on a log-scale (Arrhenius plot).

Optoelectronics

N. Finger, E. Gornik, P.O. Kellermann, T. Maier

**Institut für Festkörperelektronik, Technische Universität Wien,
Floragasse 7, A-1040 Vienna, Austria**

1. Wavelength-graded laser array

(P.O. Kellermann, N. Finger and E. Gornik (cooperation with University Stuttgart))

The wavelength division multiplexing (WDM) scheme is utilized to increase significantly the transmission rate of optical communication systems. Monolithic arrays of wavelength-graded laser diodes are considered as a compact choice for WDM light sources.

Fig. 1: Wavelength graded laser array.

We are developing a wavelength-graded surface-emitting laser array, which is based on contradirectional surface-mode coupling. The wavelength of single array elements can be adjusted after the processing by just changing the optical thickness of a surface waveguide. Phase matching of the surface-mode and the laser-mode (propagating in the dielectric surface waveguide and in the horizontal cavity respectively) is achieved by a surface relief grating in the top cladding of the laser waveguide. The grating causes radiation losses of the laser-mode (dominated by the emission into the substrate). The losses are reduced significantly in a narrow spectral range by the excitation and feedback process of the surface-mode. The linewidth of this resonance is comparable to the longitudinal Fabry-Perot mode spacing of the laser cavity, thus providing an effective mode selection mechanism, which leads to single-mode emission. The surface-mode couples both to the active region and into the vacuum light cone resulting in surface emission.

This surface-mode coupling concept is now used to realize a wavelength-graded array with visible red GaInP/AlGaInP lasers. Lasers in the visible regime are suitable to be used as emitters in optical short-range data transmission since the attenuation minimum of polymethylmethacrylate (PMMA) fibers lies near 650 nm. Holographic lithography and ion milling define the surface grating. Different thicknesses of the SiO/SiN surface waveguides are etched by ion milling yielding a wavelength spacing between the individual lasers. The total range across the array is a few nanometers. The fabrication process allows etching one element type of many arrays in one step..

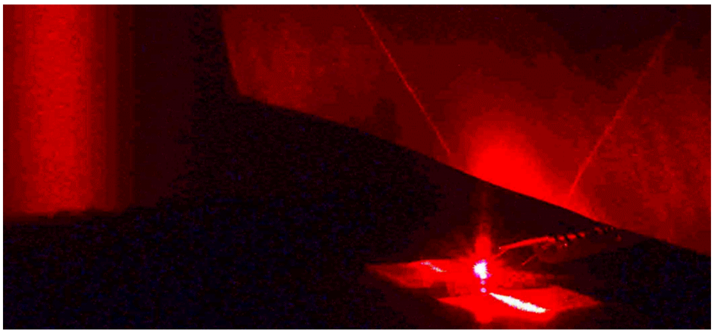

Fig. 2: The array elements emit via the surface. The intensity emitted per solid angle via the surface beam is five times larger than the one at the edges. Farfield pattern of a surface mode coupled laser: Two narrow surface beams and divergent spontaneous emission strike a paper screen (top) that is orientated parallel to the laser stripe contact. The divergent edge emission can be seen on the thermo electric cooling element and on a second paper screen (left-hand), which is orientated parallel to the cleaved facets.

2. A compact sensor for interferometric displacement measurements

(T. Maier and E. Gornik)

Interferometers based on the self-mixing effect in a single-mode laser diode are a low-cost solution for precise measurements of displacements, vibrations or absolute distances. Due to their inherent single-mode behavior and their homogenous far field patterns, vertical-cavity surface emitting lasers (VCSELs) appear especially suitable for this kind of application. Furthermore, by monolithic integration of a high-efficiency resonance-enhanced photodetector (REPD) which is used to read out the interferometric signal, a simple and compact interferometric sensor can be realized.

Our sensor consists of a GaAs-VCSEL which is surrounded by a large-area REPD (Fig. 3). The laser's 3 µm oxide aperture ensures single transverse mode operation throughout the pumping range. The top Bragg mirror of the VCSEL consists of 16.5 periods SiO_2/Si_3N_4. The detector efficiency is maximized by removing 5.5 periods of the top mirror, resulting in a peak efficiency of 62%.

The laser light is collimated and reflected back on the VCSEL with a retroreflector mounted on a piezoelectric transducer (PZT) which is driven by a sine voltage. The laser power is monitored with the integrated REPD. Due to self-mixing, the output power of the laser depends on the length of the external cavity and is modulated with a period of λ/2. The actual shape of the interferometric signal is determined by the strength of the feedback. Figure 4 shows the detector signal for several feedback levels, which are obtained by inserting various density filters in the optical path. For moderate feedback (a) the laser exhibits bistable switching between two external cavity modes, resulting in a hysteresis of the output power. The different switching levels indicate the direction of the retroreflector's movement. For decreasing feedback, the hysteresis disappears (b), and the sawtooth-like shape of the photosignal approaches a sine waveform (c). A first estimation of the dynamic range of the interferometer gives a minimum value of 15 cm.

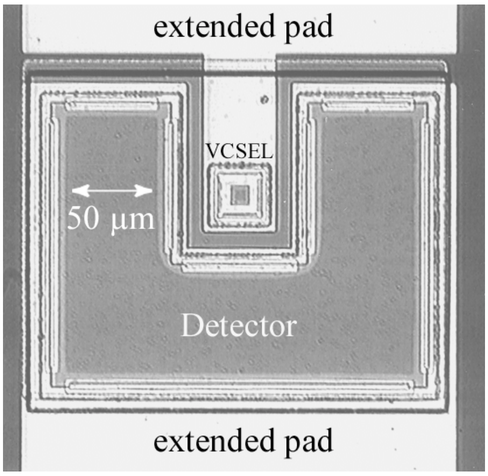

Fig. 3: Photograph of the sensor chip.

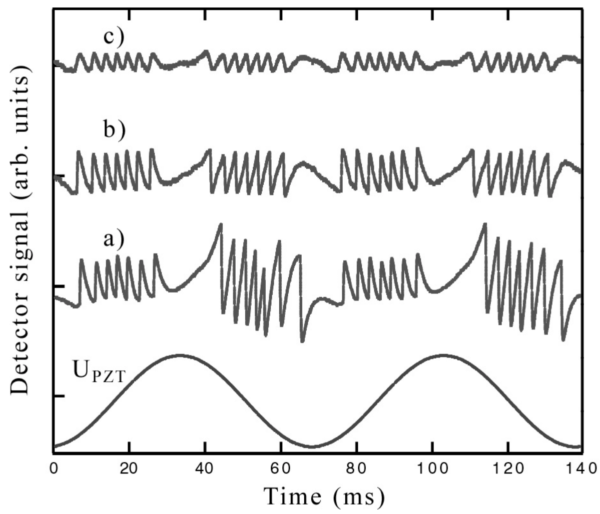

Fig. 4: Detector signals for various feedback levels (a, b, c). UPZT is the drive voltage applied to the PZT. The length of this external cavity is 20 cm.

Quantum Cascade Lasers

N. Finger, S. Gianordoli, S. Gianordoli, E. Gornik, L. Hvozdara, W. Schrenk, G.Strasser, J. Ulrich, K. Unterrainer, R. Zobl

Institut für Festkörperelektronik, Technische Universität Wien, Floragasse 7, A-1040 Vienna, Austria

1. Quadrupolar deformed microlasers on GaAs/AlGaAs

(S. Gianordoli, W. Schrenk, L. Hvozdara, G. Strasser, K. Unterrainer, N. Finger, E. Gornik)

Quantum cascade lasers (QCLs) are powerful light sources in the mid infrared, a spectral region interesting for gas sensing and pollution monitoring. Low threshold currents, high working temperatures (165 K for microcylinder lasers) and single mode emission with a side mode suppression ratio better than 20 dB are needed for many applications.

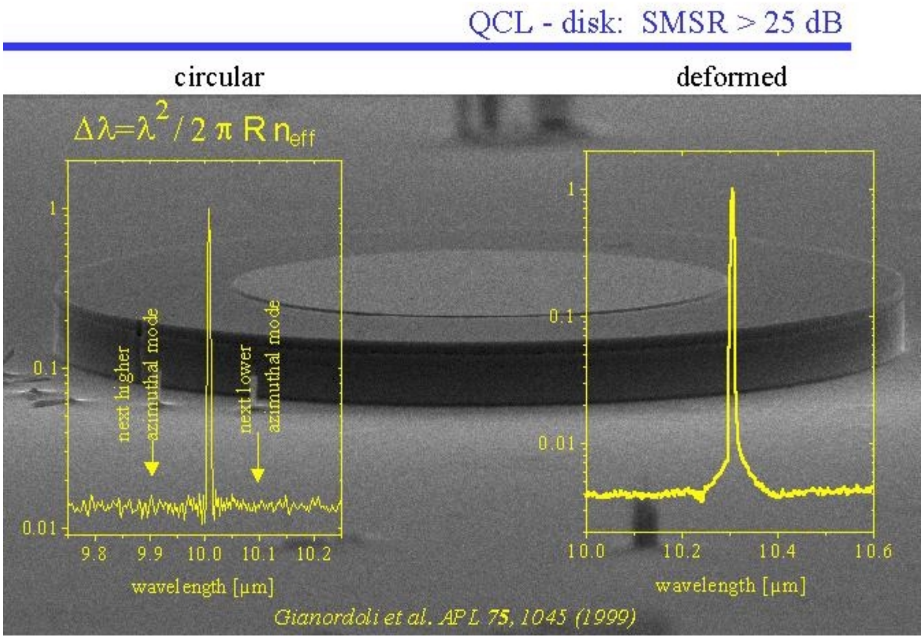

Fig. 1: Single mode spectra of microcavities.

For all driving currents, the described micro-cavity lasers exhibit single mode behavior with a side mode suppression better than 25 dB. No additional side modes are identifiable in the spectra. The positions of the next modes in the emission spectrum of the circular laser (R = 60 µm) are indicated with arrows. The large radius of the deformed micro-laser is R = 50 µm with a deformation coefficient of 0.18. Driving currents are in the range between 200 mA and 2 A, depending on the size of the lasers. Using the following formula in polar coordinates for the radius of the microlasers the so called quadrupolar shaped microlasers shown in Fig. 2 are fabricated using optical lithography and dry etching.

$$r(\phi) = \frac{R}{\sqrt{1+2\varepsilon}} \sqrt{1+2\varepsilon\cos(2\phi)}$$

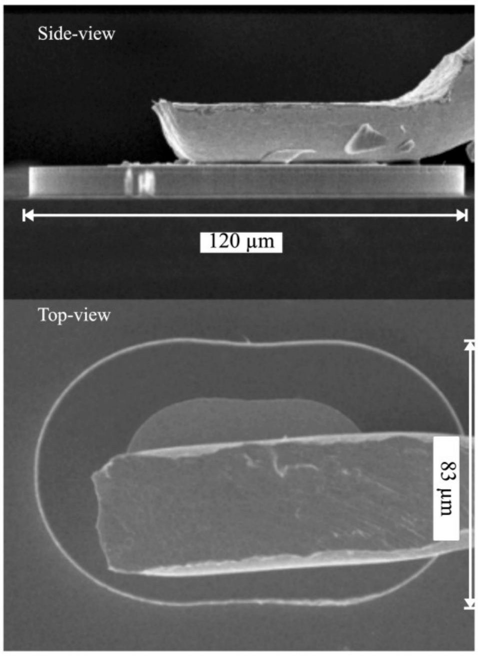

Fig. 2: Top and side view of bonded microcavities.

The side-view and top-view scanning electron pictures of a typical microlaser are depicted in Fig. 2. The etched depth is around 10 µm. For the depicted quadrupolar shaped laser the larger radius has a value R = 60 µm, the smallest value for the radius is 41.7 µm and the deformation is e = 0.22. This results in an active area of 7854 μm^2. For this large deformation the resonator gets concave. In spite of this fact a resonant mode exists and the laser is operating. The distance between the shaped top Au contact and resonator edge is 20 µm. The bonding wire is clearly seen on both views . For a deformation of e = 0.22 the shape of the microlaser rim starts to get concave. This displays excellent quality of the used technology.

2. Self-aligned coupled cavity GaAs/AlGaAs mid-infrared quantum cascade lasers

(L. Hvozdara, G. Strasser, K. Unterrainer, E. Gornik)

Since the introduction of quantum cascade lasers (QCLs) by Faist et al. in 1994 they have undergone a very dynamic development and reached a state of the art among the mid-infrared (MIR) radiation sources. Besides the traditional ridge Fabry-Perot (F-P) geometry, many modifications like distributed feedback-lasers, microcylindrical, quadrupolar as well as disk lasers have been fabricated and characterized.

We present a novel, monolithic, self-aligned focused ion beam cut coupled cavity GaAs/AlGaAs Quantum Cascade Laser emitting in the range of λ = 9.4 µm. Separate pulsing of two optically coupled laser sections enables control of the lasing in single mode regime and in multimode regime. Single mode operation with side mode suppression ratio better than 25 dB is demonstrated. Mode control over two 3.6 cm^{-1} spaced single modes is shown. Optical output intensity modulation in a range of 20 dB is achieved. The laser exhibits a peak output power in the range of 200 mW at cryogenic conditions.

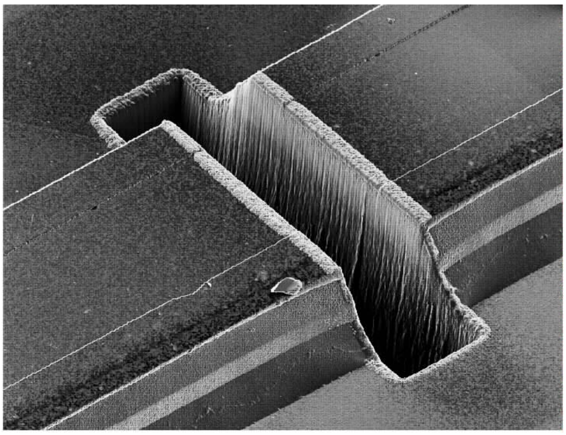

Fig. 3: SEM picture of the FIB processed gap on the $FIBC^3$ laser.

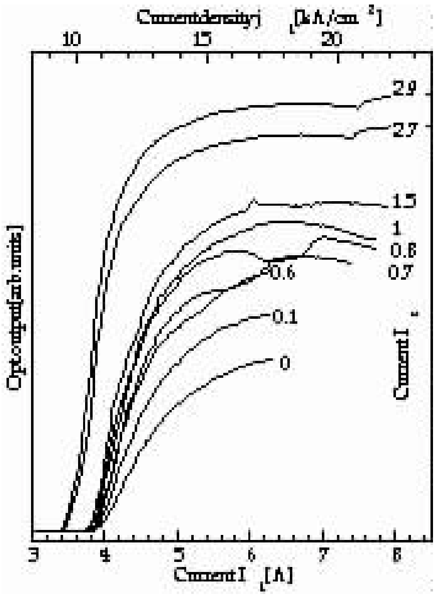

Fig. 4: Optical output vs. current (L-I). The current through the shorter laser section is given as a parameter.

A laser ridge fabricated by common lithographic techniques is modified by trenching a gap perpendicularly across the laser resonator. The extended contact is separated by a shallower trench, in order to enable separate current driving of the two laser sections. The obtained Fib-Cut Coupled Cavity ($FIBC^3$) laser (Fig. 3) is ideally self-aligned, mechanically stable and its fabrication is highly reproducible. This modification converted a two-terminal device into a three terminal device. An independent control of currents through the two sections enables modulation of the output intensity, mode control and single mode operation. Figure 4 shows typical output characteristics (L-I) of a FIBC3 laser with two sections of non-equal lengths. I_L represents the current driven through the longer section (x-axis) and I_S stands for the current driven through the shorter section (parameter). Variation of I_S from 0 to 2.9 A leads to an increase of the total output intensity by factor of three in the saturation regime. A modulation range of 20 dB in the linear regime has been found. Differential efficiency in the linear regime rises by a factor of 4.1.

3. Development of a terahertz quantum cascade laser

(J. Ulrich, R. Zobl, G. Strasser, K. Unterrainer, E. Gornik)

Quantum cascade lasers are today feasible with vacuum wavelengths up to 17 µm. In order to extend their range into the far infrared, i. e. down to terahertz frequencies, we have designed cascade structures with a level separation of less than the longitudinal optical (LO) phonon energy. Thereby, LO-phonon emission – being the fastest non-radiative scattering channel in the mid-infrared lasers – should be suppressed.

Our emitters are made up of 50 periods of a chirped $Al_{0.15}Ga_{0.85}As/GaAs$ superlattice. Figure 5 displays the conduction band structure. The radiative transition takes place between the first two subbands of a wide quantum well. Multiple ridges were processed for electroluminescence measurements. Using two different spectrometers, a Fourier-transform spectrometer and a magnetically tunable InSb cyclotron resonance detector, we have observed spontaneous emission at 17.3 meV (4.3 THz) with a linewidth of 1.3 meV (see Fig. 6). This is consistent with the calculated energy difference of 17.1 meV. The detected optical power has been roughly estimated from the detector sensitivity to be 10 pW.

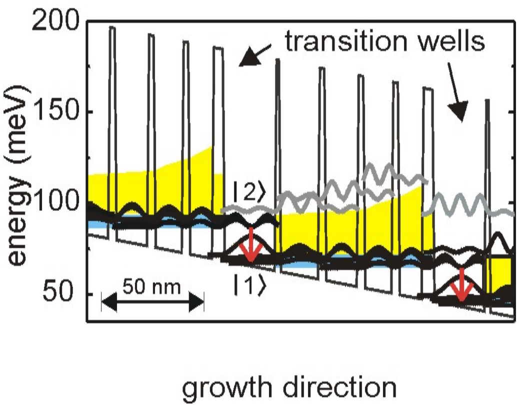

Fig. 5: Conduction band diagram of a terahertz quantum cascade laser.

The main reason for the relatively low power is the low internal quantum efficiency, i.e., the radiative transition rate over the non-radiative rate. The output power could be enhanced by a factor of two by reducing the non-radiative scattering rate in a magnetic field perpendicular to the epitaxial layers. Thereby, the in-plane motion is quantized into Landau levels and electron-electron-scattering is significantly suppressed. The enhancement of the line intensity exhibits characteristic oscillations stemming from resonant tunneling between the two Landau-fans. These results prove directly that the emission from the cascade emitter is limited by fast electron-electron-scattering, which can be controlled by a magnetic field.

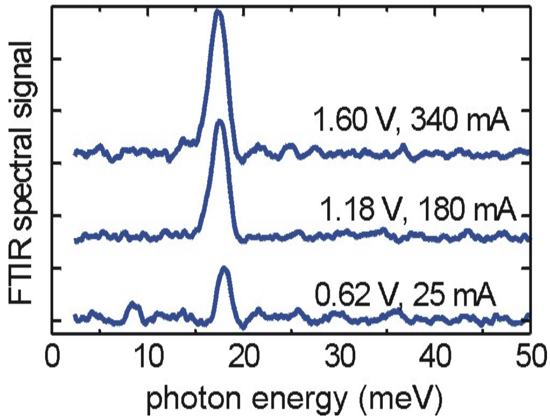

Fig. 6: Emission spectra of a terahertz quantum cascade laser.

4. Distributed Feedback Quantum Cascade Lasers

(W. Schrenk, N. Finger, S. Gianordoli, L. Hvozdara, G. Strasser, E. Gornik)

Quantum cascade lasers are powerful light sources in the mid infrared, a spectral region interesting for gas sensing and pollution monitoring. Since the demonstration of the QCLs in 1994 in the InGaAs/InAlAs system grown on InP, the laser performance has been improved dramatically. For many applications there is a need for continuous tunable single mode sources, which can be realized by distributed feedback (DFB) lasers.

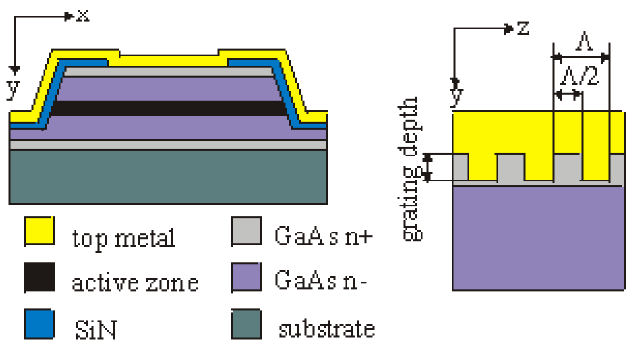

Fig. 7: Schematic cross sections of the DFB QCL and the grating region.

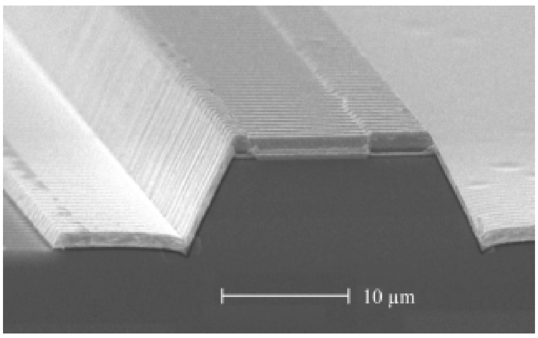

Fig. 8: Image of a fabricated device.

We fabricated distributed feedback quantum cascade lasers in the GaAs/AlGaAs material system, emitting at a wavelength of $\lambda = 10$ µm. The chosen laser design allows a simple fabrication technology without regrowth. The first order grating (grating period Λ =1.6 µm) used for distributed feedback is etched into the surface of the upper cladding layer and covered with gold (Fig. 7 and Fig. 8). A deep etched ridge is used for lateral optical and electrical confinement. Vertical light confinement is achieved by a double plasmon enhanced optical waveguide. The active zone of our QCLs is based on intersubband transitions and consists of 30 periods of injector/active cell.

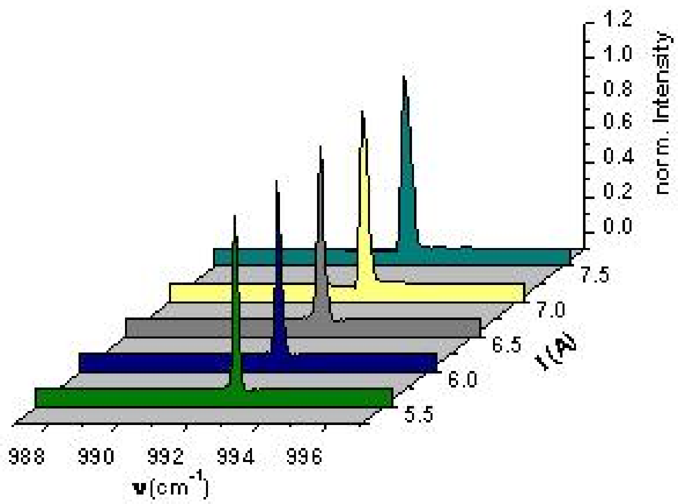

Fig. 9: Normalized emission spectra.

Single mode emission (Fig. 9) is observed with a linewidth smaller than $\Delta\nu = 0.2$ cm^{-1}, limited by the measurement setup. The emission wavenumber can be tuned continuously with the temperature at a rate of $d\nu/dT = 0.048$ cm^{-1}/K. We measured a coupling coefficient of $\kappa = 24$cm^{-1}, which is in good agreement with the numerical calculations based on a rigorous Floquet-Bloch theory.

THz and FIR Spectroscopy

R. Bratschitsch, W. Fischler, R.A. Höpfel, R. Kersting, T. Müller, G. Strasser, J. Ulrich, K. Unterrainer, R. Zobl

Institut für Festkörperelektronik, Technische Universität Wien, Floragasse 7, A-1040 Vienna, Austria

1. Coherent THz emission from optically pumped parabolic quantum wells

(R. Bratschitsch, T. Müller, R. Kersting, G. Strasser, K. Unterrainer)

We present experiments which show that modulation doped parabolic quantum wells (PQWs) emit coherent THz radiation corresponding to the intersubband plasmon when excited by near infrared femtosecond laser pulses. The samples used in the experiments are modulation doped GaAs/AlGaAs PQWs, with widths in the range of 1200 - 2000 Å and carrier sheet densities of 1.7×10^{11} – 5×10^{11} cm^{-2}. We perform THz autocorrelation (AC) measurements using near infrared laser pulses. The Fourier transform of the recorded AC signal gives the spectrum of the coherent THz radiation emitted by the PQW.

Figure 1 shows the spectrum of a modulation doped PQW (W = 1400 Å, n_{2D} = 5×10^{11} cm^{-2}) excited by 780 nm (τ = 80 fs) laser pulses. The density of the optically generated carriers is kept well below the carrier density due to the modulation doping inside the PQW.

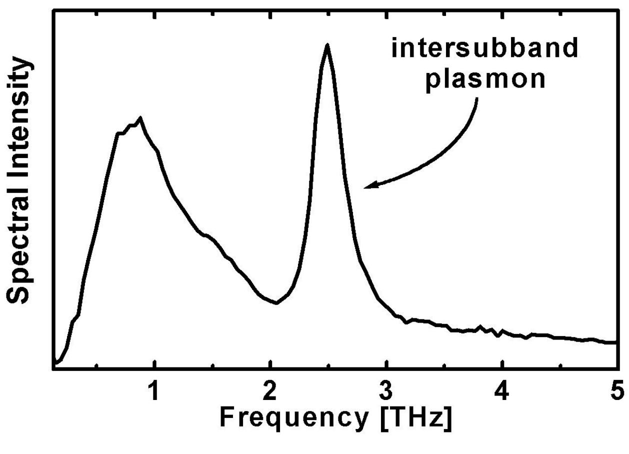

Fig. 1: THz emission of the 1400 Å PQW excited by 780 nm laser pulses (T = 5 K).

The spectrum of the emitted THz radiation consists of two components, a broad one around 0.8 THz due to THz generation at the surface of the sample and a narrow one (FWHM: 0.3 THz) with a center frequency of 2.55 THz. The narrowband emission results from the oscillation of the carriers inside the PQW at the intersubband plasmon frequency. The narrowband PQW emission can be excited within a wide range of excitation wavelengths (815 – 760 nm). The combination of the designability of the transition frequency, the narrowband emission, and the absence of any processing of the sample make modulation doped PQWs attractive and easy-to-use THz emitters.

2. Few-cycle MIR emission from quantum beats

(T. Müller, R. Bratschitsch, G. Strasser, K. Unterrainer)

We report on the emission of few-cycle mid-infrared radiation from coherent charge oscillations in a semiconductor quantum well. We use 10 fs optical pulses to excite two quantized states in an asymmetric step quantum well, which was designed to maximize the optical interband and intersubband matrix elements. The coherent excitation of these states creates a coherent superposition of eigenstates. The polarization associated with the transitions then shows quantum beats due to the different energies of the transitions involved. The spacing of the two quantum states is 140 meV which corresponds to a beat frequency of about 33 THz. Even at room temperature more than 15 cycles of the oscillation can be observed before dephasing. The spectrum of the emitted radiation is obtained by a autocorrelation measurement. Fourier transform of the autocorrelation trace then gives the spectrum, which agrees very well with the results obtained from the numerical solution of the Liouville equation.

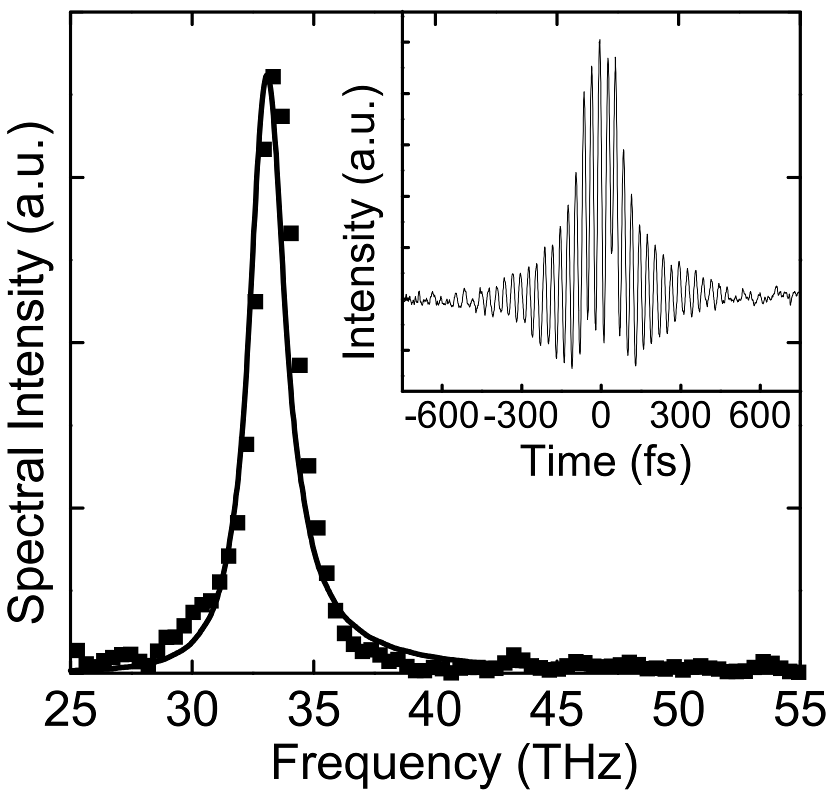

Fig. 2: The figure shows the measured (squares) and the calculated (line) spectrum of the emitted MIR radiation at room temperature. The autocorrelation signal is shown in the inset.

3. THz modulators and varactors

(R. Kersting, R. Bratschitsch, G. Strasser, K. Unterrainer (INTERACT collaboration))

We have shown in previous works that intersubband transitions in semiconductor heterostructures can be used to modulate free propagating THz pulses. However, modulation amplitudes have been low (1 – 5%). The purpose of the work was to design semiconductor heterostructures with increased modulation properties. The new structures have been grown by molecular beam epitaxy. Modulator devices have been fabricated and tested in terms of modulation amplitude and cut-off frequency. In addition, we performed time-resolved THz emission experiments on a varactor similar to that used by the RAL and Lille groups in their mixing experiments. We achieved the time-resolved data by photoexcitation of the varactor with 65 fs laser pulses at a wavelength of 800 nm. The excitation density is about $5x10^{16}$ cm^{-3}. The THz pulse coming from the varactor was time-resolved by mixing the emission with a broadband THz pulse having a bandwidth of about 5 THz. The center frequency of the THz emission from the varactor was about 2.2 THz showing that the upper limit for the mixing technique could be around 2 THz.

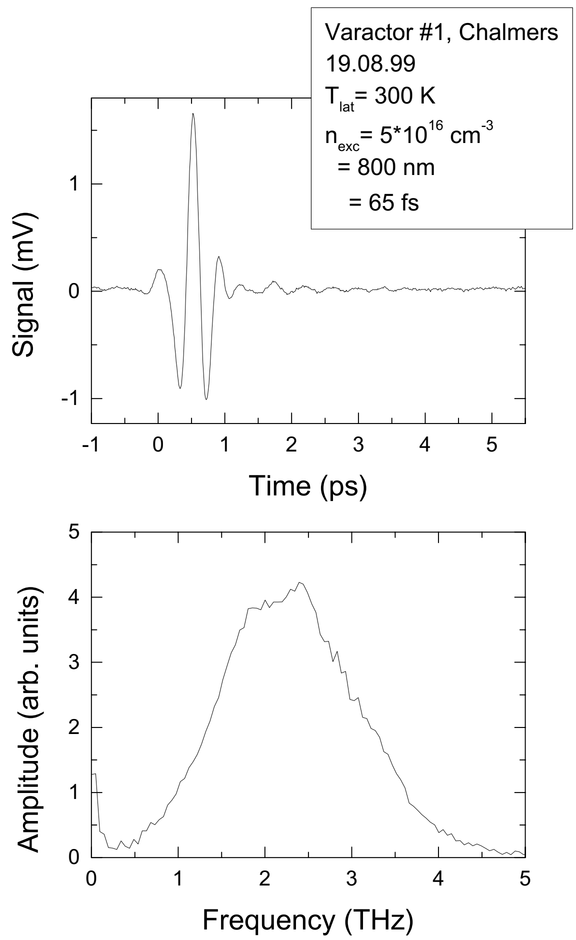

Fig. 3: The figure shows auto correlation and spectrum of the THz emission from a varactor similar to that used by the RAL and Lille groups in their mixing experiments. The varactor is excited with 65 fs laser pulses at a wavelength of 800 nm. The excitation density is about $5x10^{16}$ cm^{-3}.

4. Heavy hole/light hole quantum beats in symmetric and asymmetric double quantum wells

(W. Fischler, R.A. Höpfel, R. Bratschitsch, G. Strasser, K. Unterrainer)

We investigate optically excited quantum beats (QBs) in different GaAs/AlGaAs quantum well structures. The set of samples consists of symmetric double quantum wells (sDQW) and asymmetric double quantum wells (aDQW). Using a conventional pump-probe configuration (femtosecond near infrared pulses) we measure the time evolution of the change in sample reflectivity. Depending on the excitation energy we excite not only the well known QB between the first heavy hole and the first light hole electronic states (hh1/lh1-QB) but also a second one between the second heavy hole and light hole states (hh2/lh2-QB). In the case of an aDQW (Fig. 4(a)), both QBs are energetically separated and have different beat frequencies because of different hh-lh splittings in the wide and the narrow well. The damping times are constant over the energetic window where the QBs can be observed. In contrast, in the case of a sDQW the beat frequencies are nearly the same and the QBs are energetically not separated any more. But surprisingly, the signature of both QBs is revealed in a clear reduction of the measured damping when both oscillations are excited simultaneously. This behavior is interpreted as a consequence of the fact that the coherent polarizations of both QBs have the same sign and, therefore, interfere constructively.

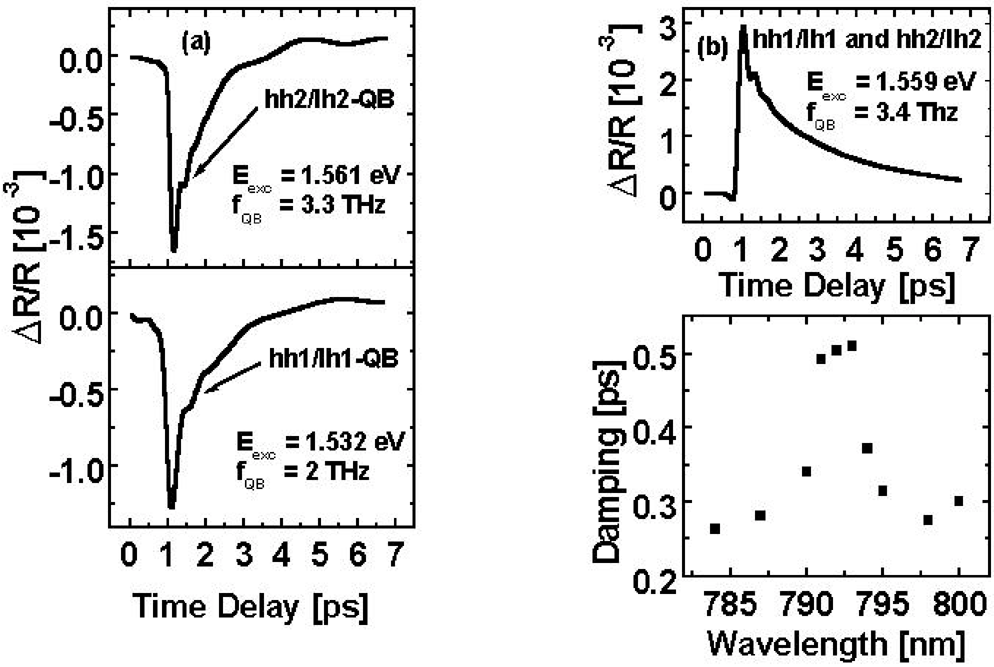

(a) (b)

Fig. 4: (a) aDQW: Reflectivity traces for two different excitation energies; (b) sDQW: Both QBs are simultaneously excited. Bottom: Reduction of damping.

5. Measurement of hot electron temperatures in parabolic quantum wells

(R. Zobl, J. Ulrich, G. Strasser, K. Unterrainer)

The validity of the Kohn theorem in PQWs was verified in a series of electroluminescence experiments (see Kohn). An additional magnetic field B whose axis was tilted at various angles with respect to the sample's growth axis was applied to produce the characteristic mode dispersion $\omega_{\pm}(B)$ of two coupled harmonic oscillators (see Kohn, Fig. 5). In the measured FIR emission spectra the peak positions fully confirm the simple center of mass calculation (in the Heisenberg picture) for the dispersion. The FIR emission intensities $I_d(\omega)$ therefore must follow the simple blackbody law $I_{bb}(\omega, T_e)$ for an ensemble of pure harmonic oscillators radiating at the frequencies ω_+ and ω_-, respectively. Since there are two easy to evaluate, background free emission lines, their absolute intensities together with their intensity ratio uniquely identify the electron temperatures T_e involved. The exact determination of T_e even by the use of an *uncalibrated* detector (i.e. with unknown responsivity V/W) therefore allows for a reasonable estimate about the actual terahertz radiation output of the wells (Fig. 5). At some 100 mW electrical input power electron temperatures exceed 70 K yielding an integral FIR emission in the 10^{-7} W range per cm^2 emissive area.

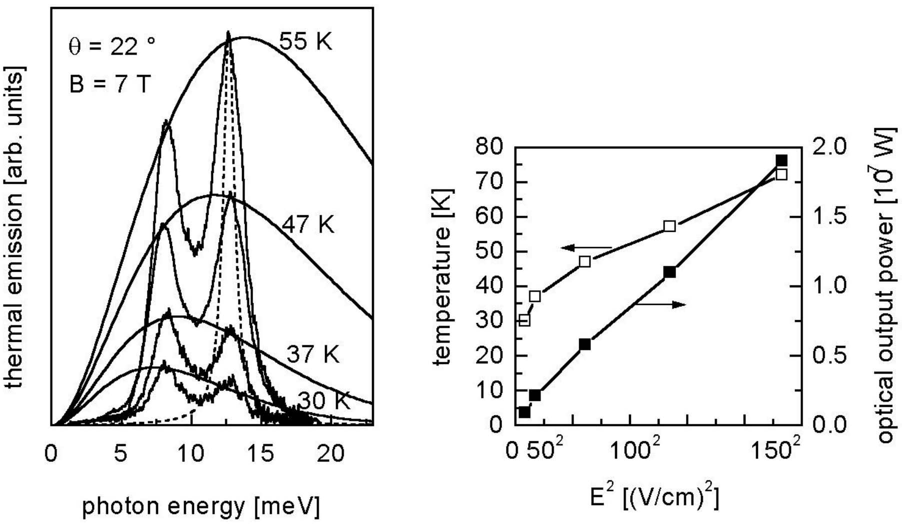

Fig. 5: Extraction of electron temperatures in a PQW: At $\theta = 22°$ magnetic field tilt angle and $B = 7$ T the 'oscillator strengths' $f_{\pm}$ become equivalent with respect to the spatial orientation of the dipole oscillators corresponding to ω_+, ω_-. The measured intensities, integrated over all contributing emission angles, then only differ by their blackbody weight $I_{bb}(\omega_{\pm}, T_e)$.

The left of Fig. 5 shows detected optical intensities $I_d(\omega)$ for an electrical input power of 25 mW, 50 mW, 220 mW, and 510 mW. The dashed line represents a Lorentzian model of the emission lines with their actual FWHM linewidth of 1.1 meV. Planck's radiation law $I_{bb}(\omega, T_e)$ is plotted for the four electron temperatures T_e that satisfy $I_d(\omega_{\pm}) = \alpha I_{bb}(\omega_{\pm}, T_e)$ using a common scaling factor α. The right of Fig. 5 shows electron temperatures and optical output power vs E^2 of electric driving field. No saturation in emission intensity is found.

6. Coherent THz plasmons in GaAs/AlGaAs superlattices

(R. Bratschitsch, R. Kersting, T. Müller, G. Strasser, and K. Unterrainer)

In contrast to the electrons in bulk material, the electrons in a superlattice reside inside a miniband. Depending on the miniband width (which can be designed by the well and barrier widths) the miniband can be filled with electrons to a certain level by doping the superlattice. In our experiments we use four different superlattices, 70 (50, 40, 40) periods of 50 Å (75, 100, 200) wells and 20 Å (20, 25, 25) barriers, with a width of the first electron miniband of 55 meV (26, 10, 2). The superlattices are all n-doped with n = $1x10^{17}$ cm^{-3}. This carrier concentration results in a filling percentage of the first electron miniband of 19% (39, 86, 100) (Fig. 6).

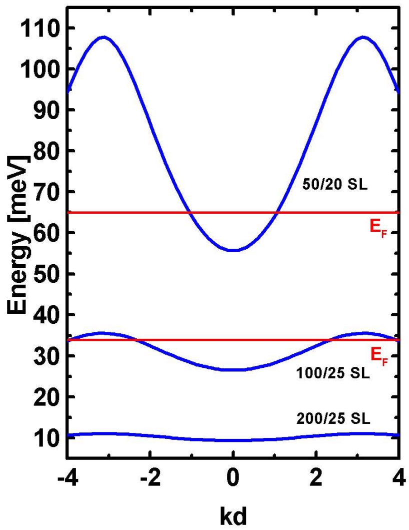

Fig. 6: First electron miniband for the 50/20, 100/25 and 200/25 superlattice. The Fermi energy is denoted by E_F.

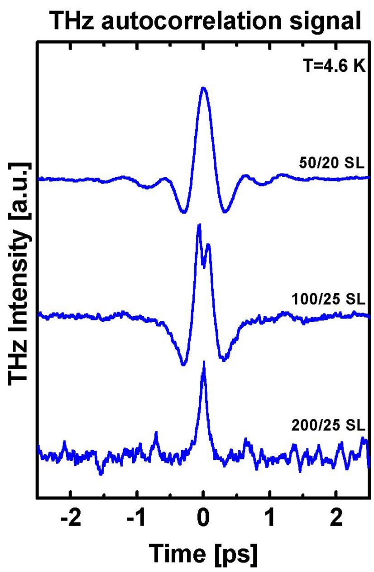

Fig. 7: THz autocorrelation signals of the 50/20, 100/25, and 200/25 superlattices, recorded at T = 4.6 K.

Figure 7 shows the THz autocorrelation function for the three different superlattices recorded at T = 4.6 K. While the autocorrelation signal for the superlattice with the full electron miniband (200/25) shows no oscillation the electrons in the 100/25 superlattice (86% miniband filling) begin to oscillate but this oscillation is strongly damped. For the 50/20 superlattice with a miniband filling of 19%, several oscillations can be seen. The frequency of the oscillations in the 50/20 superlattice is dependent on the optically generated carrier density ($n_{opt} = 1x10^{16} – 1x10^{18}$ cm^{-3}). However, this dependence cannot be explained by a simple plasma frequency formula where the bulk effective mass of the electron is replaced by the effective mass of the electron inside the miniband.

In contrast to the THz emission experiments mentioned above, electrons that are optically generated by a femtosecond laser pulse can also perform plasma oscillations in a previously empty miniband. For this purpose we used the 200/25 superlattice which has a full first electron miniband but an empty second one. If the wavelength of the exciting laser pulses is tuned above the second miniband a strongly damped oscillation of the injected electrons appears.

Thermal saturation of a superlattice can be established if the thermal energy k_BT becomes larger than the miniband width. In this case the miniband becomes uniformly occupied although not full and the conductivity (mobility) decreases drastically. This decrease in mobility should also be seen in the THz oscillations. Two superlattices with a miniband width of 55.4 meV and 26.2 meV were grown and the THz autocorrelation functions were recorded for both samples at T = 4.6 K and 300 K. At low temperature both samples show distinct oscillations because in both cases the thermal energy k_BT is much smaller than the miniband width. At room temperature the superlattice with the wide miniband (Δ = 55.4 meV) still shows the oscillations because k_BT = 26 meV is smaller than the miniband width but the oscillations in the superlattice with the narrow miniband are strongly damped because k_BT is as large as the miniband width.

In summary, we have shown that dopant electrons or optically injected electrons in a superlattice begin to oscillate when excited by femtosecond laser pulses. These plasmons can not only be detected at low temperature but also at T = 300 K. The oscillations can be prevented when the miniband is nearly full or full or when the miniband is thermally saturated.

FIB Technology

E. Bertagnolli, H. Langfischer, A. Lugstein, H.D. Wanzenböck

**Institut für Festkörperelektronik, Technische Universität Wien,
Floragasse 7, A-1040 Vienna, Austria**

1. Focused Ion Beam technology — a new approach for the sub 100nm microfabrication regime

(A. Lugstein, H.D. Wanzenböck, E. Bertagnolli)

1.1 Analytical

Cross-sectioning exposes device structures for direct examination but conventional sample preparation procedures are difficult, time consuming, and grossly destructive. Cross sections formed by focused ion beam (FIB) milling are easier and much faster than the conventional sample preparation process provided by cleaving, polishing, and etching. Using exemplary microelectronic devices, the analytical feasibilities of FIB were exploited revealing an imaging resolution down to 5 nm (Fig. 1).

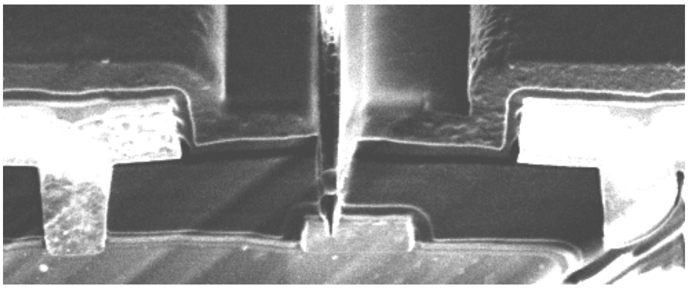

Fig. 1: Cross section of an inhomogeneous channel device.

1.2 Novel QCL-Laser Device

In collaboration with the QCL-Laser group (L. Hvozdara, G. Strasser), a successful modification of GaAs/AlGaAs mid infrared quantum cascade lasers has been demonstrated. By a single step maskless focused ion beam modification a novel monolithic mid infrared quantum cascade laser with self-aligned focused ion beam was generated. This tunable device was named FIB cut coupled cavity laser (FIBC3) and due to its novelty, a patent thereof is already pending.

By the same way a QCL integrated with monolithic one-dimensional photonic bandgap mirrors has been fabricated. The mirrors are composed of two precisely defined grooves trenched across the laser ridge (Fig. 2).

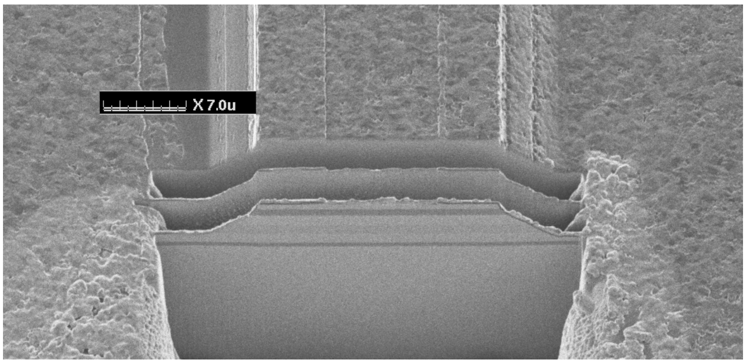

Fig. 2: FIB Image of the QCL with monolithic one dimensional photonic bandgap.

1.3 Inhomogeneous channel devices

In order to overcome the leakage/IDSAT tradeoff of sub-100 nm devices, recent investigations focus on an optimized MOSFET incorporating a sharp sublithographic dopant peak preferably on the source side of the channel. In cooperation with the Simulation Group of Siegfried Selberherr (Institute for Microelectronics, Technical University Vienna), we started the exploration of this device family by using localized ion implantation beams to fabricate laterally tailored doping profiles along the channels. First results show the feasibility of modifying the channel by FIB. Proper post-treatment reduces the defect levels to an insignificant level, thus opening the way to do basic work on these novel devices.

1.4 In situ diagnostic

In order to quantify the solid-beam interaction (charging, heating, defect generation etc.) and the residual damage done by the ion beam impinging the surface, the influence of focused ion beam on device performances will be studied in situ. Therefore the focused ion beam system has been enlarged by a new setup, enabling electrical parameterization of devices during beam exposure.

2. FIB-based tungsten metallization

(H. Langfischer, A. Lugstein, H. D. Wanzenböck, E. Bertagnolli)

Objective of the work is the development of a direct write metallization scheme enabling to contact and to interconnect sub-100 nm devices.

In a first step, the process windows and the fundamental mechanisms of deposition and etch reactions are under investigation. Therefore, pattern transfer, pattern alignment, layer formation, and layer characterization are primary concerns. Patterned W-layers were deposited on thermally grown silicon oxide via local decomposition of adsorbed molecular layers of volatile metal organic tungsten precursor gases (e.g. $W(CO)_6$) by focused Ga^+ ion beams. Primary effects are substrate intermixing and substrate erosion underneath the tungsten line, consuming tens of nanometers of substrate material. The chemical composition of the layers was evaluated by secondary ion mass spectroscopy (SIMS) measurements of as-grown metal pads. In Fig. 3, the SIMS depth profiles of W and C ions and W-Si molecule ions, acting as an indicator for the Si substrate, are depicted showing a homogeneous composition of the deposited metal layer. Approaching the interface, however, a clear pile-up is seen, suggesting atomic mixing with the substrate due to recoil effects.

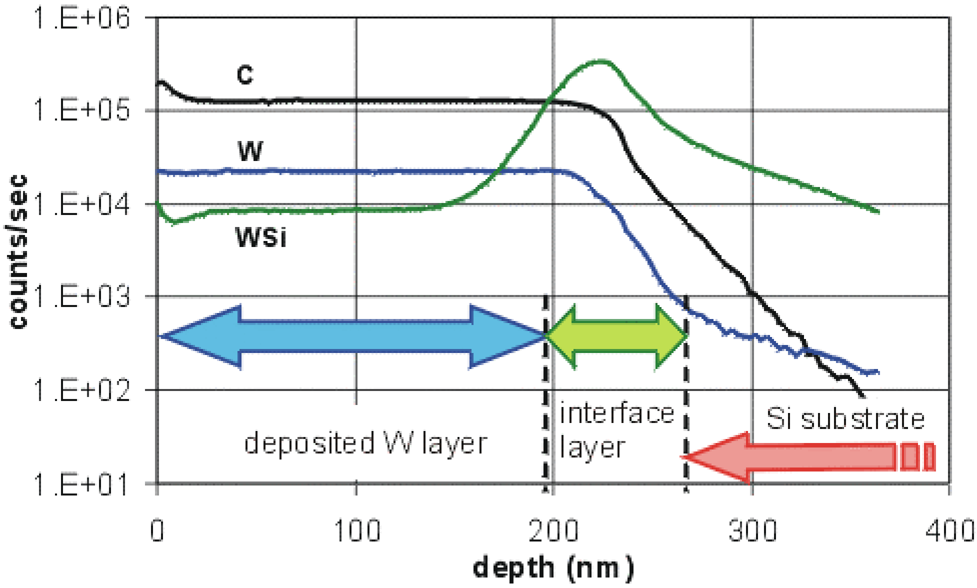

Fig. 3: SIMS depth profile of C, W and WSi. The pile-up in the WSi concentration indicates the atomic mixing at the interface layer.

In order to perform electrical measurements, tungsten squares are connected to Al contact pads (60 x 60 μm^2) in a van der Paw arrangement, allowing electrical probing (Fig. 4).

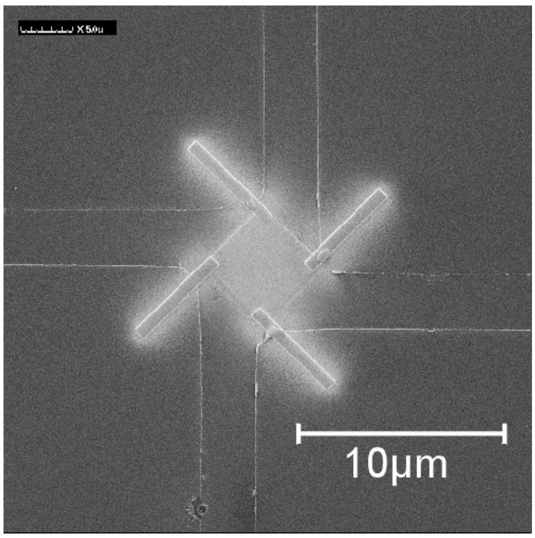

Fig. 4: SEM picture of a FIB tungsten test device.

The electrical and analytical characterization of the FIB induced metallization allowed to corroborate the dependence of the material properties on the variation of the deposition parameters. The sheet resistance of the layers amounts typically to 3 Ohms per square. The resistivity of the metal was calculated to be in a typical range of 200 – 300 μΩcm.

The maximum current densities, indicating the robustness of the material, were estimated to 3.5 10^6 A/cm^2. As expected, the electrical properties of the material were found to correlate with the composition of the tungsten layer, hosting Ga, C, Si and O. Auger spectra of the W-layer on SiO_2 indicated a significant presence of C and Ga and trace levels of Si and O. By balancing the pulse rate of the impinging beam with the adsorption efficiency, the relative Ga contamination of the layers could be drastically reduced.

The obtained results demonstrated that FIB based metal layers of W are a promising choice for local front-end metallization regarding layer homogeneity, sheet resistance, and maximum current density. Most crucial from the point of view of contact metallization is the incorporation of Gallium and the substrate mixing effect due to the high energy of the impinging ions.

Characterization of Microelectronic Devices

C. Fürböck, E. Gornik, M. Litzenberger, D. Pogany

Institut für Festkörperelektronik, Technische Universität Wien, Floragasse 7, A-1040 Vienna, Austria

1. Temperature distribution in Smart Power ESD protection devices

(M. Litzenberger, C. Fürböck, D. Pogany, E.Gornik (in cooperation with Infineon Technologies, Munich, Germany)

The temperature distribution during and after an electrostatic discharge (ESD) has been investigated with ns time- and µm spatial resolution in ESD protection devices that are used in Smart Power integrated circuits for the automobile industry.

In this experiment the devices are stressed with ESD pulses of various current levels resulting in a heating of the device and a consequent change of the refractive index in the silicon (thermooptic effect). The change in the refractive index is measured with a heterodyne interferometric method via the phase shift in an infrared laser beam. The laser beam is directed from the chip backside on the device under investigation. It passes through the Si bulk and the active area of the device, is reflected on the front side metallization, passes back through the device and is focused on a detector, where it interferes with a reference beam that has a slightly different wavelength. From the resulting heterodyne signal the phase shift evolution in the probing laser beam during the ESD pulse is evaluated using a FFT algorithm. For the mapping of the temperature distribution, the active area of the device is automatically scanned with the laser beam, while the device is synchronously stressed with ESD pulses. The phase shift in the laser beam gives a measure for the integral of the refractive index change and therefore for the temperature increase along the laser beam path. To estimate the actual maximum temperature increase in the device, thermal simulations have been used to calculate the temperature distribution in the device along the laser beam path. From these data a correlation between the measured phase shift and the maximum temperature increase was derived.

Figure 1 shows the cross section of the temperature distribution in a vertical npn transistor ESD protection device after stressing with currents from 0.2 A to 1.2 A. It can clearly be seen that the device is active (temperature increase) in the p+ regions of the structure, and inactive (no temperature increase) in the n+ (emitter) region (see inset), indicating that the bipolar transistor is not turned on and the device is operating before snapback. Also a slightly asymmetric shape of the temperature increase with higher values on the cathode side (left in the figure) can be identified. This asymmetry is due to the distributed resistance of the buried layer, resulting in a higher electric field and consequently in a higher current density at the cathode edge side of the device. Figure 2 shows the relation between the maximum temperature increase and the power of the ESD pulse, measured in four different types of ESD protection structures. It can be seen that the maximum temperature increase scales linearly with the pulse power. This is expected as the heat dissipated in the devices is proportional to the power of the stressing pulse, for the short times during the pulses. The results of measurements in many different types of ESD protective structures – in bipolar and also in CMOS technology – show that the method can identify critical parts in the layout and the functionality of the devices, even before they fail. This information is of great value for the device optimization, and this has already led to the improvement of the ESD ruggedness of the protection structures.

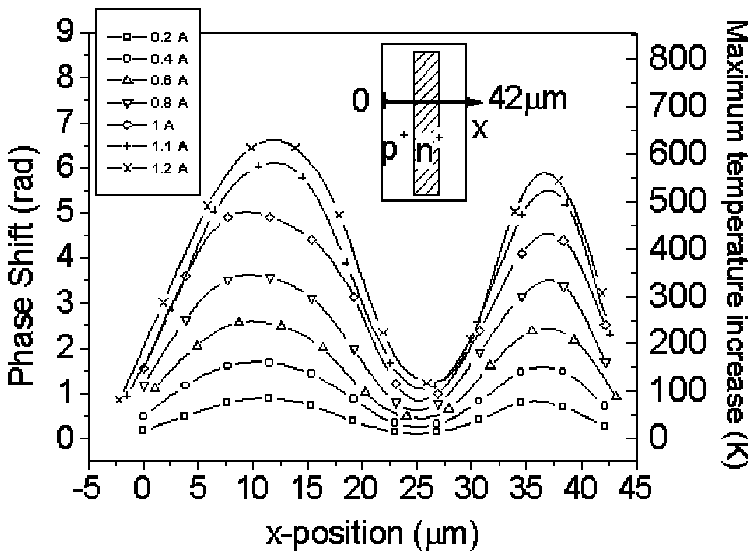

Fig. 1: The distribution of the phase shift and temperature in an ESD protection structure after stressing with an ESD pulse, shown for pulse currents from 0.2 A to 1.2 A. The layout of the structure (top view) and the location of the cross section are shown in the inset.

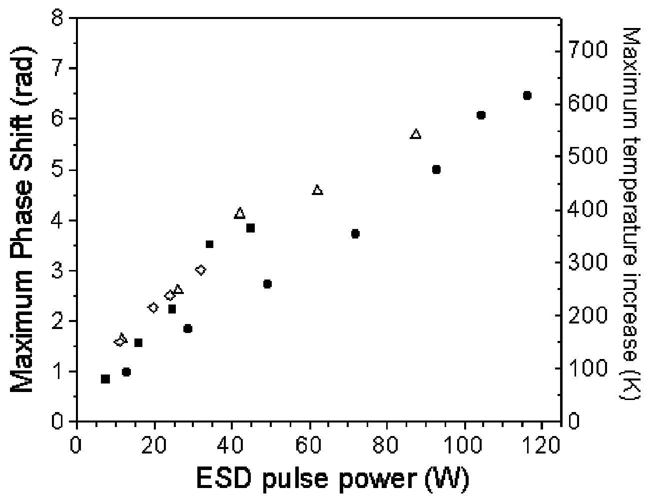

Fig. 2: The maximum phase shift and the maximum temperature increase depending on the ESD pulse power for 4 different device types (different symbols). As expected, the maximum temperature scales linearly with the power dissipation in the ESD protection device.

2. Laser interferometric method for ns-time scale thermal mapping of Smart Power ESD protection devices during ESD stress

(C. Fürböck, M. Litzenberger, D. Pogany, and E. Gornik)

Monitoring of breakdown homogeneity, temperature distribution, and thermal dynamics is of prime interest for the design and development of ESD protection structures. Self-heating effects during an ESD event are known to limit the performance and reliability of ESD protection devices. At our institute we use a laser interferometric thermal mapping technique to monitor the homogeneity of bipolar transistor action and temperature dynamics during ESD stress in ESD protection devices which are operated in the snap-back regime. The measured temperature profiles are compared to a thermal simulation and correlated with the positions of ESD damage obtained by backside IR microscopy. Critical places in the devices are identified under stressing conditions where no irreversible damage occurs which is important from the point of view of reliability evaluation and failure analysis.

The devices presented here are vertical pn diodes and laterally asymmetric npn transistor structures (see inset in Fig. 3). The temperature evaluation is based on monitoring the temperature-induced increase in the refractive index (thermo-optical effect) by measuring the phase changes of a non-absorbed infrared laser beam λ = 1.3 µm) probing the device active region. The extracted phase shift (Fig. 3) is proportional to the integral of the temperature change along the probe beam path. The devices are stressed with 150 ns long current pulses. To estimate the temperature in the device we have simulated the vertical temperature profile in the device.

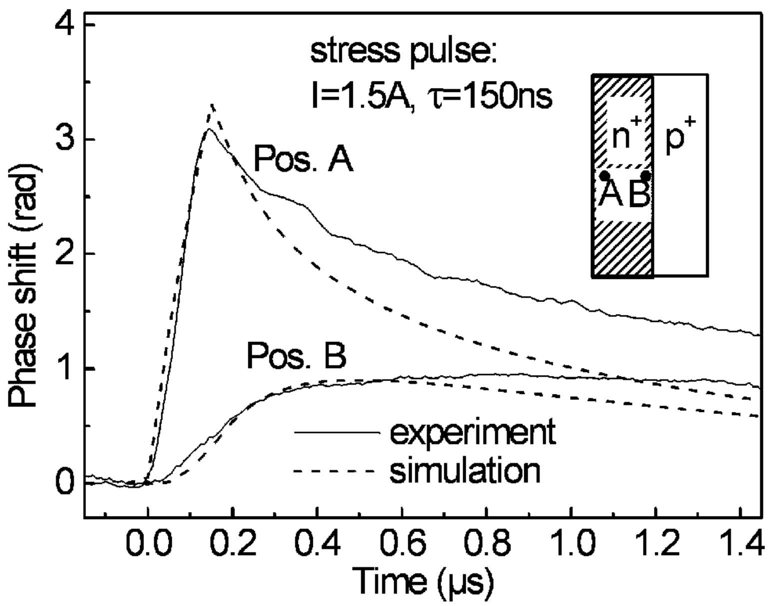

Fig. 3: Measured and simulated phase shift evolution for two positions in the asymmetric structure stressed by 1.5 A pulse of 150 ns duration. The delay in the signal maximum for the position B arises from the heat transfer from the dominant heat source (position A). The simplified layout of the structure is given in the inset.

At the position of the heat source, the phase shift exhibits a steep increase during the pulse and a decrease of the signal after current turn-off due to cooling of the device (Fig. 3, Pos. A). At positions outside the heat source the phase signal shows a delayed and reduced increase, which is caused by heat transfer from the dominant heat source (Pos. B). The simulated phase signal shows quantitative and qualitative agreement with the experiments during and after the ESD pulse, respectively (Fig. 3). At lower stress currents the temperature rise is homogeneous along the device width, whereas at higher current stress two hot spots are developed at the corners of the emitter area. (Fig. 4). These temperature peaks are well correlated with the position of the ESD damage found from infrared microscopy observation (Fig. 5).

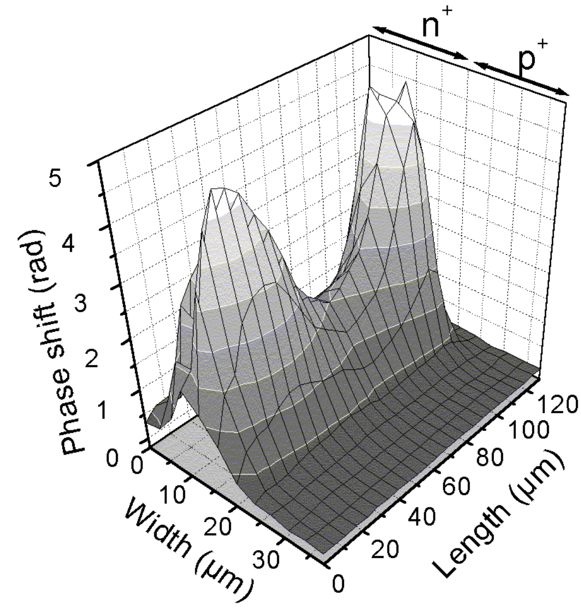

Fig. 4: Spatial distribution of the measured phase shift in an asymmetric structure at the end of a pulse with I = 1.5 A.

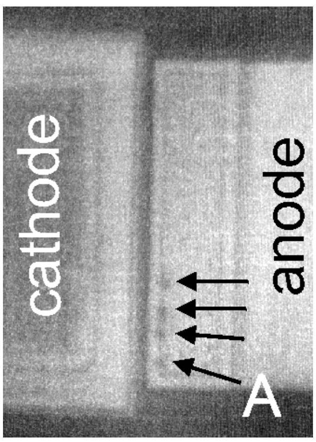

Fig. 5: IR image of the asymmetric structure which has been subjected to 4 ESD pulses of 1.9 A. The dark spots are indicated by arrows. The position of the first dark spot is denoted by 'A'.

Our interferometric thermal mapping technique has shown a strong capability for investigating breakdown homogeneity, temperature distribution, and thermal dynamics in Smart Power ESD protection devices on a ns time scale with high spatial resolution. The increased temperature at the edge and corners of the n+ region of the asymmetric structure explains the position of the ESD damage in this device type. The IR camera observation of the ESD damages has revealed that the critical regions are the edges in asymmetric structure.

This work was performed in collaboration with Infineon Technologies in Villach (Austria) and Munich (Germany).

3. Stress evolution of low frequency (RTS) noise and leakage current in gg-nMOSFET ESD protection devices.

(D. Pogany, M. Litzenberger, C. Fürböck, E. Gornik (in collaboration with INFINEON and Siemens))

Electrostatic discharge (ESD) protection is an important issue for CMOS circuits. From the point of view of design optimization it is important to distinguish between surface and bulk failure modes in these devices. The surface degradation mode, especially the role of hot carriers during the ESD stress, is less studied. On the other hand, analysis of low frequency noise, especially random telegraph signals (RTSs), provides a sensitive tool to study surface related stress-induced damage in Si/SiO_2 systems.

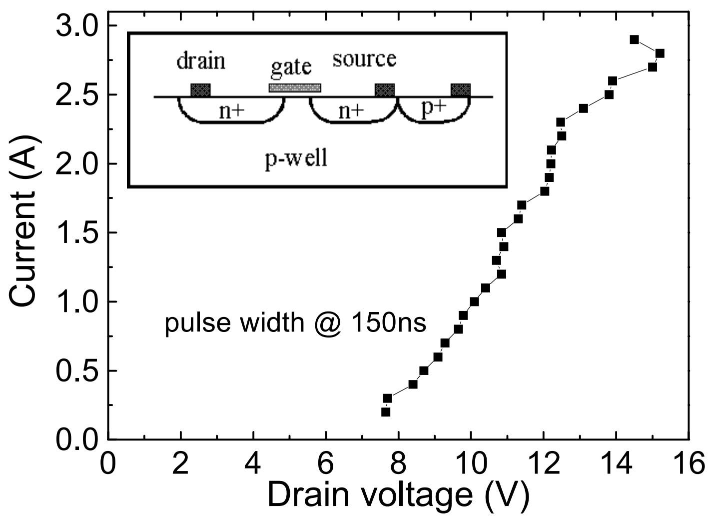

Fig. 6: Typical high current IV curve of an ESD protection device. Inset is the schematics of the structure; contact pads are indicated by black squares.

We have analyzed ESD stress-induced RTS fluctuations and leakage currents in 0.35 μm technology single finger grounded-gate (gg) n-channel MOSFETs with different layout parameters (see Fig. 6). Reverse IV curves and noise are monitored in the 0 – 3 V range after each gradually increased ESD stress pulse magnitude or number.

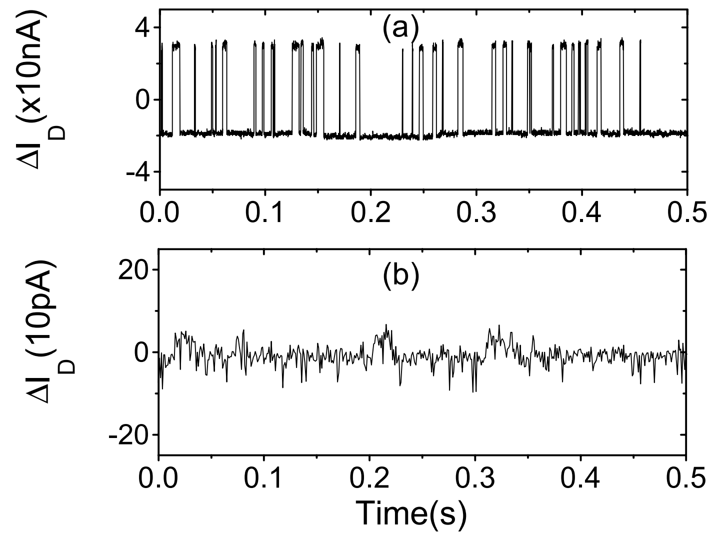

Fig. 7: Current fluctuations related to the strong non-monotone IV evolution (a) and gradual monotone IV behavior (b) in a gg-nMOS device stressed by 1.1 A and 1.6 A ESD pulse, respectively; $V_D = 2.2$ V for both cases.

The results show two different stress evolutions of leakage current and noise which are typical by (i) strong increase in the current and noise and non-monotone evolution of IV characteristics which was attributed to surface (Si/SiO_2 interface) origin of the ESD damage and by (ii) gradual monotone increase in IV characteristics and low noise which was attributed to a bulk ESD damage. The analysis of the ESD damage by the OBIC (Optical Beam Induced Current) technique supports the results of the electrical measurements.

4. Study of Random Telegraph Signal (RTS) noise in Smart Power DMOS devices

(D. Pogany and E. Gornik (in collaboration with INFINEON Technologies, Munich))

Double-diffused metal-oxide-semiconductor (DMOS) field effect transistors fabricated by smart power technology are widely used in the automotive industry as power switches. Structural or technology defects in power devices can cause a decrease in the breakdown voltage or an increase in the leakage current. It is important to identify possible sources of these defects in the early stage of technology development as they can have an impact on device reliability and lifetime. It has been shown in many studies that the leakage currents are often accompanied with the existence of excess low frequency noise. The $1/f$ or Random Telegraph Signal (RTS) noises are known as very sensitive indicators of device reliability and material quality.

We have studied low frequency current fluctuations in power multi-cell power DMOS devices in order to obtain information on the leakage current-related defects. We have established that an excess leakage current is always accompanied by an excess low frequency noise which has a form of RTS fluctuations or $1/f$ noise. The relative RTS amplitude $\Delta I_D/I_D$ as a function of I_D exhibits first a plateau followed by a roll-off having an $I_D^{-\alpha}$ dependence with $0.5 < \alpha < 1$. The typical relative RTS amplitude values at the plateau are close to 1%, but RTS fluctuations with the relative amplitude as high as 20% have also been found (see Fig. 8). The RTS noise in the frequency domain (0.1 Hz – 10 kHz range) gives rise to a Lorentzian spectrum superimposed on a $1/f$ noise background which indicates that the dominant RTS noise is governed by a Poisson process (Fig. 9). As going to higher gate biases ($V_G > 1.6$ V, inversion), the noise is dominated by a $1/f$ spectrum in any device.

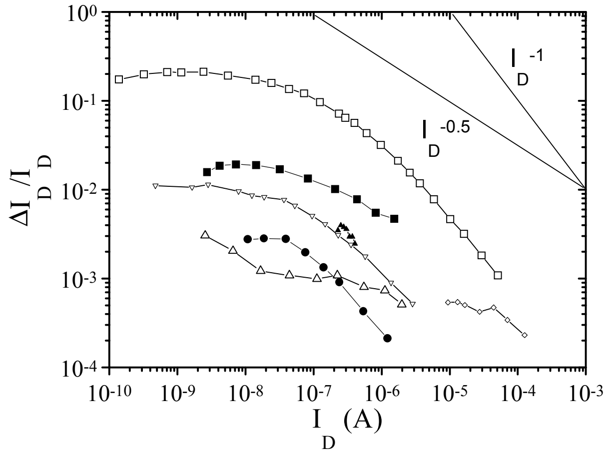

Fig. 8: Relative RTS amplitude $\Delta I_D/I_D$ as a function of I_D for seven different devices with and without the excess leakage current at $V_G = 0$. Two different slopes in the $\Delta I_D/I_D$–I_D dependence are indicated by solid lines.

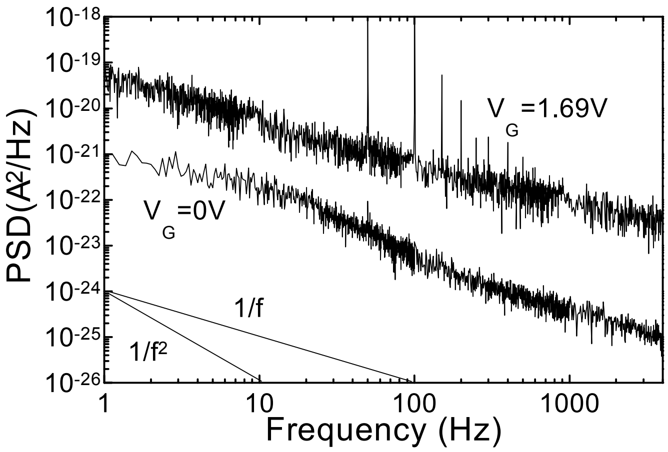

Fig. 9: Frequency dependence of power spectral density (PSD) at two different gate biases of a DMOS exhibiting RTS noise. Note the curve at V_G=1.69V is typical also for defect-free devices.

The results indicate that the basic noise mechanism in these multicell devices is similar to the noise mechanism observed in submicron MOSFETs (carrier trapping/detrapping at or near Si/SiO_2 interface under the gate oxide). For simplicity, the DMOS structure is considered as a parallel connection of submicron MOSFETs. Each of these MOSFETs exhibits RTS (or *1/f*) fluctuations which, in superposition, give rise to *1/f* noise in the inversion. The observation of the single RTS fluctuators in the devices with the excess current indicates that the leakage current and noise comes from one single or a small number of cells. The leakage current is supposed to be due to an extended defect located in the device active area. The structural analysis has revealed crystal damage in the body/drain and body/source region, which confirms the conclusion driven from the noise study.

5. Damage analysis in Smart Power technology ESD protection devices

(D. Pogany, M. Litzenberger, E. Gornik (in collaboration with INFINEON and Siemens))

Electrostatic discharge (ESD) protection devices are of great importance in smart-power technology circuits used in the automotive industry. Temperature rise during the ESD stress may induce fatal device failure due to thermal instability during the second breakdown. Analysis of the ESD damage is therefore an important issue for the design optimization of these devices. We have studied damage caused by ESD stress in Smart Power technology ESD protection devices using backside IR microscopy and IV characterization.

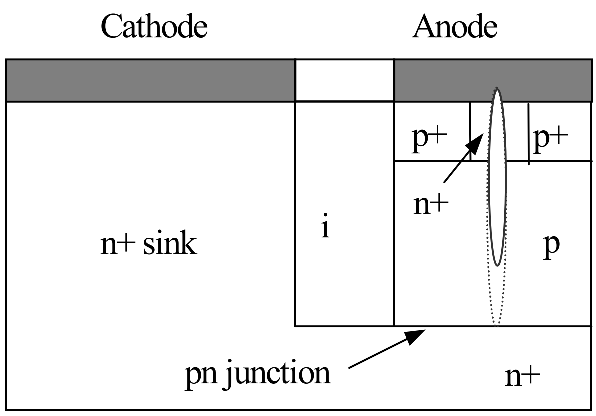

Fig. 10: Schematics cross section of a symmetric ESD protection device. The model of the damaged region is also shown: solid and dotted ellipses indicate defects outside and inside the zero bias space charge region.

Devices used in this study are vertical pn diodes and laterally symmetric and asymmetric npn transistor structures with a breakdown voltage near 60 V (see Fig. 10). The ESD damage, seen in the infrared camera as a dark spot (DS), is caused by the local thermal degradation of the Si/(contact metallization) interface due to current filamentation. In general, the successive stress causes either (i) a creation of a new DS usually accompanied with a kink in IV characteristics (new leakage path) or (ii) an increase in dimension of an already existing DS connected with a shift of the kink to lower voltages. We have also established that the increase in the reverse leakage current at low biases is always accompanied with the increase in the forward leakage current at low forward biases (Fig. 11). If the reverse current increase is observed at higher voltages, the forward current is unaffected.

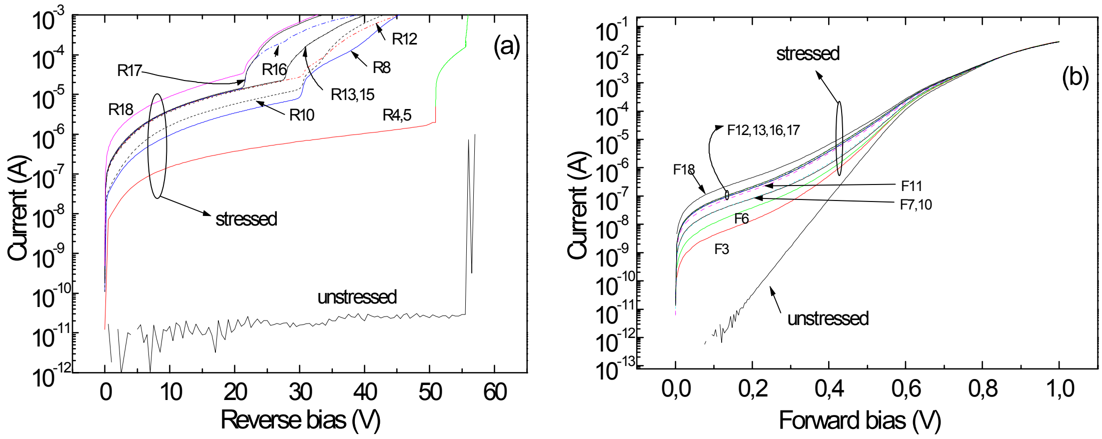

Fig. 11: Development of reverse (a) and forward bias (b) IV curves as a function of increasing stress pulse number (3 A) in an asymmetric structure exhibiting two DSs in the n+ emitter region. The same number in the numbering of the curves in (a) and (b) corresponds to the same stress level. The reverse leakage current components at V_R < 20 V and V_R > 20 V (kinks) correspond to stress evolution of either DSs. Note that the increase in the reverse current at low voltages, but not the kink component, is correlated with the increase in the forward bias leakage.

From the experiments we assume that the DS region is formed by a high density of g-r centers, probably due to diffusion of impurities from the contact metal. The progressive decrease in the kink voltage observed in the reverse IV curves is interpreted as a stress-induced penetration of the defect region through the reverse bias space charge region. The penetration of the damage into the zero-bias space charge region causes an increase in the forward current where the defects act as recombination centers. From the simulation we have estimated that the forward current increase starts to be observable when the damage penetrates 4.7 µm from the surface.

Microelectronics Technology — Cleanroom Linz

Microstructure Research: Cleanroom Linz

G. Bauer, H. Heinrich, H. Thim, G. Brunthaler

Institut für Halbleiter- und Festkörperphysik, and Institut für Mikroelektronik, Johannes Kepler Universität Linz, A-4040 Linz, Austria

The GMe supports the microstructure research in the cleanrooms of the Institut für Halbleiter- und Festkörperphysik and of the Institut für Mikroelektronik in Linz. In the field of high-frequency devices a fast frequency counter at 35 GHz for a distance sensor device was realized in 1999, capable of measuring the frequency with a 20 bit resolution in 120 microseconds. In the field of Si/SiGe devices, the activities were concentrated on the deposition of Si/SiGeC heterobipolar transistors on preprocessed wafers provided by an Austrian industrial partner. The structuring activities were concentrated on nanometer length Schottky gates. The optoelectronic activities were pursued for Er-doped Si diodes for light generation and by realizing vertical cavity surface emitting lasers for the 4 to 6 µm wavelength range. Magnetic structures were realized by depositing Fe on GaAs and ZnSe, and steps towards an in-situ optical process control for molecular beam epitaxial growth involving reflection difference spectroscopy were made. Semiconductor nanostructures like wires and dots, fabricated by self-assembled growth were investigated with respect to their elastic and optical properties.

The funding of the activities in the two cleanrooms at the University of Linz which are jointly used by three groups is of vital importance for our microstructure research activities. This basic funding allows for investigations which are made possible through additional funding coming from the FWF, FFF, the OeNB, as well as through cooperation with industrial groups as listed below.

In the following short presentations an overview is given on the achievements made in the cleanrooms in Linz in 1999. The basic equipment which is available in these clean rooms allows for MBE growth of Si-based heterostructures, of II-VI and IV-VI heterostructures, for the deposition of ferromagnetic layers like Fe on II-VI as well as III-V compounds, as well as for MOCVD growth of III-V compounds like GaAs/GaAlAs and GaAs/GaInAs. Apart from *in-situ* and *ex-situ* structural characterization, lateral patterning is made possible through equipment like optical, holographic, and electron beam lithography. Processing includes also facilities for the deposition on insulating as well as contact layers. In this respect, a major investment has been made: Equipment for the deposition of oxide and nitride layers has been purchased for the clean room of the semiconductor physics building which will be installed in 2000. Furthermore, through funds made available by the Ministry of Science and Traffic a transmission electron microscope has been ordered which will also be installed in the year 2000. This will greatly enhance our analytical possibilities for device oriented work.

Consequently, studies related to high frequency electronic and to optoelectronic devices can be performed which are described in the following.

For the section on HF-systems, a fast frequency counter at operating at 35 GHz, applied to a microwave distance sensor for short-range applications was realized. The main feature of this device is its capability to measure frequencies with a 20 bit resolution. It allows for system linearization of the oscillator characteristics.

Si-SiGe heterobipolar transistors are now widely introduced in the production for high speed bipolar and BiCMOS circuits, offering a speed advantage without sacrificing the compatibility to standard Si technologies. In Linz steps towards the optimization of the doping and composition profiles for the SiGeC HBT technology were made in a collaboration with Austria Microsystems (AMS), Unterpremstätten. Processed wafers provided by AMS were overgrown in Linz, and the essential conditions for the optimization of the layer sequence were studied.

In the field of lateral nanostructuring of Si/SiGe, work has been performed on selective Si and Si/SiGe epitaxy employing shadow masks. In particular, the lateral boundary between crystalline and polycrystalline Si areas was studied. It was shown that a defined undercut can be created thermally in a simple SiO_2 mask. This has led to the controlled deposition of Si/SiGe wire structures, which show excellent material quality as evidenced by their structural as well as by their optical (luminescence) properties.

Furthermore, work on growth instabilities found in Si homoepitaxy was pursued, extending the investigations to Si/SiGe in order to find out which role is played by the lattice strain due to the mismatch. In this respect, also studies were made towards a better understanding of the surface undulations which occur in lattice mismatched heteroepitaxy. The lateral and vertical ordering of self-organized structures has been studied in detail and the role of the anisotropy of the elastic properties for this ordering has been established quantitatively.

In the section on optoelectronics several contributions are incorporated into this report: The studies on electroluminescence from Si diodes by using Er doping were pursued, and in particular a mid-infrared vertical cavity surface emitting laser was realized, which has found international esteem. Work on reflectance difference spectroscopy was performed in order to allow for a real-time in-situ growth control in MBE as well as in MOCVD systems. In the framework of a European project, this system will be adapted for the process control of GaN in cooperation with partners from industry and from several universities.

Studies aimed towards the rapidly developing field of spintronics are being done: So far, growth studies have been performed by depositing Fe on GaAs and ZnSe, and by investigating the optical response of heterostructures containing manganese.

Project Information for 1999

Project Manager

Doz. Dr. Gerhard BRUNTHALER

Institut für Halbleiter- und Festkörperphysik, Johannes Kepler Universität Linz, A-4040 Linz, Austria

Project Group

Last Name	First Name	Status	Remarks
Bauer	Günther	University professor	
Heinrich	Helmuth	University professor	
Thim	Hartwig	University professor	
Schäffler	Friedrich	University professor	
Jantsch	Wolfgang	University professor	
Brunthaler	Gerhard	Associate professor	
Diskus	Christian	Associate professor	
Krenn	Heinz	Associate professor	
Palmetshofer	Leopold	Associate professor	
Springholz	Gunther	Associate professor	
Sitter	Helmut	Associate professor	
Heiss	Wolfgang	Assistant professor	
Kolmhofer	E.	Assistant professor	
Lübke	Kurt	Assistant professor	
Binder	Fritz	Technician	
Fuchs	Othmar	Technician	
Hinterreiter	Marion	Technician	
Kainz	Ursula	Technician	
Katzenmayer	Hans	Technician	
Rabeder	Klaus	Technician	
Wirtl	Elisabeth	Technician	
Stepikhova	Margarita	Guest	
Bierleutgeb	Karin	Ph.D. student	
Bonanni	Alberta	Ph.D. student	
Daniel	Anke	Ph.D. student	
Kocher	Gudrun	Ph.D. student	

Last Name	First Name	Status	Remarks
Montaigne-R.	Alberto	Ph.D. student	
Mühlberger	Michael	Ph.D. student	
Pinczolits	Michael	Ph.D. student	
Prechtl	Gerhard	Ph.D. student	
Raab	Anneliese	Ph.D. student	
Roch	Tomas	Ph.D. student	
Sandersfeld	Nils	Ph.D. student	
Schelling	Christoph	Ph.D. student	
Schwarzl	Thomas	Ph.D. student	
Seyringer	Heinz	Ph.D. student	
Stangl	Julian	Ph.D. student	
Wiesauer	Karin	Ph.D. student	
Zhuang	Yan	Ph.D. student	
Grillberger	C.	Diploma student	
Landsiedl	M.	Diploma student	
Lengauer	G.	Diploma student	
Raiser	S.	Diploma student	
Schraml	S.	Diploma student	

Publications in Reviewed Journals

1. M. Helm, W. Hilber, G. Strasser, R. De Meester, F.M. Peeters, A. Wacker: "*Continuum Wannier-Stark ladders strongly coupled by Zener resonances in semiconductor superlattices*", Physical Review Letters **82** , 3120-3123 (1999).
2. A. Prinz, G. Brunthaler, Y. Ueta, G. Springholz, G. Bauer, G. Grabecki, T. Dietl: "*Electron localization in n-Pb $_{1-x}$ Eu$_x$Te*", Physical Review B **59**, 12983-12990 (1999).
3. M. Pinczolits, G. Springholz, G. Bauer: "*Molecular beam epitaxy of highly faceted self-assembled IV-VI quantum dots with bimodal size distribution*", Journal of Crystal Growth **201/202**, 1126-1130 (1999).
4. G. Springholz, T. Schwarzl, W. Heiss, H. Seyringer, S. Lanzerstofer, H. Krenn: "*MBE growth of highly efficient lead salt-based Bragg mirrors on BaF$_2$ (111) for the 4 – 6 µm wavelength region*", Journal of Crystal Growth **201/202**, 999 -1004 (1999).
5. V. Holy, J. Stangl, S. Zerlauth, G. Bauer, N. Darowski, D. Lübbert, U. Pietsch: "*Lateral arrangement of self-assembled quantum dots in an SiGe/Se superlattice*", Journal of Physics D (Applied Physics) **32**, A234-A238 (1999).
6. J. Grim, V. Holy, J. Kubena, J. Stangl, A.A. Darhuber, S. Zerlauth, F. Schäffler, G. Bauer: "*Diffuse x-ray reflectivity of strain-compensated Si/SiGe/SiC multilayers*", Journal of Physics D (Applied Physics) **32**, A216-A219 (1999).

7. J. Grim, V. Holy, J. Kubena, A.A.Darhuber, G. Bauer, S. Zerlauth: "*X-ray reflection from self-organized interfaces in a SiGe/Si multilayer*", Semiconductor Science and Technology **14**, 32-40 (1999).

8. V. Holy, G. Springholz, M. Pinczolits, G. Bauer: "*Strain induced vertical and lateral correlations in quantum dot superlattices*", Physical Review Letters **83**, 356-359 (1999).

9. K. Herz, G. Bacher, A. Forchel, H. Straub, G. Brunthaler, W. Faschinger, G. Bauer, C. Vieu: "*Recombination dynamics in dry-etched (Cd,Zn)Se/ZnSe nanostructures: Influence of exciton localization*", Physical Review B **59**, 2888-2893 (1999).

10. O. Gauthier-Lafaye, F.H. Julien, S. Cabaret, J.-M. Lourtioz, G. Strasser, E. Gornik, M. Helm, P. Bois: "*High-power GaAs/AlGaAs quantum fountain unipolar laser emitting at 14.5 µm with 2.5% tunability*", Applied Physics Letters **74**, 1537-1539 (1999).

11. Y. Zhuang, V. Holy, J. Stangl, A.A. Darhuber, P. Mikulik, S. Zerlauth, F. Schäffler, G. Bauer, N. Darowski, D. Lübbert, U. Pietsch: "*Strain relaxation in periodic arrays of Si/SiGe quantum wires determined by coplanar high resolution x-ray diffraction and grazing incidence diffraction*", Journal of Physics D (Applied Physics) **32**, A224-A229 (1999).

12. J. Stangl, V. Holy, P. Mikulik, G. Bauer, I. Kegel, T.H. Metzger, O.G. Schmidt, C. Lange, K. Eberl: "*Self-assembled carbon-induced germanium quantum dots studied by grazing-incidence small-angle x-ray scattering*", Applied Physics Letters **74**, 3785-3787 (1999).

13. Y. Zhuang, J. Stangl, A.A. Darhuber, G. Bauer, P. Mikulik, V. Holy, N. Darowski, U. Pietsch: "*X-ray diffraction from quantum wires and quantum dots*", Journal of Materials Science: Materials in Electronics **10**, 215-221 (1999).

14. F. Schinagl, A. Bonanni, S. Holl, G. Prechtl, H. Krenn: "*Magnetic polarons in MnTe layers*", Journal of Magnetism and Magnetic Materials **198-199**, 194-196 (1999).

15. T. Schwarzl, W. Heiss, G. Kocher-Oberlehner, G. Springholz: "*CH_4/H_2 plasma etching of IV-VI semiconductor nanostructures*", Semiconductor Science and Technology **14**, L11-L14 (1999).

16. Stangl, V. Holy, A.A. Darhuber, P. Mikulik, G. Bauer, J. Zhu, K. Brunner, G. Abstreiter: "*High-resolution x-ray diffraction on self-organized step bunches of $Si_{1-x}Ge_x$ grown on (113)-oriented Si*", Journal of Physics D (Applied Physics) **32**, A71-A74 (1999).

17. C. Schelling, G. Springholz, F. Schäffler: "*Kinetic Growth Instabilities on Vicinal Si (001) Surfaces*", Physical Review Letters **83**, 995-998 (1999).

18. M. Pinczolits, G. Springholz, G. Bauer: "*Evolution of hexagonal lateral ordering in strain-symmetrized PbSe/PbEuTe quantum-dot superlattices*", Physical Review B **60**, 11524-11529 (1999).

19. G. Grabecki, J. Wrobel, T. Dietl, K. Byczuk, E. Papis, E. Kaminska, A. Piotrowska, G. Springholz, M. Pinczolits, G. Bauer: "*Quantum ballistic transport in constrictions of n-PbTe*", Physical Review B **60**, R5133-R5136 (1999).

20. T. Schwarzl, W. Heiss, G. Springholz: "*Ultra-high-finesse IV-VI microcavities for the midinfrared*", Applied Physics Letters **75**, 1246-1248 (1999).

21. M. Helm: "*The basic physics of intersubband transitions*", *in*: "Intersuband Transitions in Quantumwells: Physics and device applications", Semiconductors and Semimetals Vol. **62**, eds. H.C. Liu and F. Capasso (Academic Press 1999), p. 1-99.

22. M. Helm: "*Infrared Semiconductor Sources*", in: "Long-wavelength infrared emitters based on quantum wells and superlattices", ed.: M. Helm (Gordon and Breach 1999) p.1.

23. W. Heiss, G. Prechtl, D. Stifter, H. Sitter, G. Springholz, T. Riemann, F. Bertram, D. Rudloff, J. Christen, G. Bley, U. Neukirch, J. Gutowski, J. Liu: "*Luminescence of ZnCdSe/ZnSe ridge quantum wires*", Applied Physics Letters **75**, 974-976 (1999).

24. A. Bonanni, G. Prechtl, W. Heiss, F. Schinagl, S. Holl, H. Krenn, H. Sitter, D. Stifter, K. Hingerl: "*Reflectance difference spectroscopy and magneto-optical analysis of digital magnetic heterostructures*", Journal of Vacuum Science Technology B **17**, 1722-1727 (1999).

25. M. Berti, D. De Salvador, A. V. Drigo, J. Stangl, F. Schäffler, S. Zerlauth, G. Bauer: "*Behaviour of metastable $Si_{1-y}C_y$ epilayers under 2MeV Alpha particles irradiation*", *in*: Lattice Mismatched Thin Films, ed. by E.A. Fitzgerald (The Minerals, Metals & Materials-Society 1999) p. 53-59.

26. M. Helm, W. Hilber, G. Strasser, R. DeMeester, F.M. Peeters: "*Minibands and Wannier-Stark ladders in semiconductor superlattices studied by infrared spectroscopy*", Brazilian Journal of Physics **29**, 652 (1999).

27. G. Strasser, L. Hvozdara, S. Gianordoli, K. Unterrainer, E. Gornik, P. Kruck, M. Helm: "*GaAs/AlGaAs quantum cascade intersubband and interminiband emitter*", Journal of Crystal Growth **201-202**, 919 (1999).

28. T. Schwarzl, G. Springholz, H. Seyringer, H. Krenn, S. Lanzerstorfer, W. Heiss: "*High-reflectivity lead-salt-based Bragg mirrors for the mid-infrared range*", IEEE Journal of Quantum Electronics **35**, 1753-1758 (1999).

29. G. Strasser, S. Gianordoli, L. Hvozdara, K. Unterrainer, E. Gronik, P. Kruck, M. Helm: "*GaAs/AlGaAs quantum cascade intersubband emitter*", Proc. 24th International Conf. on the Physics of Semiconductors, World Scientific 1999.

30. M. Schatzmayr, E. Wachmann, M. Mühlberger, C. Schelling, and F. Schäffler: "*A fully certified SiGe-BiCMOS process for ASICs and multiproduct wafers*", Proc. Int. Semicond. Dev. Res. Symp., Charlottesville, VA, Dec. 1999.

31. M. Helm, W. Hilber, G. Strasser, R. De Meester, F.M. Peeters, A. Wacker: "*Simultaneous investigation of vertical transport and intersubband absorption in a superlattice: Continuum Wannier-Stark ladders and next-nearest neighbor tunneling*", Physica B **272**, 194-197 (1999).

32. G. Springholz: *"Observation of large-scale surface undulations due to inhomogenous dislocation strain fields in lattice-mismatched epitaxial layers"*, Applied Physics Letters **75**, 3099-3102 (1999).

33. G. Springholz, T. Schwarzl, W. Heiss, H. Seyringer, S. Lanzerstorfer, H. Krenn: "*MBE growth of highly efficient lead-salt-based Bragg mirrors on (111) BaF_2 for the 4-6 µm wavelength region*", J. Cryst. Growth **201-202**, 999-1004 (1999).

34. W. Heiss, G. Prechtl, D. Stifter, G. Springholz, L. Toth: "*ZnCdSe/ZnSe quantum wires fabricated by selective molecular beam epitaxy on prepatterned GaAs substrates"*, *in:* "Current Developments of Microelectronics", ed. K. Riedling (Gesellschaft für Mikroelektronik, Wien 1999) p. 97.

35. K. Wiesauer, G. Springholz: "*Fabrication of semiconductor nanostructures by Scanning Force Microscopy"*, *in:* "Current Developments of Microelectronics", ed. K. Riedling (Gesellschaft für Mikroelektronik, Wien 1999) p. 171.

36. G. Springholz, T. Schwarzl, W. Heiss, H. Seyringer, S. Lanzerstorfer, H. Krenn: "*Fabrication of highly efficient mid-infrared Bragg mirrors from IV-VI semiconductors"*, *in:* "Current Developments of Microelectronics", ed. K. Riedling (Gesellschaft für Mikroelektronik, Wien 1999) p. 71.

37. T. Schwarzl, W. Heiss, G. Kocher-Oberlehner, G. Springholz: "CH_4/H_2 Plasma Etching of IV-VI Semiconductors", *in:* "Current Developments of Microelectronics", ed. K. Riedling (Gesellschaft für Mikroelektronik, Wien 1999) p. 197.

38. M. Mühlberger, F. Schäffler: "*Carbon Co-Doping of $Si_{1-x}Ge_x$:B Layers: Suppression of Transient Enhanced Diffusion*", *in:* "Current Developments of Microelectronics", ed. K. Riedling (Gesellschaft für Mikroelektronik, Wien 1999) p. 167.

39. H. Seyringer, B. Fünfstück, F. Schäffler: "*Electron Beam Lithography of Nanostructures*", *in:* "Current Developments of Microelectronics", ed. K. Riedling (Gesellschaft für Mikroelektronik, Wien 1999) p. 201.

40. N. Sandersfeld, H. Seyringer, G. Steinbacher, L. Palmetshofer, , S. Zerlauth, F. Schäffler: "*Modulation Doped Si/$Si_{1-x}Ge_x$-Field-Effect Transistors*", *in:* "Current Developments of Microelectronics", ed. K. Riedling (Gesellschaft für Mikroelektronik, Wien 1999) p. 189.

41. C. Schelling, G. Springholz, F. Schäffler: "*Growth Instabilities in Si Homoepitaxy*", *in:* "Current Developments of Microelectronics", ed. K. Riedling (Gesellschaft für Mikroelektronik, Wien 1999) p. 193.

42. J. Stangl, Y. Zhuang, G. Bauer, C. Rosenblad, H. von Känel: "*Fast Growth Method for the Fabrication of Modulation Doped Si/SiGe Field Effect Transistors*", *in:* "Current Developments of Microelectronics", ed. K. Riedling (Gesellschaft für Mikroelektronik, Wien 1999) p. 207.

43. Y. Zhuang, P. Mikulik, V. Holy, G. Bauer, R. Hammond, T.E. Whall, E.H.C. Parker: "*Si/SiGe Layers on Patterned Substrates for MODFET Applications*", *in:* "Current Developments of Microelectronics", ed. K. Riedling (Gesellschaft für Mikroelektronik, Wien 1999) p. 213.

44. C. Rosenblad, T. Graf, J. Stangl, C. Penn,, G. Bauer, and H. von Känel: "*SiGe heteropeitaxy at high growth rates by a new plasma enhanced CVD process*", Proceedings of the 24th International Conference on the Physics of Semiconductors, ed. D. Gershoni (World Scientific, Singapore 1999).

45. G. Grabecki, J. Wrobel, T. Dietl, K. Byczuk, E. Papis, E. Kaminska, A. Piotrowska, G. Springholz and , G. Bauer: "*Ballistic quantum transport in n-PbTe*", Proceedings of the 24th International Conference on the Physics of Semiconductors, ed. D. Gershoni (World Scientific, Singapore 1999).

46. A. Darhuber, V. Holy, J. Stangl, S. Zerlauth, G. Bauer, N. Darowski, D. Lübbert, and U. Pietsch: "*Strain and strain relaxation in SiGe dot multilayers embedded in Si*", Proceedings of the 24th International Conference on the Physics of Semiconductors, ed. D. Gershoni (World Scientific, Singapore 1999)

47. C. Pidgeon, P. Findlay, B. N. Murdin, J. Langerak, C. Ciesla, J. Oswald, A. Homer, G. Springholz, and G. Bauer: "*Auger recombination dynamics of lead salts under ps free electron laser excitaions*", Proceedings of the 24th International Conference on the Physics of Semiconductors, ed. D. Gershoni (World Scientific, Singapore 1999).

48. J. Stangl, S. Zerlauth, F. Schäffler, G. Bauer, M. Berti, D. De Salvador, A. V. Drigo, and F. Romanato: "*Deviation of lattice parameters from Vegards rule in SiGeC epilayers*", Proceedings of the 24th International Conference on the Physics of Semiconductors, ed. D. Gershoni (World Scientific, Singapore 1999).

49. A. Bonanni, D. Stifter, K. Hingerl, H. Seyringer, H. Sitter: "*Self-assembling Mn-based Nanostructures on CdTe*", Appl. Phys. Lett. **74**, 3732 (1999)

50. D. Stifter, A. Bonanni, M. Garcia-Rocha, M. Schmid, K. Hingerl, H. Sitter: "*In Situ Reflectance Difference Spectroscopy: N-Plasma Doping Process of MBE-grown ZnTe Layers*", J. Cryst. Growth **201/202**, 132 (1999)

51. A. Bonanni, D. Stifter, K. Hingerl, H. Seyringer, H. Sitter: "*In Situ Characterization of the Growth Dynamics in MBE of Mn-based II-VI Compounds: Self-organized Mn Structures on CdTe*", J. Cryst. Growth **201**, 707 (1999)

52. M. Stepikhova, L. Palmetshofer, W. Jantsch, H.J. von Bardeleben, N. Gaponenko: "*µm Infrared Photoluminescence Phenomena in Er-doped Porous Silicon*", Appl. Phys. Lett. **74** (4), 537-539 (1999)

53. W. Jantsch, S. Lanzerstorfer, L. Palmetshofer, M. Stepikhova, H. Preier: "*Different Er centres in Si and Their Use for Electroluminescent Devices*", J. Luminescence **80**, 9-17 (1999)

54. D. Stifter, A. Bonanni, K. Hingerl, H. Sitter: "*Zerstörungsfreie Messung dünner Schichten mit polarisationsoptischen Methoden*", Elektrotechnik u. Informationstechnik, 116. Jg., H. 5, p. 315 (1999)

55. D. Stifter, M. Schmid, K. Hingerl, A. Bonanni, M. Garcia-Rocha, H. Sitter: "*In Situ Reflectance Difference Spectroscopy of II-VI Compounds: A Real Time Study of N-Plasma Doping During MBE*", J. Vac. Sci. and Technol. **B17**, 1697 (1999)

56. A. Bonanni, G. Prechtl, W. Heiß, F. Schinagl, S. Holl, H. Krenn, H. Sitter: "*Reflectance Difference Spectroscopy and Magneto-Optical Analysis of Digital Magnetic Heterostructures*", J.Vac. Sci. and Technol. **B17**, 1722 (1999)

57. S. Lanzerstorfer, J.D. Pedarnig, R.A. Gunasekaran, D. Bäuerle, W. Jantsch: "*1.54 µm Emission of Pulsed-laser Deposited Er-doped Films on Si*", J. Luminescence **80**, 353-356 (1999)

58. H. Sitter, T. Nguyen Manh: "*Pristine and Ba-Doped C60 Epilayers — Growth and Characterization*", Cryst. Res. Technol. **34**, 605-614 (1999)

59. W. Heiß, G. Prechtl, D. Stifter, H. Sitter, G. Springholz, T. Riemann, F. Bertram, D. Rudloff, J. Christen, G. Bley, U. Neukirch, J. Gutowski, J. Liu: "*Luminescence of ZnCdSe/ZnSe Ridge Quantum Wires*", Appl. Phys. Lett. **75** (7), 974-976 (1999)

60. A. Bonanni, K. Hingerl, H. Sitter, D. Stifter: "*Reflectance Difference Spectroscopy of Mn Intra-Ion Transitions in p-Doped Diluted Magnetic Semiconductors*", Phys. Stat. Sol. (b) **215**, 47 (1999)

61. A. Bonanni, H. Seyringer, D. Stifter, K. Hingerl, H. Sitter: "*Self-Assembling Mn-Based Nanostructures*", Proc. Seminar "Current Developments of Microelectronics", ed. by K. Riedling, p. 81 (1999)

62. D. Papajova, H. Sitter: "*Simulation of Epitaxial Growth: A Comparison of Stochastic and Rate Equation Models*", In: Research Trends, Current Topics in Crystal Growth Research Vol. 5, 55-89 (1999)

63. J. Franc, P. Hlidek, H. Sitter, E. Belas, A.L. Toth, L. Turjanska, P. Höschl: "*Photoluminescence of Deep Levels in (CdZn)Te Correlation with Diffusion Length Measurements*", Proc. ICDS San Francisco (1999)

64. E. Belas, R. Gill, J. Franc, H. Sitter, A.L. Toth, P. Moravec, P. Höschl: "*Dynamics of Native Point Defects in H2 Plasma-Etched Narrow Gap (HgCd)Te*", Proc. ICDS San Francisco (1999)

65. M. Stepikhova, Z. Krasil´nik, W. Jantsch, L. Palmetshofer, J. v. Bardeleben: "*Er-Related Photoluminescence in Porous Silicon - Optically Active Er Centers*", Proc. Russ. Acad. Sci., Ser. of Physics, Vol. 63, N 2, pp. 400-405 (1999)

66. Z. Wilamowski, W. Jantsch, N. Sandersfeld, F. Schäffler: "*Dipolar Field, Spin Relaxation, e-e Exchange and Spin Gap in Si/SiGe Quantum Wells"*, Ann. Phys. (Leipzig) **8**, 5, 507-510 (1999)

67. W. Jantsch, Z. Wilamowski, N. Sandersfeld, F. Schäffler: "Determination of Potential Fluctuations in Modulation-Doped SiGe Quantum Wells from Conduction Electron Spin Resonance", Proc. ICDS-20 (1999)

68. W. Jantsch, S. Lanzerstorfer, L. Palmetshofer, M. Stepikhova, G. Kocher, H. Preier: "*On the Generation of Optically Active Er Centers in Si Light Emitting Diodes*", Physica B **273-274**, 944-946 (1999)

69. N. Sandersfeld, W. Jantsch, Z. Wilamowski, F. Schäffler: "*ESR Investigations of Modulation-Doped Si/SiGe Quantum Wells*", GADEST 99, ed.by H.G.Grimmeiss et al., in : Solid State Phenomena **69-70**, 191 (1999)

70. Kozanecki, H. Przybylinska, W. Jantsch, L. Palmetshofer: "*Room Temperature Photoluminescence Excitation Spectroscopy of Er^{3+} Ions in Er- and (Er^{+}Yb)-Doped SiO_2 Films*", Appl. Phys. Lett. **75** (14), 2041 (1999)

71. W. Jantsch, S. Lanzerstorfer, M. Stepikhova, H. Preier, L. Palmetshofer: "*Status, Hopes and Limitations for the Si:Er-Based 1.54 µm Emitter*", GADEST 99, ed. by H.G. Grimmeiss et al., in: Solid State Phenomena **69-70**, 53 (1999)

72. I.A. Karpovich, M.V. Stepikhova, W. Jantsch: "*Heteroepitaxial Passivation of GaAs Surfaces and Its Influence on Photosensitivity Spectra and Recombination*

Parameters of GaAs Epitaxial Layers and Semi-Insulating Materials", In: Semicond. and Insul. Mat. ed. By. Z. Lilienthal-Weber and C. Miner, IEEE Inc., p.63 (1999)

73. W. Jantsch, . Z. Wilamowski, N. Sandersfeld, F. Schäffler: "*Conduction Electron Spin Resonance in $Si/Si_{1-x}Ge_x$ Quantum Wells*", Proc. Int. Conf. Phys. Semicond., Jerusalem 1998, ed. by D. Gershoni (World Scientific, Singapore 1999)
74. S. Lanzerstorfer, W. Jantsch, M. Stepikhova, L. Palmetshofer, H. Preier: "*Which Type of Center is Responsible for the 1.54 µm Emission in Si:Er at 300 K*", Proc. Int. Conf. Phys. Semicond., Jerusalem 1998, ed. by D. Gershoni (World Scientific, Singapore 1999
75. Kozanecki, W. Jantsch, M. Stepikhova, S. Lanzerstorfer, A. Henry, J.P. Bergmann: "*Spectroscopic Characterization of Er^{3+} Ions in 6H SiC*" ,Proc. Int. Conf. Phys. Semicond., Jerusalem 1998, ed. by D. Gershoni (World Scientific, Singapore 1999
76. S. Lanzerstorfer, J.D. Pedarnig, R.A. Guansekaran, D. Bäuerle, W. Jantsch Photoluminescence at 1.5 µm Heavily Er-Doped Insulating Films on Si In: Semicond. and Insulating Mat., ed. by Z. Lilienthal-Weber and C. Miner, IEEE Inc., p. 169 (1999)
77. N.V. Gaponenko, A.V. Mydri, O.V. Sergeev, V.E. Borisenko, M. Stepikhova, L. Palmetshofer, W. Jantsch, J.C. Pivin, B. Hamilton, A.S. Baran, A.I. Rat´ko: "*On the Origin of 1.5 µm Luminescence in Porous Silicon Coated with Sol-Gel Derived Erbium Doped Fe_2O_3 Films*", J. Luminescence **80**, 399-403 (1999)
78. S. Lanzerstorfer, J.D. Pedarnig, R.A. Guansekaran, D. Bäuerle, W. Jantsch: "*1.5 µm Emission of Pulsed-Laser Deposited Er-Doped Films on Si*", J. Luminescence **80**, 353-356 (1999)
79. T. Schwarzl, G. Springholz, H. Seyringer, H. Krenn, S. Lanzerstorfer, W. Heiß: "*High Reflectivity Lead Salt Based Bragg Mirrors for the Mid Infrared Range*", IEEE J. Quantum Electronics **35**, 1753 (1999)
80. G. Springholz, T. Schwarzl, W. Heiß, H. Seyringer, S. Lanzerstorfer, H. Krenn: "*MBE Growth of Highly Efficient Lead Salt Based Bragg Mirrors on $BaF_2(111)$ for the 4-6 µm Wavelength Region*", J. Cryst. Growth **201/202**, 999 (1999)
81. H. Sitter, W. Heiss, K. Hingerl: "*Optical Characterization of Low Dimensional II-VI Compound Heterostructure*", Proc. CLACSA, Havanna 1999 (World Scientific)
82. A. Yu. Andreev, B.A. Andreev, M.N. Drozdov, H. Ellmer, V.P. Kuznetsov, N.G. Kalugin, Z.F. Krasil´nik, Yu.A. Karov, L. Palmetshofer, K. Piplits, R.A. Rubtsova, M.N. Stepikhova, E.A. Uskova, V.B. Shmagin, H. Hutter: "*Electrical and Optical Properties of Silicon Doped by Er during Sublimational Molecular Beam Epitaxy*", Proc. Russ. Acad. Sci., Ser. of Physics **63**, 392 (1999)
83. A.Yu. Andreev, B.A. Andreev, M.N. Drozdov, Z.F. Krasil´nik, M.N. Stepikhova, V.B. Shmagin, V.P. Kuznetsov, R.A. Rubtsova, E.A. Uskova, Yu.A. Karpov, H. Ellmer, L. Palmetshofer, K. Piplits, H. Hutter: "*Optically Active Layers of Silicon Doped with Erbium during Sublimational Molecular Beam Epitaxy*", Semicond. **33**, 131 (1999)

84. Yu. Suprun-Belevich, L. Palmetshofer, B.J. Sealy, N. Emerson: "*Mechanical Strain and Electrically Active Defects in Si Implanted with Ge^+ Ions*", Semicond. Sci. Technol. **14**, 565 (1999)

85. B.A. Andreev, A.Yu. Andreev, H. Ellmer, H. Hutter, Z.F. Krasil´nik, V.P. Kuznetsov, S. Lanzerstorfer, L. Palmetshofer, K. Piplits, R.A. Rubtsova, N.S. Sokolov, V.B. Shmagin, M.V. Stepikhova, E.A. Uskova: "*Optical Er-Doping of Si during Sublimational Molecular Beam Epitaxy*", J.Cryst .Growth **201/202,** 534 (1999)

Submitted / in print:

1. G. Springholz, J. Stangl, M. Pinczolits, V. Holy, P. Mikulik, P. Mayer, K. Wiesauer, G. Bauer, D. Smilgies, H.H. Kang, L. Salamanca-Riba: "Nearly perfect 3D ordering in IV-VI quantum dot superlattices with ABCABC... vertical stacking sequence", Physica E, in print.
2. G. Springholz, M. Pinczolits, V. Holy, P. Mayer, K. Wiesauer, T. Roch, G. Bauer: "Self-organized growth of three-dimensional IV-VI semiconductor quantum dot crystals with fcc-like vertical stacking and tunable lattice constant", Surface Science, in print.
3. J. Stangl, V. Holy, J. Grim, G. Bauer, J. Zhu, K. Brunner, G. Abstreiter, O. Kienzle, F. Ernst: "Structural investigation of Si/SiGe superlattices on vicinal (113) oriented Si", Thin Solid Films 351 (1999), in print.
4. V. Holy, G. Springholz, M. Pinczolits, G. Bauer: "Lateral ordering in quantum dot PbSe/PbEuTe superlattices", Proceedings of the 9th International Conference on Narrow Gap Semiconductors, ed. M. von Ortenberg (Berlin 1999), in print.
5. V. Holy, J. Stangl, G. Springholz, M. Pinczolits, G. Bauer, I. Kegel, T.H. Metzger: "Lateral and vertical ordering of self-assembled PbSe quantum dots studied by high-resolution x-ray diffraction", Physica B, in print.
6. D. De Salvador, M. Petrovich, M. Berti, F. Romanato, E. Napolitani, A. Drigo, J. Stangl, S. Zerlauth, M. Mühlberger, F. Schäffler, G. Bauer, P.C. Kelires: "Lattice parameter of Si1-x-yGexCy alloys", Physical Review B, in print.
7. G. Springholz: "Molecular Beam Epitaxy of IV-VI Heterostructures and Superlattices", in: "Lead Chalcogenides: Physics and Applications", eds. D. Khoklov, Gordon and Breach, in print.
8. M. Helm, W. Hilber, G. Strasser, R. DeMeester, F.M. Peeters, A. Wacker: "Interminiband spectroscopy of biased superlattices", Physica E, in print.
9. N. Sandersfeld, W. Jantsch, Z. Wilamowski, F. Schäffler: "ESR investigations of modulation-doped Si/SiGe quantum wells", Thin Solid Films, in print.
10. F. Schäffler: "Silicon-Germanium", in: "Properties of Advanced Semiconductor Materials", eds. M.E. Levinshtein, S.L. Rumyantsev, M.S. Shur, John Wiley & Sons, New York 1999, in print.
11. M. Mühlberger, C. Schelling, N. Sandersfeld, H. Seyringer, F. Schäffler: "High-Speed Transport in Si/Si1-x-yGexCy Heterostructures", Thin Solid Films, in print.
12. T. Schwarzl, W. Heiss, G. Springholz: "High finesse IV-VI microcavities for the mid infrared", Physica E, in print.

13. W. Heiss, G. Prechtl, D. Stifter, H. Sitter, G. Springholz, T. Riemann, F. Bertram, D. Rudloff, J. Christen, G. Bley, U. Neukirch, J. Gutowski, J. Liu: "Luminescence of ZnCdSe/ZnSe ridge quantum wires", Physica E, in print.

14. C. Rosenblad, J. Stangl, E. Müller, G. Bauer, H. von Känel: "Strain relaxation of SiGe graded buffers grown at very high rates", EMRS 1999, in print.

15. H. Beyer, J. Nurnus, H. Böttner, A. Lambrecht, G. Springholz, G. Bauer: "MBE and Themoelectric Properties of PbTe/Pb1-xSrxTe MQW Structures", Proc. 9th International Conference on Narrow Gap Semiconductors, 1999, in print.

16. W. Heiss, T. Schwarzl, G. Springholz: "Lead-salt based Bragg mirrors and microcavities for the mid-infrared", Proc. 9th International Conference on Narrow Gap Semiconductors, 1999, in print.

17. T. Schwarzl, W. Heiss, G. Springholz, M. Aigle, H. Pascher: "6 µm vertical cavity surface emitting laser based on IV-VI semiconductor compounds", Electronics Letters, in print.

18. G. Strasser, S. Gianordoli, L. Hvozdara, W. Schrenk, K. Unterrainer, E. Gornik, M. Helm: "Intersubband and interminiband GaAs/AlGaAs quantum cascade lasers at 10 microns", Physica E, in print.

19. F. Schäffler: "Electron and Hole Mobilities", SiGe EMIS Data Review, ed. E. Kasper, in print.

20. Y. Zhuang, C. Schelling, T. Roch, A. Daniel, F. Schäffler, G. Bauer, J. Grenzer, U. Pietsch, S. Senz: "Investigation of inhomogeneous in-plane strain relaxation in Si/SiGe quantum wires by high resolution x-ray diffraction", Mat. Res. Soc. Symp. Proc., in print.

21. C. Schelling, G. Springholz, F. Schäffler: "New kinetic growth instabilities in Si (001) homoepitaxy", Thin Solid Films, submitted.

22. C. Penn, G. Bauer, F. Schäffler, S. Glutsch: "Band Ordering of the Pseudomorphic Si1-xGex/Si Heterostructure: The Fundamental Role of Excitons", Thin Solid Films, in print.

23. Y. Zhuang, C. Schelling, J. Stangl, C. Penn, S. Senz, F. Schäffler, A. Daniel, and U. Pietsch, G. Bauer: "Structural and optical properties of Si/Si1-xGex wires", Thin Solid Films, in print.

24. Y. Zhuang, U. Pietsch, J. Stangl, V. Holy, N. Darowski, J. Grenzer, S. Zerlauth, F. Schäffler, G. Bauer: "In-plane strain and shape analysis of Si/SiGe nanostructures by grazing incidence diffraction", Physica B, XSNS 6, Holland, in print.

25. C. Penn, F. Schäffler, G. Bauer, P. C. M. Christianen, J. C. Maan, and S. Glutsch: "Magnetoluminescence Investigations on Si/Si0.76Ge0.24 Quantum Wells", Physical Review B, submitted.

26. G. Springholz, M. Pinczolits, P. Mayer, V. Holy, G. Bauer, H. H. Khang, and L. Salamanca-Riba: "Tuning of lateral and vertical correlations in self-organized PbSe/PbEuTe quantum dot superlattices", Physical Review Letters, in print.

27. G. Springholz, T. Schwarzl, M. Aigle, H. Pascher, and W. Heiss: "4.8 µm vertical emitting PbTe quantum well lasers based on high finesse EuTe/PbEuTe microcavities", Applied Physics Letters, submitted.

28. H. H. Kang, L. Salamanca-Riba, M. Pinczolits, G. Springholz, V. Holy, and G. Bauer: “TEM investigation of self-organized PbSe quantum dots as a function of spacer layer thickness and growth temperature”, Proceedings of the Materials Research Society, submitted

29. D. Papajova, M. Vesely, H. Sitter: “A Study of the Surface Roughness Using a Temperature Activated Rate Equation Model”, Mat. Sci. in Semicond. Processing

30. L. Bocanek, B. Handlirova, J. Humlicek, T. Nguyen Manh, H. Sitter: “Temperature Dependence of Optical Spectra of C60 Thin Films”, Fullerence Sci. and Technol.

31. P. Hanzalek, I. Ohlidal, H. Sitter: “Reflectance of Thin Films with Non-Uniform Thickness”, J. Opt. Eng.

32. D. Ferraud, J. Cibert, C. Bourgognon, S. Tatarenko, A. Wasiela, G. Fishman, A. Bonanni, H. Sitter, S. Kolesnik, J. Jaroszynski, T. Dietl: “Carrier Induced Ferromagnetic Interaction in p-Doped ZnMnTe Epilayers”, J. Cryst. Growth

33. A. Bonanni, K. Hingerl, W. Hilber, H. Sitter, D. Stifter: “In Situ Reflectance Difference Spectroscopy of Intra-Mn Transitions in Highly N-Doped II-VI Diluted Magnetic Semiconductors”, J. Cryst. Growth

34. A. Bonanni, K. Hingerl, H. Sitter, D. Stifter: “Reflectance Difference Spectroscopy: A Powerful Tool for in Situ Investigations of II-VI Compounds with Mn”, Thin Solid Films

35. N. Sandersfeld, W. Jantsch, Z. Wilamowski, F. Schäffler: “ESR Investigations of Modulation-Doped Si/SiGe Quantum Wells”, IJC-Si, Japan 1999

36. M. V. Stepikhova, B.A. Andreev, V.B. Shmagin, Z.F. Krasil´nik, V.P. Kuznetsov, V.G. Shengurov, S.P. Svetlov, W. Jantsch, L. Palmetshofer, F. Schäffler, H. Ellmer: “Pecularities and Advantages of Optically Active Si:Er and Si1-xGex Layers Grown by the Sublimation MBE Method”, IJC-Si, Japan 1999

37. Z. Wilamowski, W. Jantsch, N. Sandersfeld, F. Schäffler: “Spin Properties of the Two-Dimensional Electron Gas”, Physica B

38. W. Jantsch, Z. Wilamowski, N. Sandersfeld, F. Schäffler: “Electric and Magnetic Field Fluctuations in Modulation-Doped Si/SiGe Quantum Wells”, Physica E

39. G. Springholz, T. Schwarzl, M. Aigle, H. Pascher, W. Heiss: “4.8 µm Vertical Emitting PbTe Quantum Well Lasers Based on High Finesse EuTe/Pb1-xEuxTe Microcavities”, Appl. Phys. Letters

40. T. Schwarzl, W. Heiss, G. Springholz, M. Aigle, H. Pascher: “6 µm Vertical Cavity Surface Emitting Lasers Based on IV-VI Semiconductor Compounds”, Electronic Letters

41. G. Prechtl, W. Heiss, S. Mackowski, A. Bonanni, G. Karczewski, H. Sitter, W. Jantsch: “Single Antiferromagnetic MnTe (Sub)monolayers in CdTe/CdMgTe Quantum Wells”, Semicond. Sci. and Technol.

42. T. Schwarzl, W. Heiss, G. Springholz: “High Finesse Mid Infrared Microcavities Based on Lead Salts”, Physica E

43. K. Bierleutgeb, H. Sitter, H. Krenn, H. Seyringer: “A Comparative Study of Iron Films on II-VI and III-V Semiconductors”, Proc. SLATES, Catargena 1999, Phys. stat. sol.

44. K. Hingerl, W. Hilber, R.E. Balderas-Navarro, A. Bonanni, H. Sitter, D. Stifter: “Surface Stress-Induced Optical Bulk Anisotropies”, Phys. Rev. Lett.

45. Yu.P. Rakovich, A.G. Rolo, M.V. Stepikhova, M.I. Vasilevskiy, M.J.M. Gomes, M.V. Artemyev, W. Jantsch, W. Heiss, G. Prechtl: “Absorption and Photoluminescence Study of CdS Quantum Dots: The Role of Host Matrix and Nanocrystal Size and Density”, Proc. MRS Spring Meeting 1999

46. W. Heiss, T. Schwarzl, G. Springholz: “Lead Salt Based Bragg Mirrors and Microcavities for the Mid Infrared”, World Scientific

Presentations

Invited Talks:

1. G. Bauer: “Magnetic Semiconductor Superlattices”, 9th Brazilian Workshop on Semiconductor Physics, Belo Horizonte, Brasilien, Feb. 1999.
2. M. Helm: “Minibands and Wannier-Stark ladders in semiconductor superlattices studied by infrared spectroscopy”, 9th Brazilian Workshop on Semiconductor Physics, Belo Horizonte, Feb. 1999.
3. W. Heiss, T. Schwarzl, G. Springholz: “Lead Salt based Bragg Mirrors and Microcavities for the Mid-Infrared”, 9th International Conference on Narrow Gap Semiconductors, Berlin, 27.9.-1.10. 1999.
4. V. Holy, G. Springholz, M. Pinczolits,G. Bauer: “Lateral Ordering in Quantum Dot PbSe/PbEuTe Superlattices”, 9th International Conference on Narrow Gap Semiconductors, Berlin, 27.9.-1.10, 1999.
5. F. Schäffler: “High-Speed Transport in Si/SiGeC Heterostructures”, Int. Joint Conference on Si Epitaxy and Heterostructures, Zao, Mijagi, Japan, Sept. 1999.
6. F. Schäffler: “Application of Silicon-Based Heterostructures in Microelectronics”, Semicond. Dev. Res. Symp., Charlottesville VA, USA, Dec. 1999.
7. G. Springholz, M. Pinczolits, V. Holy, G. Bauer: “Self-organized growth of three-dimensional quantum dot crystals with fcc-like vertical stacking and tunable lattice constant”, 18th European Conference of Surface Science, 21. - 24.9. 1999, Vienna, Austria.
8. G. Springholz, M. Pinczolits, V. Holy, G. Bauer: “Self-organized growth of semiconductors quantum dot crystals”, Annual Meeting of the Austrian Physical Society, 20. - 25.9. 1999, Innsbruck, Austria.
9. G. Springholz: “Fabrication of Semiconductor Nanostructures and their Characterization by High Resolution X-ray Diffraction Techniques”, 28th International School on Physics of Semiconducting Compounds, 6.-11.6.1999, Jaszowiec, Poland.
10. J. Stangl, V. Holy, G. Springholz, M. Pinczolits, P. Mikulik, G. Bauer: ”Vertical and Lateral Arrangement in Dot Superlattices”, Spring Meeting of the Materials Research Society, San Fransisco, USS, 5.-9. April 1999.
11. M. Helm: “Infrarotspektroskopie von Halbleitern”, Heraeus-Ferienkurs “Festkörperspektroskopie”, TU Dresden, BRD, 6.10. 1999.

12. F.Schäffler: "Silicon-Based Heterostructures for High-Speed Device Applications", Electronic Materials and Devices Seminar, Princeton NJ, USA, Dec. 1999.
13. G. Springholz: "Molecular Beam Epitaxy and in situ Reflection High-Energy Electron Diffraction Growth Studies of IV-VI Semiconductor Heterostructures", Fraunhofer Institut für physikalische Meßtechnik, 23.2.1999, Freiburg , Germany.
14. M. Helm: "Mid-infrared detectors and lasers based on intersubband transitions in quantum wells", Institute of Industrial Science, Tokyo University (Roppongi), Tokyo, Japan, 2.8.1999.
15. M. Helm: "Interminiband spectroscopy of semiconductor superlattices", Institute of Industrial Science, Tokyo University (Roppongi), Tokyo, Japan, 29.6.1999.
16. M. Helm: "Minibands and Wannier-Stark ladders in superlattices studied by infrared spectroscopy", Dept. of Basic Science , Tokyo University (Komaba), Tokyo, Japan, 25.6.1999.
17. M. Helm: "Minibands and Wannier-Stark ladders in superlattices studied by infrared spectroscopy", RIEC, Tohoku University, Sendai, Japan, 23.6.1999.
18. M. Helm: "Minibands and Wannier-Stark-ladders in semiconductor superlattices studied by infrared spectroscopy", Institut für Festkörperelektronik, TU Wien, 17.5.1999.
19. H. Sitter, K. Hingerl, W. Heiß: "Optical Characterization of Low Dimensional II-VI Compound Heterostructures", IX Latin American Congress on Surface Science and its Applications, Havanna, July 1999
20. K. Bierleutgeb, H. Sitter, H. Krenn, H. Seyringer: "A Comparative Study of Iron Films on II-VI and III-V Semiconductors", IX Latin American Congress on Surface Science and its Applications, Havanna, July 1999
21. W. Heiss, T. Schwarzl, G. Springholz: "Lead Salt Based Bragg Mirrors and Microcavities for the Mid Infrared", 9th Int. Conf. On Narrow Gap Semiconductors, Berlin, Sept.-Oct. 1999
22. W. Jantsch, S. Lanzerstorfer, M. Stepikhova, H. Preier, L. Palmetshofer: "Status, Hopes and Limitations for the Si:Er-Based 1.54 µm Emitter", GADEST 99, Höör, Schweden, Sept. 1999

Conference presentations (talks and posters):

1. G. Springholz, T. Schwarzl, W. Heiß, H. Seyringer, S. Lanzerstorfer and H. Krenn: "*Fabrication of highly efficient mid-infrared Bragg mirrors from IV-VI semiconductors*", Current Topics in Microelectronics, 3.3. - 6.3.1999, Bad Hofgastein, Austria.
2. K. Wiesauer and G. Springholz: "*Fabrication of Semiconductor Nanostructures by Scanning Force Microscopy*", Current Topics in Microelectronics, 3.3. - 6.3.1999, Bad Hofgastein, Austria.
3. M. Pinczolits, G. Springholz, V. Holy and G. Bauer: "*Nearly perfect 3D ordering in IV-VI quantum dot superlattices*", Gordon Research Conference on Thin Films and Crystal Growth Mechanisms, 20.6. - 25.6.1999, Plymouth, NH, USA.

4. T. Schwarzl, W. Heiss and G. Springholz: "*High finesse IV-VI microcavities for the mid infrared*", International Conference on Modulated Semiconductor Structures, 12.7 - 16.7.1999, Fukuoka, Japan.
5. G. Springholz, M. Pinczolits, V. Holy, G. Bauer, H. H. Khang, L. Salamanca-Riba: "*Nearly perfect three dimensional ordering in IV-VI quantum dot superlattices with ABCABC... vertical stacking sequence*", International Conference on Modulated Semiconductor Structures, 12.7 - 16.7.1999, Fukuoka, Japan.
6. G. Springholz, M. Pinczolits, V. Holy , P. Mayer, G. Bauer, H. H. Kang and L. Salamanca-Riba: "*Three dimensional ordering in PbSe/PbEuTe quantum dotsuperlattices with ABCABC...vertical stacking sequence*", 9th International Conference on Narrow Gap Semiconductors, Berlin, 27.9.-1.10.1999.
7. T. Schwarzl, W. Heiss and G. Springholz: "*High Finesse Lead Salt Microcavities for the 4-7 μm Spectral Region*", MIOMD, Aachen, 17.9.-20.9,.1999.
8. G. Springholz, M. Pinczolits, V. Holy, G. Bauer, H. H. Kang, L. Salamanca-Riba: "*Vertical and lateral correlations in self-organized quantum dot superlattices*", Fall Meeting of the Materials Research Society, 28.11. - 3.12.1999, Boston, USA.
9. W. Heiss, G. Prechtl, D. Stifter, H. Sitter, G. Springholz, L. Toth (poster): "*ZnCdSe/ZnSe Quantum Wires Fabricated by Selective Molecular Beam Epitaxy on Prepatterned GaAs Substrates*": Current Topics in Microelectronics, 3.3. - 6.3.1999, Bad Hofgastein, Austria.
10. M. Pinczolits, G. Springholz, V. Holy and G. Bauer (poster): "*Molecular beam epitaxy of quantum dot crystals*", Current Topics in Microelectronics, 3.3. - 6.3.1999, Bad Hofgastein, Austria.
11. G. Springholz and K. Wiesauer (poster): "*Depth resolution for scanning tunneling microscopy imaging of misfit dislocations in heteroepitaxial layers and multilayers*", Gordon Research Conference on Thin Films and Crystal Growth Mechanisms, 20.6. - 25.6.1999,Plymouth, NH, USA.
12. W. Heiss, G. Prechtl, D. Stifter, H. Sitter, G. Springholz, T. Riemann, F. Bertram, D. Rudloff, J. Christen, G. Bley, U. Neukirch, J. Gutowski and J. Liu (poster): "*Luminescence of ZnCdSe/ZnSe ridge quantum wires*", International Conference on Modulated Semiconductor Structures, 12.7 - 16.7.1999, Fukuoka, Japan.
13. M. Pinczolits, G. Springholz, V. Holy and G. Bauer (poster): "*Self-organized growth and hexagonal lateral ordering in PbSe/PbEuTe quantum dot superlattices*", 18th European Conference on Surface Science, 21.-24.9.1999, Vienna, Austria.
14. H. H. Kang, L. Salamanca-Riba, G. Springholz, M. Pinczolits and G. Bauer (poster): "*Transmission electron microscopy investigations of self-organized PbSe/PbEuTe quantum dot superlattices*", Fall Meeting of the Materials Research Society, 28.11. - 3.12.1999, Boston, USA.
15. K. Bierleutgeb, H. Sitter, H. Krenn and H. Seyringer: "*A comparative Study of Iron Films on II-VI- and III-V-semiconductors*", 15th Latinamerican Symposium on Solid State Physics, Cartagena de Indias, Colombia, Nov. 1999.
16. C.Penn, S.Glutsch, G.Bauer and F.Schäffler: "*Band Ordering of the Pseudomorphic* $Si_{1-x}Ge_x$*/Si Heterostructure: The Fundamental Role of Excitons*", Int. Joint Conf. Si, Zao, Miyagi, Japan, Sep. 1999

17. C. Penn, P.C.M. Christianen, F. Schäffler, J.C. Maan, G. Bauer: "*Type II band alignment and exciton wave-functions in $Si/Si_{1-x}Ge_x$ quantum wells*", 9th International Conference on Modulated Semiconductor Structures (MSS9), July 12-16, 1999, Fukuoka, Japan.
18. N.Sandersfeld, W.Jantsch, Z.Wilamowski, F.Schäffler: "*ESR Investigations of Modulation-Doped Si/SiGe Quantum Wells*", Int. Joint Conf. Si, Zao, Miyagi, Japan, Sep. 1999
19. Y.Zhuang, C.Schelling, J.Stangl, S.Senz, F.Schäffler, A.Daniel, U.Pietsch, G.Bauer: "*Structural and Optical Properties of $Si/Si_{1-x}Ge_x$ Wires*", Int. Joint Conf. Si, Zao, Miyagi, Japan, Sep. 1999
20. C.Schelling, G.Springholz, F.Schäffler: "*New Kinetic Growth Instabilities in Si(001) Homoepitaxy*", Int. Joint Conf. Si, Zao, Miyagi, Japan, Sep. 1999
21. M.Schatzmayr, E.Wachmann, M.Mühlberger, C.Schelling, F.Schäffler: "*A Fully Certified SiGe-BiCMOS Process for ASICS and Multiproduct Wafers*", Semic. Dev. Res. Symp., Charlottesville VA, USA, Dec. 1999
22. Y. Zhuang, U. Pietsch, J. Stangl, N. Darowski, T. Roch, V. Holy, G. Bauer, S. Zerlauth, F. Schäffler: "*Investigation of inhomogenous strain relaxation in dry-etched SiGe/Si quantum wires using GID*", MRS 1999, Boston, USA, December 1999.
23. Y. Zhuang, V. Holy, J. Stangl, N. Darowski, J. Grenzer, U. Pietsch, S. Zerlauth, F. Schäffler, G. Bauer: "*In-plane strain and shape analysis of Si/SiGe nanostructures by grazing incidence diffraction*", 6th International Conference on Surface X-ray and Neutron Scattering, Sept. 1999, Nordwijkerhout, Netherlands.
24. T. Roch, J. Stangl, A. Darhuber, G. Bauer, Jian-hong Zhu, K. Brunner, G. Abstreiter: "*Self-organized SiGe quantum dots and wires on vicinal Si(001) substrate correlated laterally by step bunches*", 4th Autumn School ("X-ray scattering from Surfaces and Thin Layers"), Smolenice, Slowakei, 22.-25. September 1999.
25. A. Daniel, J. Stangl, E. Höflinger, G. Bauer, C. Rosenblad, H. Von Känel: "*Anisotropic Strain Relaxation in Graded SiGe Buffers Grown by Low Energy Plasma Enhanced Chemical Vapor Deposition*", 4th Autumn School ("X-ray Scattering from Surfaces and Thin Layers"), Smolenice, Slowakei, 22.-25. September 1999.
26. M. Helm, W. Hilber, G. Strasser, R. DeMeester, F. M. Peeters, A. Wacker: "*Interminiband spectroscopy of biased superlattices*", 5th Int. Conf. on Intersubband Transitions in Quantum Wells, Bad Ischl, Austria, Sept. 1999.
27. M. Helm: "*Infrared spectroscopy of biased superlattices*", Adriatico Research Conference on "High-Field Transport in Superlattices", Trieste, Italy, Aug. 1999
28. M. Helm, W. Hilber, G. Strasser, R. DeMeester, F. M. Peeters, A. Wacker: "*Simultaneous investigation of vertical transport and intersubband absorption in a superlattice: continuum Wannier-Stark ladders and next-nearest neighbor tunneling*", 11th Int. Conf. on Nonequilibrium Carrier Dynamics in Semiconductors (HCIS-11), Kyoto, Japan, July 1999

29. G. Strasser, S. Gianordoli, L. Hvozdara, W. Schrenk, K. Unterrainer, E. Gornik, M. Helm: "*Intersubband and interminiband GaAs/AlGaAs quantum cascade lasers at 10 microns*", 9th Int. Conf. on Modulated Semiconductor Structures, Fukuoka, Japan, July 1999
30. R. H. J. De Meester, F. M. Peeters, M. Helm: "*Optical absorption of biased semiconductor superlattices*", 7th Int. Symposium: Nanostructures - Physics and Technology 1999, St. Petersburg, Russia, June 1999
31. M. Helm, W. Hilber, G. Strasser, R. DeMeester, F. M. Peeters: "*Mid-infrared spectroscopy of biased superlattices*", EUROPTO Conference on THz Spectroscopy and Applications, Munich, BRD, June 1999
32. A.G. Rolo, M.V. Stepikhova, M.I. Vasilevskiy, M.J.M. Gomes, Yu.P. Rakovich, M.V. Artemyev, W. Jantsch, W. Heiss, G. Prechtl: "*Absorption and Photoluminescence Study of CdS Quantum Dots: The Role of Host Matrix and Nanocrystal Size and Density*", Spring Meeting of the Mat. Res. Soc., San Francisco, USA, April 1999
33. Z. Wilamowski, W. Jantsch, N. Sandersfeld, F. Schäffler: "*Spin Properties of the Two-Dimensional Electron Gas*", Int. Conf Low Temperature Physics, Helsinki, Finnland 1999
34. Z. Wilamowski, W. Jantsch, N. Sandersfeld, F. Schäffler: "*Dipolar Field, Spin Relaxation, e-e Exchange and Spin Gap in Si/SiGe Quantum Wells*", Int. Conf. On Correlation, Hamburg 1999
35. W. Jantsch, S. Lanzerstorfer, L. Palmetshofer, M. Stepikhova, G. Kocher, H. Preier: "*On the Generation of Optically Active Er Centers in Si Light Emitting Diodes*", Int. Conf. Defects in Semicond., Berkeley, CA, July 1999
36. W. Jantsch, Z. Wilamowski, N. Sandersfeld, F. Schäffler: "*Determination of Potential Fluctuations in Modulation-Doped SiGe Quantum Wells from Conduction Electron Spin Resonance*", Int. Conf. Defects in Semicond., Berkeley, CA, July 1999
37. W. Jantsch, Z. Wilamowski, N. Sandersfeld, F. Schäffler: "*Electric and Magnetic Field Fluctuations in Modulation-Doped Si/SiGe Quantum Wells*", EP2DS-13, Ottawa, Canada, August 1999
38. N. Sandersfeld, W. Jantsch, Z. Wilamowski, F. Schäffler: "*ESR Investigations of Modulation-Doped Si/SiGe Quantum Wells*", Int. Joint Conf. On Si Epitaxy and Heterostructures, Japan, Sept. 1999
39. M.V. Stepikhova, B.A. Andreev, V.B. Shmagin, Z.F. Krasil´nik, V.P. Kuznetsov, V.G. Shengurov, S.P. Svetlov, W. Jantsch, L. Palmetshofer, F. Schäffler, H. Ellmer: "*Peculiarities and Advantages of Optically Active Si:Er and $Si_{1-x}Ge_x$ Layers Grown by the Sublimation MBE Method*", Int. Joint Conf. On Si Epitaxy and Heterostructures, Japan, Sept. 1999
40. N. Sandersfeld, W. Jantsch, Z. Wilamowski, F. Schäffler: "*ESR Investigations of Modulation-Doped Si/SiGe Quantum Wells*", GADEST 99, Höör, Schweden, Sept. 1999

41. T. Schwarzl, W. Heiss, G. Springholz: "*High Finesse Lead Salt Microcavities for the 4-6 μm Spectral Region*", 3rd Int. Conf. Mid-Infrared Optoelectronics Materials and Devices, Aachen, Sept. 1999

42. W. Heiß, G. Prechtl, D. Stifter, H. Sitter, G. Springholz, T. Riemann, F. Bertram, D. Rudloff, J. Christen, G. Bley, U. Neukirch, J. Gutowski, L. Toth: "*Exciton Dynamics in ZnCdSe/ZnSe Redge Quantum Wires*", 9th Int. Conf. Modulated Semicond. Structures, Fokuoka, Japan, July 1999

43. G. Prechtl, W. Heiss, A. Bonanni, S. Mackowski, G. Karczewski, H. Sitter, W. Jantsch: "*Antiferromagnetic Phase Transition in A Single MnTe Monolayer*", 9th Int. Conf. Modulated Semicond. Structures, Fokuoka, Japan, July 1999

44. T. Schwarzl, W. Heiss, G. Springholz: "*High Finesse Mid Infrared Microcavities Based on Lead Salts*", 9th Int. Conf. Modulated Semicond. Structures, Fokuoka, Japan, July 1999

45. G. Springholz, T. Schwarzl, W. Heiss, H. Seyringer, S. Lanzerstorfer, H. Krenn: "*Fabrication of Highly Efficient Mid Infrared Bragg Mirrors from IV-VI Semiconductors*", Aktuelle Entwickungen der Mikroelektronik, Bad Hofgastein, Austria, March 1999

46. W. Heiss, G. Prechtl, D. Stifter, H. Sitter, G. Springholz, L. Toth: "*ZnCdSe/ZnSe Quantum Wires by Epitaxy on Prepatterned GaAs Substrates*", Aktuelle Entwickungen der Mikroelektronik, Bad Hofgastein, Austria, March 1999

47. T. Schwarzl, W. Heiß, G. Kocher-Oberlehner, G. Springholz: "*CH_4/H_2 Plasma Etching of IV-VI Semiconductors*", Aktuelle Entwickungen der Mikroelektronik, Bad Hofgastein, Austria, March 1999

48. Bonanni, G. Prechtl, W. Heiß, F. Schinagl, S. Holl, H. Krenn, H. Sitter, D. Stifter, K. Hingerl: "*Reflectance Difference Spectroscopy and Magneto-Optical Analysis of Digital Magnetic Heterostructures*", 26th Conf. On the Physics and Chemistry of Semicond. Interfaces, San Diego, USA, Jan. 1999

49. H. Sitter, G. Matt, A.Y. Andreev, C.J. Brabec, D. Badt, H. Neugebauer, N.S. Sariciftci: "*Highly Ordered Crystalline Thin Film Bilayers of Para-Hexaphenyl and C60 Grown by Hot Wall Epitaxy*", MRS Fall Meeting, Boston, Dec. 1999

50. D. Stifter, M. Schmid, K. Hingerl, A. Bonanni, M. Garcia Rocha, H. Sitter: "*In Situ Reflectance Difference Spectroscopy of II-VI Compounds: A Real Time Study of N Plasma Doping During Molecular Beam Epitaxy*", PCSI-26, San Diego, Jan. 1999

51. Bonanni, K. Hingerl, H. Sitter, D. Stifter: "*Reflectance Difference Spectroscopy of Mn Intra Ion Transitions in p-Doped Diluted Magnetic Semiconductors*", Int. Conf. Solid State Spectroscopy, Schwäbisch Gmünd, Germany, Sept. 1999

52. Bonanni, H. Sitter, K. Hingerl, D. Stifter: "*Reflectance Difference Spectroscopy of Enhanced Mn Intra Ion Transitions in p-Doped Diluted Magnetic Semiconductors*", EMRS Spring Meeting, Strasbourg, May 1999

53. G. Neuwirt, K. Hingerl, D. Stifter, A. Bonanni, K. Bierleutgeb, H. Sitter: "*An Algorithm to Determine the Composition and Growth Rate from in-situ Spectral Ellipsometry Data*", EMRS Spring Meeting, Strasbourg, May 1999

54. W. Hilber, A. Bonanni, H. Sitter, D. Stifter, K. Hingerl: "*Reflectance Difference Spectroscopy: A Powerful Tool for in-situ Investigations of II-VI Surfaces*", European Conf. Surf. Sci. ECOSS, Vienna, Sept. 1999

Doctor's Theses

1. Dipl.-Ing. Wolfgang Hilber: "Vertikaler Transport, heiße Elektronen und Metall-Isolator Übergang in Halbleiter-Übergittern: elektrische und optische Untersuchungen", Linz, 1999.
2. Dipl.-Ing. Christian Penn: "Electronic Properties of Si/SiC Heterostructures", Linz, 1999.
3. Dipl.-Ing. Sven Lanzerstorfer: "Charakterisierung von Er-dotiertem Si", Linz, 1999.
4. M.Sc. Alberta Bonani: "Growth and Characterization of Semimagnetic Multilayer Structures", Linz, 1999.

Habilitations

1. Dipl.-Ing. Dr. Gunther Springholz: "Molekularstrahlepitaxie von IV-VI Halbleitern: Wachstumsprozesse und Herstellung von Heterostrukturen", Linz 1999.

Cooperations

1. Siemens München, Dr.Heide
2. Daimler Benz Reserach Laboratories Ulm, Dr. Presting, Dr. König
3. VOEST ALPINE, Linz, Dr.Angerer,
4. Siemens Villach,
5. AMS Unterpremstätten
6. KEBA, Linz, Ing.G.Krippner
7. Institut für Halbleiterphysik, Frankfurt/Oder
8. Sektion Physik, Ludwig-Maximilians Universität München
9. Physics Department, Cornell University
10. ETH, Zürich
11. ESRF Grenoble
12. DESY, Hasylab, Hamburg
13. FOM Institute Rijnhuizen, Niederlande
14. Walter Schottky Institut, TU München
15. IBM Research Center, Yorktown Heights
16. Institut für Festkörperelektronik, TU Wien
17. Philips Almelo, Niederlande
18. Heriot Watt University, Edinburgh, Scotland

19. University of Southampton, England
20. High Pressure Research Center, Warschau, Polen
21. Institue of Physics, Polish Academy of Sciences, Warschau
22. TU Berlin, Institut für Festkörperphysik
23. Universität Würzburg
24. Universität Bayreuth
25. Universität Bremen
26. Purdue University, Lafayette, IN, USA
27. MIT, Cambridge, MA, USA
28. NIST, Gaithersburg, MD, USA
29. Nanoelectronics Research Center, University of Glasgow, Scotland
30. University of Warwick, Coventry, England
31. North Carolina State University, NC, USA
32. IAF Freiburg
33. CENG Grenoble
34. Universität Paderborn
35. INSA, Lyon
36. Université de Montpellier
37. ELETTRA, Triest
38. Universiteit Instelling, Antwerpen, Niederlande
39. TASC Triest
40. ENEA, Roma
41. CNRSM-PASTIS, Brindisi
42. Akademie der Wissenschaften, Troits, Moskau
43. High Magnetic Field Lab., Grenoble
44. Siemens München, Zentrale Technik, Bereich Halbleiter
45. Fraunhofer-Institut (IAF) Freiburg (Chiptechnologie)
46. TU-München (Mikrowellentechnik)

Fast Frequency Measurement Applied to a Microwave Distance Sensor

A. Stelzer, C. G. Diskus, K. Lübke

Microelectronics Institute, Johannes Kepler University Linz, A-4040 Linz, Austria, Altenberger Str. 69

Design and characteristics of a fast frequency counter at 35 GHz for a distance sensor are presented. The signal received from the target is measured using six-port technology, and therefore accurate frequency measurement is essential. The frequency counter is capable of measuring the frequency in 120 microseconds with a 20-bit resolution.

1. Introduction

The presented frequency counter is part of a precision microwave distance sensor for short range applications [1]. A varactor tuned Gunn-oscillator serves as a signal source. The microwave signal is transmitted and received via a single corrugated horn-lens combination. Magnitude and phase of the reflected wave are measured using a six-port device [2]. Due to the frequency dependence of the calibration parameters highly accurate measurements are possible only at the calibration points. The accuracy of the distance measurement directly depends on the accuracy of the frequency measurement. The frequency counter is used both for linearizing the Gunn-diode characteristic for fast frequency sweeps and for controlling the actual frequency in interferometer mode of operation [3].

2. Experimental

2.1 Frequency Counter

Figure 1 shows the block diagram of the module consisting of dynamic and static dividers, a gating circuit realized in GaAs-MESFET technology, and a standard counter module. The frequency counter provides a very high measuring rate and a resolution of 20 bit. These requirements can only be met by directly counting the RF signal instead of using the conventional approach of down-conversion. The 35 GHz signal is fed to a dynamic frequency divider reducing the frequency to 8.75 GHz. The dynamic divider was provided by the Fraunhofer Institute for Applied Solid-State Physics (IAF), Freiburg/Breisgau, Germany [4]. This signal is counted directly by using a 8.75 GHz gating circuit followed by cascaded static dividers. By inserting the gate at this high frequency it is possible to achieve the needed 20-bit resolution with a gating time of only 120 μs. A taper matches the coaxial Wiltron-”K” connector input of the module to the coplanar input of the chip [5]. The modules are connected together with bonding wires.

The gating module controls the operation of the following static divider chain. The measurement accuracy depends on the timing accuracy of the gate. The time base is built with a temperature stabilized quartz-oscillator. The gating module is controlled by signals generated from a programmable logic device (PLD) to switch the RF on and off.

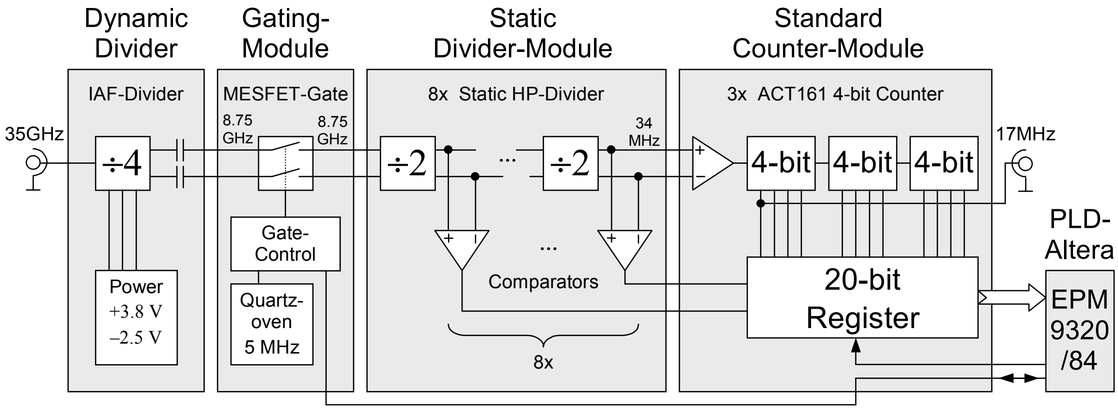

Fig. 1: Block diagram of the 35 GHz frequency counter.

The digital counter consists of eight static dividers and three integrated 4-bit counters. The counter value is transferred to a data latch while the counter chain is stopped. Therefore static dividers operating down to DC are used. The counter values are sampled using comparators that are attached to the high frequency line via resistive TEE structures. A fast comparator converts the differential signal to a logic signal compatible with 5 V logic. The logic outputs of each divider stage are combined at this module, stored in a register, and transferred to the PLD.

2.2 Gating Circuit

The circuit combines two functions. Primarily, the gating of the RF-signal is accomplished by switching transistors on and off. The second function is a logic operation, which is required for generating the gating signal. To guarantee a high accuracy of the counter, attention is paid to supply a gating signal with very precise rising and falling edges. This is done by combining the timing signal of a reference counter (realized in a PLD) and the edges of the clock signal provided by a temperature controlled crystal oscillator (TCXO). Instead of using high speed logic gates, the logic operation is carried out by the RF transistors.

Figure 2 shows the schematic of the gating circuit. The gates of the transistors T_2 are excited by the clock signal of the TCXO. The transistors T_1 and T_3 are used to switch on or to switch off the gate regardless of the clock signal. The transistors used for this gating chip are 0.5 µm GaAs-MESFETs. A scanning electron microscope picture of the chip is shown in Fig. 3. The transistors T_1 and T_2 are half as wide as the transistors T_3.

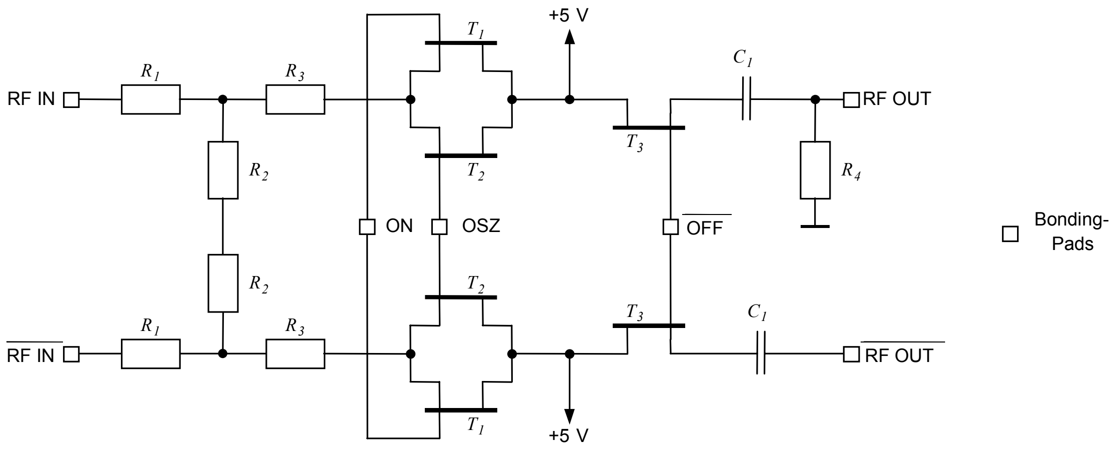

Fig. 2: Schematic of the 8.75 GHz gating-circuit realizing the logic operation $\overline{\text{OFF}} \wedge (\text{ON} \vee \text{OSC})$.

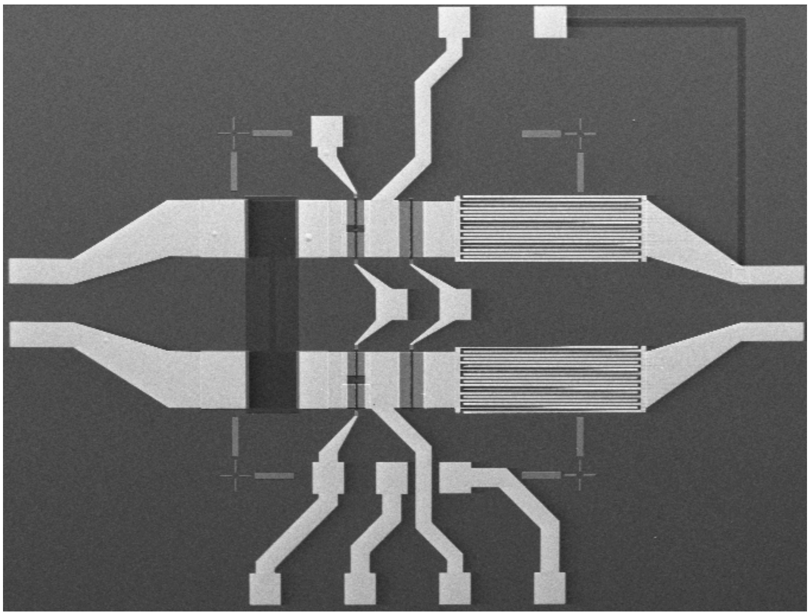

Fig. 3: Scanning electron microscope picture of the 8.75 GHz gating circuit.

The frequency counter-module described above is used in two modes of operation. One mode is to create the voltage/frequency characteristic of the voltage controlled oscillator. With this data in memory it is possible to select arbitrary frequencies of operation. For instance, a very fast linear frequency sweep can be generated.

The second mode of operation is used for selecting a frequency point with high accuracy. Because of the fast measuring cycle it is possible to implement a closed loop control for frequency adjustment. In contrast to the offset drift of the voltage/frequency characteristic, the derivative of this characteristic remains stable. Hence, the selected frequency point can be reached in two steps using a gradient technique, resulting in an overall settling time of 240 µs.

3. Conclusion

The presented frequency counter and six-port are used to determine the phase of the reflected signal in a high precision distance sensor. The frequency counter allows in-system linearization of the oscillator characteristics for fast and linear frequency sweeps. Furthermore, a frequency control loop provides a precise Gunn frequency for the high accuracy interferometer mode. A frequency accuracy of ±0.3 kHz @ 35 GHz was achieved. The measurement time was 120 µs for the frequency measurement and 6 µs for the six-port phase measurement.

Acknowledgements

The authors would like to thank M. Hinterreiter and J. Katzenmayer for fabricating and testing the devices. This work was supported by the Austrian Science Foundation (FWF) under Contract number P11424-ÖPY.

References

[1] A. Stelzer, C. G. Diskus, H. W. Thim, “A Microwave Position Sensor with Sub-Millimeter Accuracy”, *Digest to the IEEE MTT-S International Microwave Symposium*, June 13-19, 1999, Anaheim, California, vol. 4, pp. 1599-1602.

[2] G. F. Engen, “An Improved Circuit for Implementing the Six-Port Technique of Microwave Measurements”, *IEEE Transactions on Microwave Theory and Techniques*, Vol. MTT-25, No. 12, December 1977, pp. 1080-1083.

[3] G. S. Woods, D. L. Maskell, M. V. Mahoney, “A High Accuracy Microwave Ranging System for Industrial Applications”, *IEEE Transactions on Instrumentation and Measurement,* Vol. 42, No. 4, Aug. 93, pp. 812-816.

[4] Z. Lao, W. Bronner, A. Thiede, M. Schlechtweg, A. Hülsmann, M. Rieger-Motzer, G. Kaufel, B. Raynor, M. Sedler, “35-GHz Static and 48-GHz Dynamic Frequency Divider IC´s Using 0.2-µm AlGaAs/GaAs-HEMT´s”, *IEEE Journal of Solid-State Circuits*, Vol. 32, No. 10, Oct. 97, pp. 1556-1562.

[5] A. Stelzer, C. G. Diskus, A. Thiede, K. Lübke, A. L. Springer, “A 35 GHz Frequency Divider Module”, *IEEE Workshop on MMIC Design, Packaging, and System Applications*, Oct. 22-23, 1998, Freiburg/Brsg., pp. 111-112.

SiGe Technology

N. Sandersfeld, H. Seyringer, G. Lengauer, M. Mühlberger, C. Schelling, L. Palmetshofer, F. Schäffler

Abteilung für Halbleiterphysik, Universität Linz

We report on the cleanroom activities in Linz with respect to Si-based technology. Two main topics are treated: molecular beam epitaxy (MBE) of Si and $Si/Si_{1-x-y}Ge_xC_y$ heterostructures, and e-beam nanolithography. In the former field we report on kinetic and strain-induced growth instabilities and their application for self-organized growth, the growth of modulation-doped Si/SiGe heterostructures with high mobilities and high carrier concentrations, and on the deposition of $Si/Si_{1-x-y}Ge_xC_y$ heterobipolar transistors on pre-processed wafers provided by an industrial partner. The structuring activities are concentrated on nanometer-lengths Schottky gates with T or Γ cross section realized by multi-resist-layer e-beam lithography and lift-off.

1. Molecular beam epitaxy

1.1 Kinetic versus strain induced growth instabilities

The lattice mismatch of 4% between pure Si and pure Ge has important implications for epitaxial growth. One of the most prominent features is the Stranski-Krastanov growth mode, which breaks up a compressively strained epitaxial film into islands. This growth mode is widely exploited for growing so called self-organized dots of the heteromaterial with the larger lattice constant. This works particularly well with InAs on GaAs, where the InAs dots can become small enough to show zero-dimensional behavior ("quantum dots"), and the first lasers have been demonstrated in this material combination.

Ge dots on Si are another example that found widespread interest in recent years. In the Si/SiGe heterosystem also strain-induced step bunching has been studied intensively [1], which was considered as a precursor to Stranski-Krastanov island formation. The basic idea behind strain-induced step bunching on slightly misoriented Si(001) substrates is that the strain of a SiGe layer causes an arrangement of flat terraces and macrosteps with a period that is typically 10 to 20 times larger than the natural terrace spacing at a particular miscut [2]. Several experiments seemingly supported that concept [3].

We recently discovered kinetic step bunching on the surface of homoepitaxial Si layers on miscut substrates [4], the appearance of which closely resembles the morphology that has so far been associated with strain-induced step bunching. But, since lattice-mismatch-induced stress is certainly absent in the homoepitaxial layers, and self-organization phenomena are potentially useful for the fabrication of nanostructures, it is important to distinguish strain-induced and kinetic growth instabilities. For this purpose we extended our homoepitaxial growth studies to $Si_{1-x}Ge_x$ films with Ge concentrations between 5 and 50%. To separate the kinetic growth effects of the Si buffer from the strain effects of the SiGe layers, each epilayer sequence was deposited simultaneously on three 18x18 mm^2 substrates with different miscuts: One singular (001) substrate with miscut < 0.1°, and two substrates with miscuts around 1° and miscut azimuths along [100], and [110], respectively. Also, the deposition temperature for the Si buffer layer (typical 1000 Å thick) was varied between 500 °C, where we found the maximum corrugation height of the 1° miscut samples, and 750 °C, where the buffer layers are atomically smooth with an uncorrelated rms roughness of typically 2 – 3 Å.

The outcome of our experiments is rather surprising: We found no indication for strain-induced step-bunching under either of the conditions where such an effect was claimed in the literature. Whenever we start with a smooth silicon buffer, the subsequent SiGe layer remained smooth up to a maximum Ge concentration $x_{m.}$ beyond which the films disintegrated into Stranski-Krastanov islands rather than linear step bunches. x_m depends on the deposition temperature, and amounts to about 50% at 550 °C. Vice versa, whenever we started with a kinetically step-bunched Si buffer, the subsequent $Si_{1-x}Ge_x$ film with $x < x_m$ virtually replicated the morphology of the substrate (Fig. 1). This finding also applies to Si/SiGe superlattices, the morphological appearance of which depends exclusively on the morphology of the initial Si buffer.

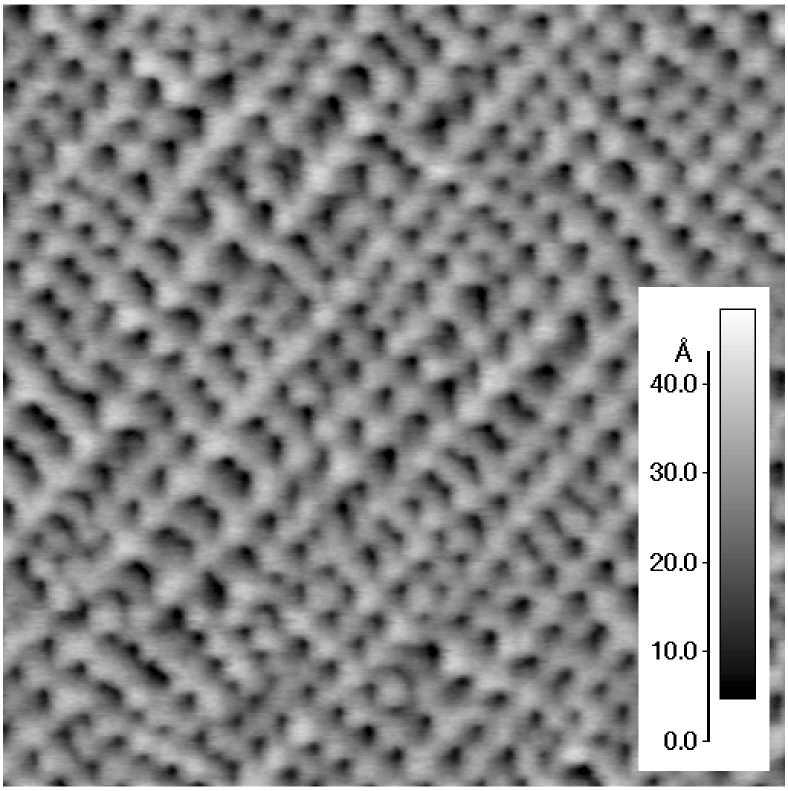

Fig. 1: 25 Å of $Si_{0.75}Ge_{0.2}$ deposited on top of a kinetically roughened Si buffer layer on a 1° miscut Si (001) substrate. No strain-induced effects are observed: the SiGe layer just replicates the morphology of the buffer. Compare also Ref. [4].

These results are important for a variety of growth phenomena in Si/SiGe epitaxy: (i) By optimizing the Si buffer, the interfaces between the Si barriers and a pseudomorphic SiGe hole channel can be made almost atomically flat. Interface roughness scattering, which has been discussed in the literature as a relevant scattering mechanism in such quantum well structures [5], can this way be suppressed. (ii) Step bunching associated with a Si buffer can be converted into an inhomogeneous strain field by adding a SiGe film that replicates the morphology. Such an arrangement has already been used for aligning subsequent Ge dots [6], but the mechanism has incorrectly been attributed to strain-induced step bunching of the SiGe film. With our new results, the pattern formation can now be efficiently designed, because it is entirely due to the morphology of the Si buffer, which can be varied by fine-tuning of the miscut and growth parameters [4].

1.2 Growth of modulation-doped Si/SiGe FETs

So far, we have tried to optimize the low temperature mobilities of Si/SiGe modulation-doped structures, in order to establish the best possible growth conditions. However, for FET applications the channel conductivity has to be optimized, which requires a compromise between carrier density and mobility. We therefore tried to increase the number of carriers in the channel by doping both SiGe barriers, and to keep the mobility high, by retaining the undoped spacers adjacent to the strained Si channel. Such a layout was optimized by self-consistent calculations, which yield asymmetric doping concentrations because of the symmetry-breaking presence of the Schottky gate. For a given spacer thickness, which was applied to either side, the doping concentrations where adjusted such that under conditions of maximum carrier transfer into the channel both doping supply layers are completely depleted.

The main problem with the additional doping layer on the substrate side of the channel is dopant segregation into the spacer, and even into the channel. To reduce this effect low-temperature doping and a subsequent thermal flash-off of excess dopants was applied for the doping supply layer on the substrate side. The thermal-flash-off has the additional benefit of an annealing step, which reduces the number of defects that might have formed during the low temperature doping.

The results are promising: We measured on double sided doped Si/SiGe MODFET structures carrier densities of $1.3 \cdot 10^{12}$ cm^{-2}, and still maintained low-temperature mobilities of 65,000 cm^2/Vs. For comparison, a typical MOSFET has under such conditions a mobility that is at least a factor of 5 lower.

1.3 $Si/Si_{1-x-y}Ge_xC_y$ Heterobipolar Transistor (HBT)

SiGe-HBTs are now widely introduced into the production lines for high speed bipolar and BiCMOS circuits, because they offer a speed advantage of at least a factor of two without sacrificing the compatibility to standard Si technologies. A general problem of Si technology is transient enhanced diffusion (TED) of the only useful acceptor element, boron, upon injection of Si self interstitials. The latter are created during thermal oxidation and also during the annealing step of the emitter implant. As has been reported in our last annual report, the addition of less than 0.5 at.% of carbon to the SiGe base can drastically reduce transient enhanced boron diffusion of the base dopant into collector and emitter. Therefore, several HBT producing semiconductor companies and manufacturers of chemical vapor deposition (CVD) reactors are presently working on a reliable process for the controlled deposition of $Si_{1-x-y}Ge_xC_y$:B base layers. CVD is the standard epitaxial deposition technique for Si, mainly because of the high throughput and the excellent reproducibility. On the other hand, changing growth parameters in a CVD process is a tedious task, because of the complex growth kinetics and chemistry. MBE is much more flexible, because of the large supersaturation and the absence of gas phase and surface chemical reactions. It is therefore an obvious step to optimize doping and composition profiles by MBE, and subsequently transfer the results to the CVD reactor in the production plant.

With this in mind we started a FFF-funded collaboration with Austria Mikrosysteme (AMS) in Unterpremstätten. The efforts to develop optimized HBT profiles with SiGeC base are twofold. On the one hand, layer sequences are deposited on unstructured substrates, large-area implanted and annealed. These reference samples serve for structural investigations. They are mainly characterized by x-ray, SIMS and optical spectroscopy to optimize the Ge, carbon and boron profiles. Even more important is the electrical characterization on real devices that have seen the complete fabrication process. For this purpose we overgrow by MBE preprocessed wafers provided by AMS. These have seen all process steps prior to the deposition of the $Si_{1-x}Ge_x$:B or $Si_{1-x-y}Ge_xC_y$:B base layer, and were subsequently reintroduced into the production line and processed to operational circuits. With some adjustments to our regular cleaning and epi-deposition process, we were able to demonstrate device-quality epi-layers. Also, the MBE process was found to be compatible with the CMOS part of the circuits, which was almost completed before MBE overgrowth. With these results an essential precondition for the optimization of the layer sequence has been fulfilled. The next steps will now be to optimize the HBTs with respect to their electrical and structural properties under genuine fabrication conditions.

2. E-beam lithography

2.1 Shadow masks for selective silicon epitaxy

While epitaxial layers allow vertical structuring with resolutions down to the thickness of an atomic layer, lateral nanostructuring is limited by the lithographic resolution, which is in most cases further hampered by inhomogeneous damage induced by reactive ion etching (RIE). Selective epitaxy is an alternative, which allows vertical and lateral structuring as the epilayers are deposited. This requires an adequate mask layer on the substrate, which has to be compatible with the epitaxial process and permits selective growth in the windows that expose the substrate.

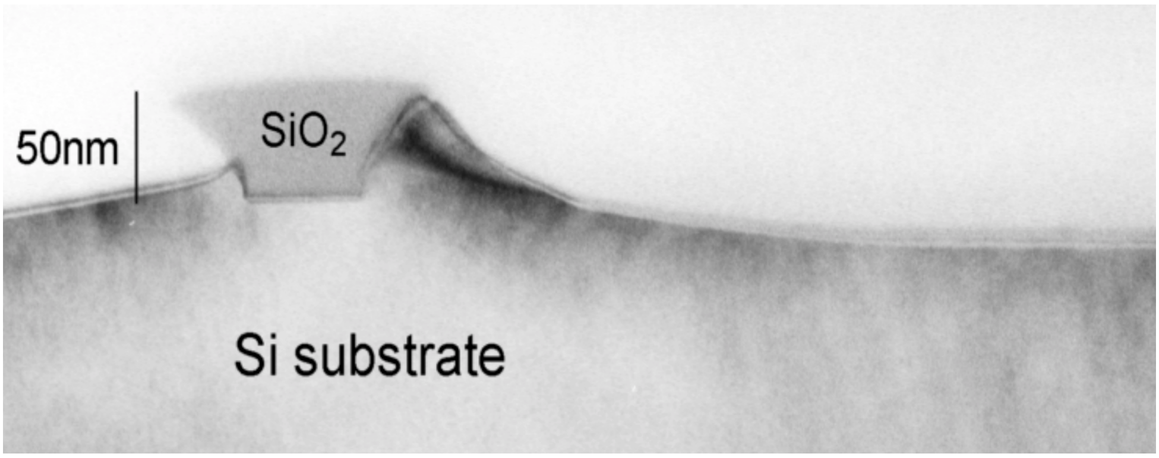

Fig. 2: Cross sectional TEM micrograph of a SiO_2 wire on a Si substrate after thermal heating at 950 °C in an UHV environment.

For Si epitaxy an SiO_2 mask is perfectly suited: It leads to epitaxial growth in the windows and to polycrystalline growth on the mask in the case of MBE and low-temperature CVD.

Under certain CVD growth conditions it is even possible to suppress deposition on the SiO_2, which is then a truly selective process, in contrast to the aforementioned standard c-Si/poly-Si process, which is occasionally referred to as “differential” epitaxy.

One of the main problems of differential epitaxy is the lateral boundary between the c-Si and poly-Si areas: Poly grains tend to grow into the c-Si areas and thus reduce the lateral resolution with respect to the resolution of the mask. Even worse, this boundary is electrically not well defined and can introduce undesired leakage currents. To overcome this problem, shadow masks have been introduced, which provide an undercut of the mask layer to separate the c-Si and the poly-Si areas by a physical gap. Frequently, a Si_3N_4/SiO_2 mask is employed, which is structured by RIE in a first step and then treated with an isotropic etchant that selectively attacks the lower lying SiO_2 layer to create the undercut. Because the second step is usually a wet chemical process (HF or BHF), the achievable resolutions are limited.

We could show that a defined undercut can be created thermally in a simple SiO_2 mask [7]. The basic mechanism is the same that is exploited for the thermal desorption of a natural oxide prior to MBE growth. A Si atom from the substrate has to diffuse to the SiO_2 surface to create SiO, which desorbs at high enough temperatures: $Si + SiO_2 \rightarrow 2\ SiO\uparrow$. In our experiments it turned out that at about 900 °C, when this reaction sets in, the surface mobility of Si atoms in the epi-windows is unexpectedly high, which leads to a significant mass transport. Since Si wets SiO_2, a surface flow of Si atoms toward the flanks of the SiO_2 mask occurs. These act as sinks because of the thermal desorption of SiO that consumes one Si atom for every SiO_2 molecule desorbed. Since the main source for the additional Si atoms is the exposed Si surface, SiO_2 desorption is more pronounced where the SiO_2 flanks are in contact with the Si substrate. This leads to the desired undercut, as is illustrated in Fig. 2.

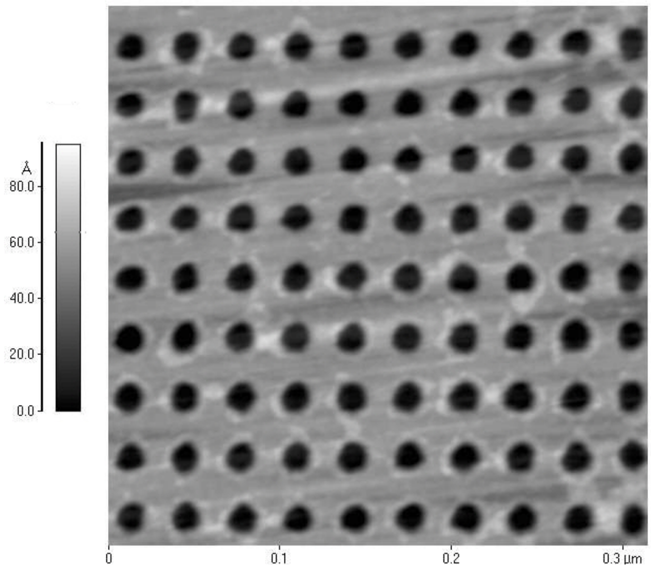

Fig. 3: E-beam lithographically structured dot-array with 150 Å diameter dots transferred into an SiO_2 layer by reactive ion etching.

It shows a cross sectional TEM micrograph of an array of SiO_2 wires, which had a rectangular cross section before the thermal treatment. The trapezoidal shape revealed in the figure is caused by the described mass transport at 950 °C in the UHV atmosphere of the MBE chamber, and can be fine-tuned by adjusting the temperature and the duration of the annealing step.

By proper exploitation of this mechanism we expect to be able to create shadow masks with lateral dimensions much smaller than had been possible so far. Figure 3 shows as a precondition a dot mask with hole diameters of 150 Å fabricated by e-beam lithography and RIE. The next step will now be to thermally create a shadow mask that leaves the upper diameter of the windows untouched, while producing the negative slope of the flanks. This way SiGe or Ge quantum dots could be deposited in an organized, and thus addressable, way.

2.2 Nanometer-length Schottky gates

Based on the five-layer transistor FET process with Schottky gate and implanted Ohmic contacts, which has been presented in the last report, the main emphasis was now put on the implementation of Schottky gates structured by e-beam lithography. Initially, we employed a single layer of PMMA for the lift-off process of the Pd/Au Schottky gates. With this simple process the parameters for mark recognition and exposure where derived. We also optimized the mesa separation of the devices, which is a critical process in Si because the surface is not naturally depleted as in most III-V materials. It turned out that mesa structuring prior to gate deposition is beneficial, especially when the gates overlap slightly with the mesa flanks. This way, complete pinch-off without any spurious parallel channel could be achieved. Figure 4 shows in the upper part SEM micrographs of a complete transistor without gate pad (right hand side), and of the gate region (left hand side) of a transistor with a 100 nm gate. The lower part shows the I-V characteristics of this device, which demonstrates the excellent pinch-off behavior at a gate voltage of –0.3 V. Due to the high Schottky barrier of 0.9 eV for Pd on n-Si, forward-bias voltages up to 0.4 V could be applied without significant leakage currents. The rather small absolute current levels are due to the relatively large gap between source and drain, which adds series resistance, and the relatively low carrier concentrations of this particular device, which was still based on a single-sided doping supply layer. The new double-sided doped layer sequences and a mask redesign with reduced source/drain gap will significantly improve these shortcomings.

After demonstrating the capability of our e-beam system to produce 100 nm gates with a single layer approach, multi-layer resist schemes were implemented to reduce the Ohmic resistance along the metal gate structure. This is important for high-frequency applications, and is usually achieved by gates with a T or Γ shaped cross sections. This way the contact area, and thus the effective gate length, can be kept in the nanometer range, whereas a low Ohmic resistance is achieved by the lateral expansion of the cross section above the contact area.

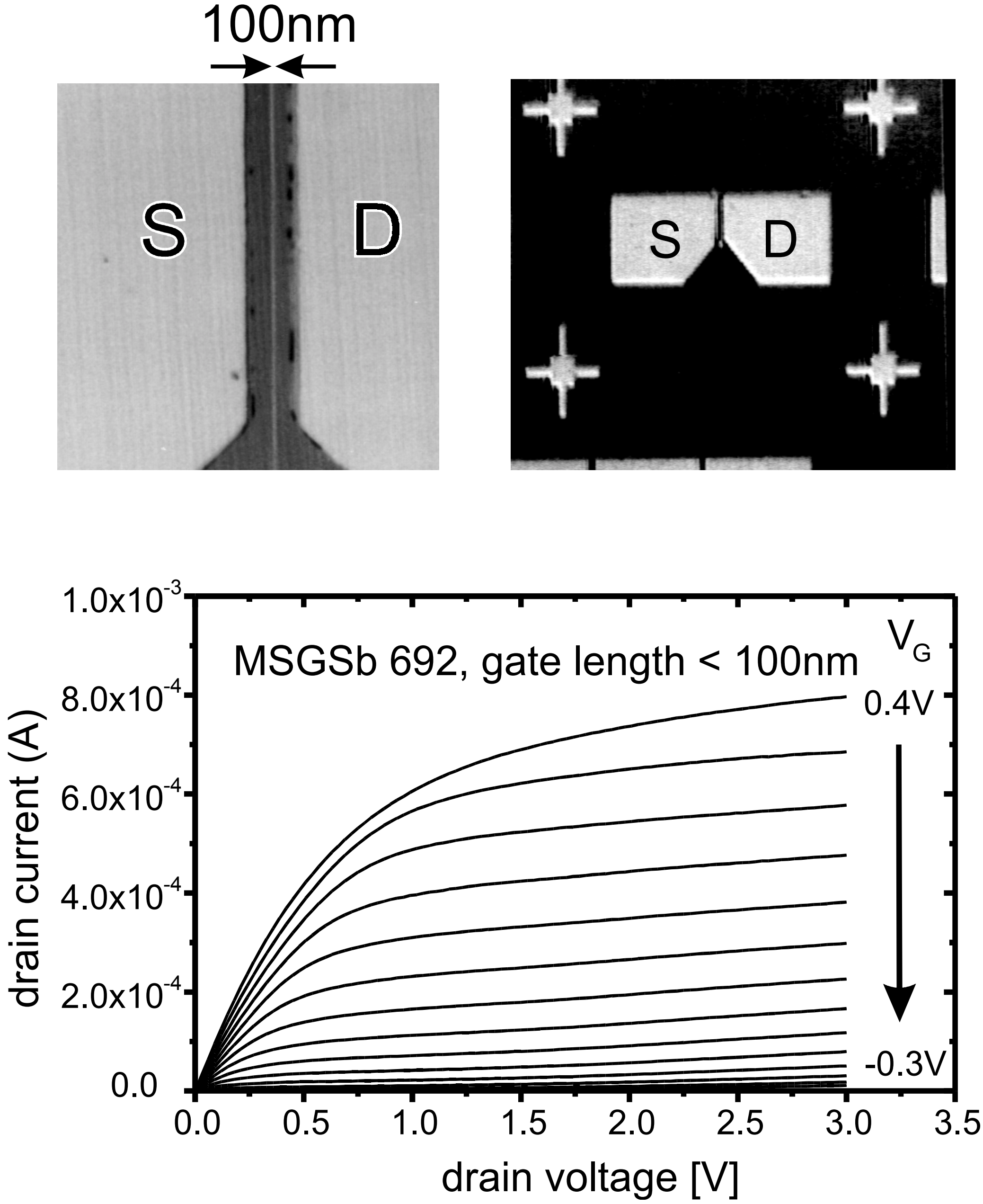

Fig. 4: SEM micrographs and I-V characteristics of a Si/SiGe MODFET with 100 nm gate.

Figure 5 shows an example of a T gate fabricated this way. The process involved three layers of resist, namely low sensitivity PMMA layers in the contact area and as a top resist, and a high sensitivity copolymer in between. e-beam exposure consists of three lines written with different doses: The middle line defines the contact area, which yields about 150 nm gate length in the depicted example. The two outer lines define the wings of the T, and were kept at a low enough dose to expose the copolymer, but not the PMMA layers. This scheme creates a negative flank due to the insensitive upper PMMA layer and such allows for easy lift-off even of gate films whose thickness approaches that of the three layer resist system. Further improvements aim now toward higher aspect ratios by employing thicker resist layers. This requires an optimization process, because thicker layers are concomitant with reduced resolution.

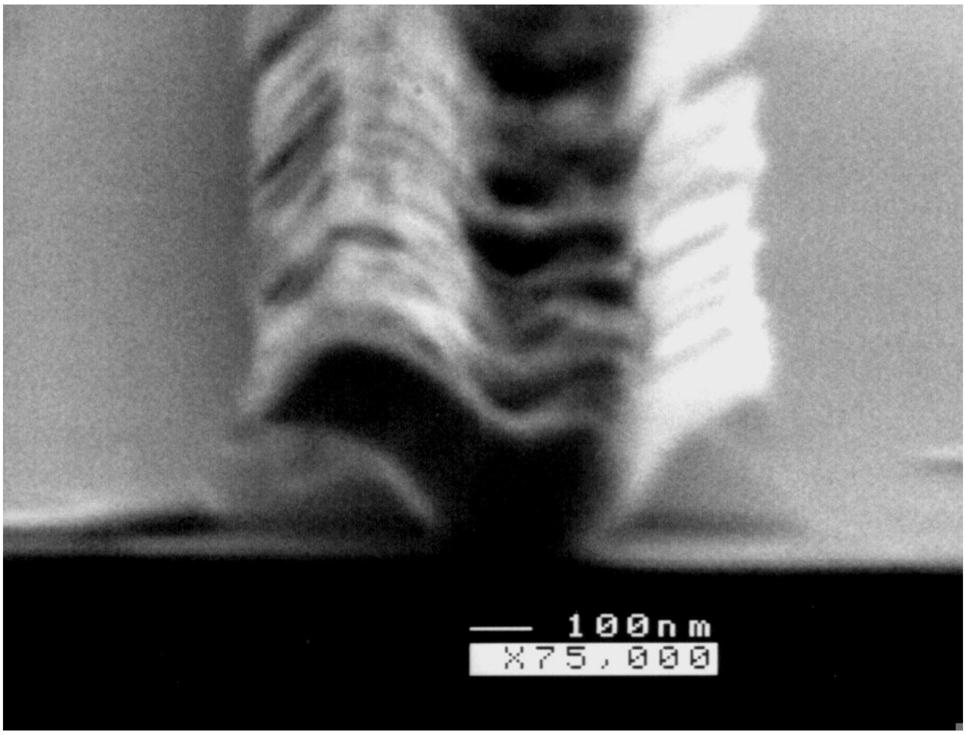

Fig. 5: Cross section of a T gate with a gate length of 150 nm.

Acknowledgements

Collaboration with M. Schatzmayr (AMS), and AMS funding in connection with the FFF-Project "SiGe-Technology" are gratefully acknowledged. We also thank S. Senz (MPI Halle, Germany) for providing x-sectional TEM micrographs, and B. Voigtländer (FZ Jülich, Germany) for giving us access to his in-situ STM installation.

References

[1] Y.H.Phang, C.Teichert, M.G.Lagally, L.J.Peticolos, J.C.Bean, E.Kasper, *Phys. Rev. B* **50**, 14435 (1994)

[2] J.Tersoff, Y.H.Phang, Z.Zhang, M.G.Lagally, *Phys. Rev. Lett.* **75**, 2730 (1995)

[3] C.Teichert, J.C.Bean, M.G.Lagally, *Appl. Phys. A* **67**, 675 (1998)

[4] C.Schelling, G.Springholz, F.Schäffler, *Phys. Rev. Lett.* **83**, 995 (1999)

[5] T.E.Whall, J. Cryst. *Growth* **157**, 353 (1995)

[6] J.Zhu, K.Brunner, G.Abstreiter, *Appl. Phys. Lett.* **73**, 620 (1998)

[7] Y.Zhuang, C.Schelling, J.Stangl, C.Penn, S,Senz, F.Schäffler, T.Roch, A.Daniel, J.Grenzer, U.Pietsch, G.Bauer, *"Structural and Optical Properties of Si/Si$_{1-x}$Ge$_x$ Wires"*, Thin Solid Films (in print)

Si/SiGe Nanolithography and Si/SiGe Wires

Y. Zhuang, C. Schelling, A. Daniel, T. Roch, M. Mühlberger, F. Schäffler, G. Bauer

Institut für Halbleiter- und Festkörperphysik, Johannes Kepler Universität Linz, A-4040 Linz, Austria

S. Senz

Max-Planck-Institut für Mikrostrukturforschung, D-06120 Halle, Germany

$Si/Si_{1-x}Ge_x$ nanostructures (wires) were grown by local solid source molecular beam epitaxy using three kinds of masks: Si, SiO_2, and SiO_2/Si_3N_4. Photoluminescence measurements were performed to establish their electronic properties and to find out the most appropriate fabrication method. Their structural properties were studied by transmission electron microscopy to obtain information on the shape of cross sections, and by x-ray coplanar and grazing incidence diffraction, which yielded depth-dependent in-plane strain distribution in the wires as well as in the substrate, which was compared to results of finite element calculations.

1. Introduction

Reactive ion etching of Si/SiGe quantum wells is known to result in structures with sidewall defects, which drastically decrease their luminescence efficiency [1], [2]. Consequently, several groups have developed techniques for the direct growth of Si/SiGe quantum wells with finite lateral widths, i.e. of wires, using local solid source [3] – [5] or gas source molecular beam epitaxy (MBE) [6], [7]. In particular, by local MBE growth through shadow masks Si/SiGe wire-like structures were fabricated with lateral dimensions down to 100 nm [5]. Ge rich self-organized quantum dots down to 70nm were selectively grown into windows defined by holes in SiO_2 masks by Kim et al. [6].

We report on selectively grown Si/SiGe multilayers using three different kinds of masks: Si, SiO_2 and SiO_2/Si_3N_4. It turns out that on patterned substrates the conventional cleaning step to remove the oxide by heating the wafers up to 950 °C results in a remarkable change of the substrate surface profile indicating significant mass transport [8] – [10]. Photoluminescence was observed from wire structures for all three types of masks, however. The highest efficiency was obtained with deep etched Si masks. We investigated the structural properties of locally grown heterostructures by using transmission electron microscopy (TEM) and high resolution x-ray diffraction. With the latter technique we obtain information on the strain status of the locally grown Si/SiGe wires, their lattice relaxation and the strain status of the substrate close to the surface, induced by patterning and overgrowth. The experimental results on the lattice strain are compared with finite element calculations.

2. Experimental

2.1 Sample preparation

Periodic $Si/Si_{1-x}Ge_x$ wire structures were grown by MBE through three different kinds of shadow masks, shown schematically in Figs.1 and 2, which represent the SiO_2, the SiO_2/Si_3N_4 shadow masks, and the deep etched Si mask. In the first sample series (Fig. 1 (a)), a 105 nm thick thermal SiO_2 layer was laterally structured into wires with periods of 800 nm. In the grooves on the Si surface, $Si/Si_{1-x}Ge_x$ multilayer structures were deposited. In the second series (Fig. 1 (b)), the thermal SiO_2 layer was capped with a 150 Å Si_3N_4 layer. After reactive etching, the SiO_2 layer was selectively etched by HF to create an undercut and thus lead to a Si_3N_4 shadow mask. $Si/Si_{1-x}Ge_x$ multilayers were grown on the Si(001) substrate through this Si_3N_4 shadow mask. In the third series, the 105 nm thick thermal SiO_2 layer was laterally structured into wires with periods of 800 nm and then the Si was deep etched to about 300 nm. Holographic lithography was performed using an Ar ion laser operating at a wavelength of 458nm, the plasma etching was performed in an Oxford Plasmalab with a parallel plate reactor. For Si etching, a mixture of SF_6 with CH_4 was used, for Si_3N_4 and SiO_2, a mixture of CF_4 with H_2.

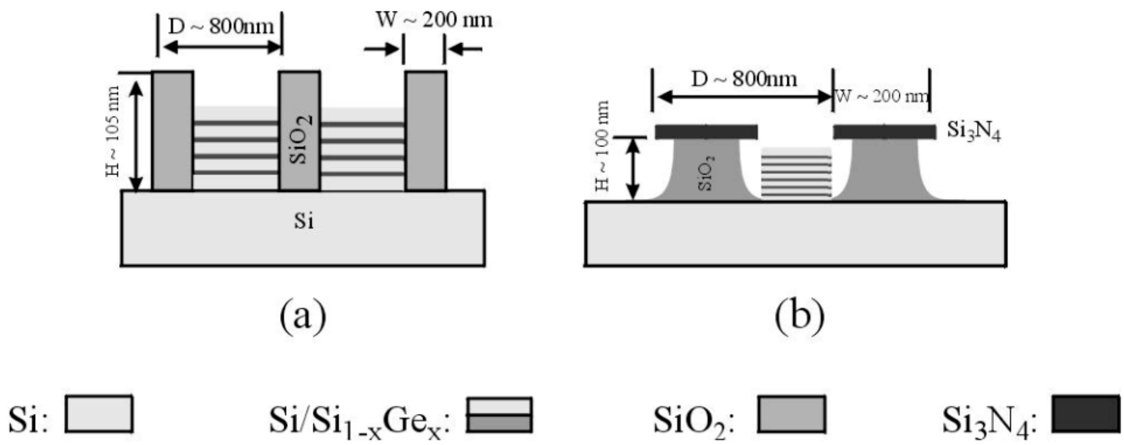

Fig. 1: Sketch of the Si/SiGe MQW wire grown through a SiO_2 and a SiO_2/Si_3N_4 shadow mask with lateral periods of about 800 nm.

2.2 Experimental results: photoluminescence

Prior to the growth of $Si/Si_{1-x}Ge_x$ MQWs on the patterned substrates, a 6 minutes thermal annealing step at 950 °C was employed to desorb the oxide layer generated during an HF free RCA cleaning procedure. From the TEM we find that this thermal-cleaning procedure leads to a significant mass transport and change of the surface profile. This mass transport is absent for a cleaning procedure involving a thermal treatment at only 650 °C. The Si substrate remains flat, and the MQW structure does not wet the etched SiO_2 wires.

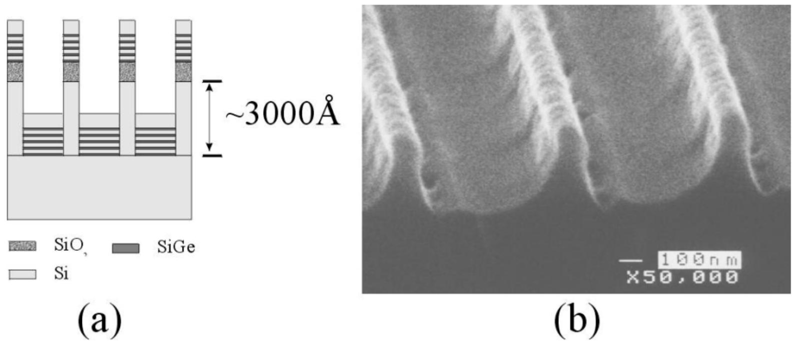

Fig. 2: (a) Sketch of the Si/SiGe MQW wires grown is deep etched Si; (b) scanning electron micrograph cross sectional view after MBW wire growth.

Photoluminescence spectra from the selectively grown Si/$Si_{1-x}Ge_x$ MQWs for the two kinds of masks shown in Fig.1 are presented in Fig.3. For these samples the conventional cleaning step at 950 °C was performed. The PL spectra were acquired at 4.2 K using an excitation laser wavelength of 488 nm, normal incidence and a power density of 0.4 W/cm^2. For the Si_3N_4 shadow mask a lift-off was performed by selective wet chemical etching. The observed Si/$Si_{1-x}Ge_x$ MQW PL lines correspond to the no-phonon line (NP), and its transverse optical phonon replica (TO). Signatures from the Si/$Si_{1-x}Ge_x$ quantum wells with finite lateral size are clearly observed for growth through both kinds of masks. It also turned out that the overall PL intensity of the wire structures is smaller for those grown between the SiO_2 wires, which exhibit high defect densities at the side wall boundaries to the oxide. Compared to such samples, a significant improvement of the luminescence efficiency (Fig. 4) is obtained for those grown into deep etched Si (Fig.2) , for which the cleaning step at 950°C was performed. The intensity from the Si/SiGe wires is higher than that from the Si substrate, which demonstrates the high PL efficiency from the wires. The FWHM of the PL lines from the wires is of the order of 10 meV, comparable to that of quantum wells. This clearly offers further possibilities for the fabrication of such high performance devices which need local epitaxial overgrowth. The lateral wire width does not yet induce any quantum confinement, this can only be observed for sizes smaller than about 40nm.

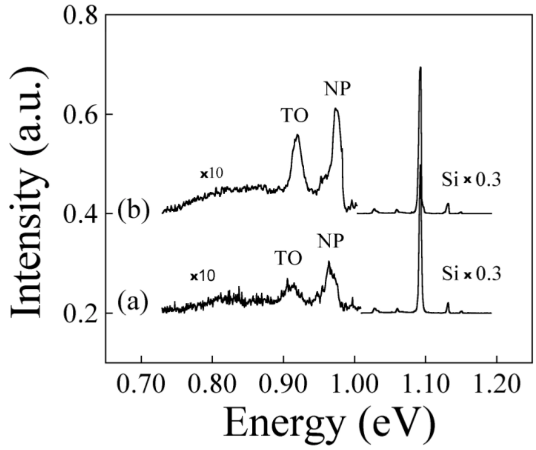

Fig. 3: PL spectra of Si/SiGe wire structure growth through the periodic SiO_2 mask (a) and through the SiO_2/Si_3N_4 mask (b).

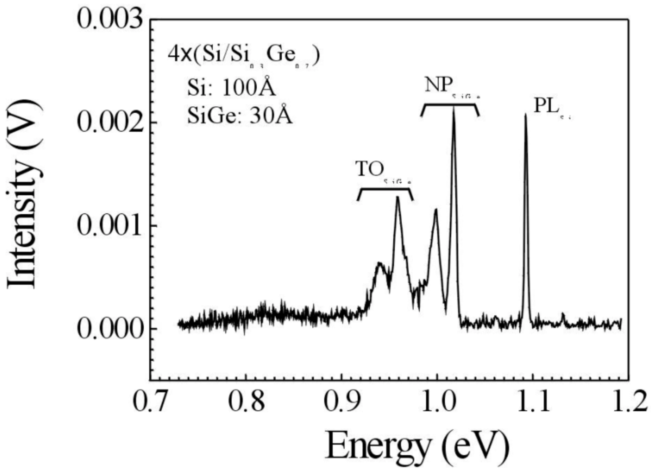

Fig. 4: PL spectra of Si/SiGe wire structure growth through the periodic SiO_2 mask in the deep etched Si wires (sample SEM shown in Fig. 2 (b)).

2.3 Strain investigations

For the strain analysis we use high angle x-ray diffraction and grazing incidence diffraction (GID) for resolving changes of the strain status with depth from the free surface and a comparison with finite element calculations. HRXRD measurements were performed for obtaining the average in-plane and vertical strain tensor components ε_{xx} and ε_{zz}, using reciprocal space maps around the (004) and the (224) reciprocal lattice points [7]. In Fig. 5, three q_x-scans (q_x denotes the x component of $q = 4\pi\sin\theta_B/\lambda$, θ_B is the Bragg angle and λ the wavelength), recorded in the vicinity of the (224) reciprocal lattice point are shown.

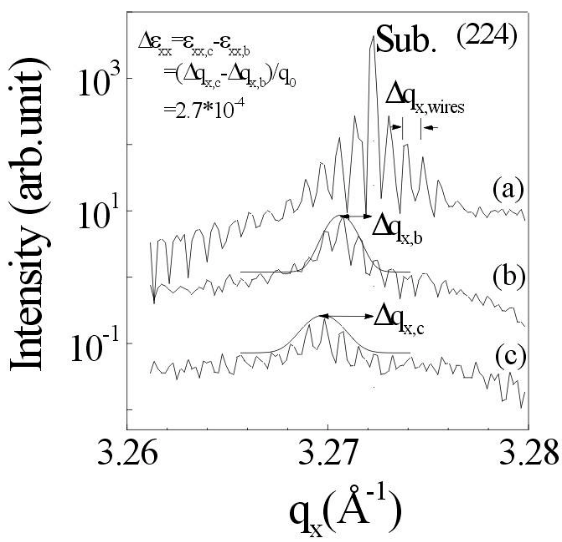

Fig. 5: X-ray diffraction of wire sample: q_x-scans in the (224) reciprocal space map across the substrate (a), the SL_0 peak (b) before removing the wire mask, and after removal of the shadow mask (c) .

Due to the orientation of the scattering vector perpendicular to the wires, several grating peaks appear, which reflect the lateral periodicity D of the wires: $D = 2\pi/\Delta q_{x,wires}$. Curve a is a scan through the Si substrate, b and c are scans through the 0^{th} order Si/SiGe superlattice peak (SL_0) corresponding to data obtained on a wire sample (Fig. 1 (b)) before and after the removal of the Si_3N_4/SiO_2 mask, respectively. From the shift of the envelope maxima for the wire samples (Fig. 5 (b) and (c)) with respect to the substrate peak (a), the mean in-plane strain $<\varepsilon_{xx}>$ is obtained to be $<\varepsilon_{xx,a}> = 4.8\times10^{-4}$ and $<\varepsilon_{xx,b}> = 7.5\times10^{-4}$, respectively. Apparently, after removing the SiO_2/Si_3N_4 mask (Fig.5 (c)) the in-plane lattice relaxation of the SiGe/Si wire structure becomes *larger*.

In order to explain these observations, finite element (FEM) calculations were performed to describe the inhomogeneous strain distribution present in the wires. The calculated results (Fig. 6 (a), (b)) clearly show that the strain distribution is very inhomogeneous. In $Si_{1-x}Ge_x$ MQW layers the maximum strain relaxation occurs close to the edge of the wires. The in-plane strain is larger at the top of the wires than it is at the bottom, reflecting the larger relaxation at the top. The strain extending into the Si substrate has both tensile and compressive components. The presence of the SiO_2 mask causes a tensile force to the substrate, which reduces the in-plane lattice relaxation in the SiGe wires (Fig. 6 (a)) . Removing the SiO_2 mask (Fig. 6 (b)), the tensile force disappears, leading to further elastic lattice relaxation in the substrate and consequently to an enhancement of the relaxation in the Si/SiGe wires.

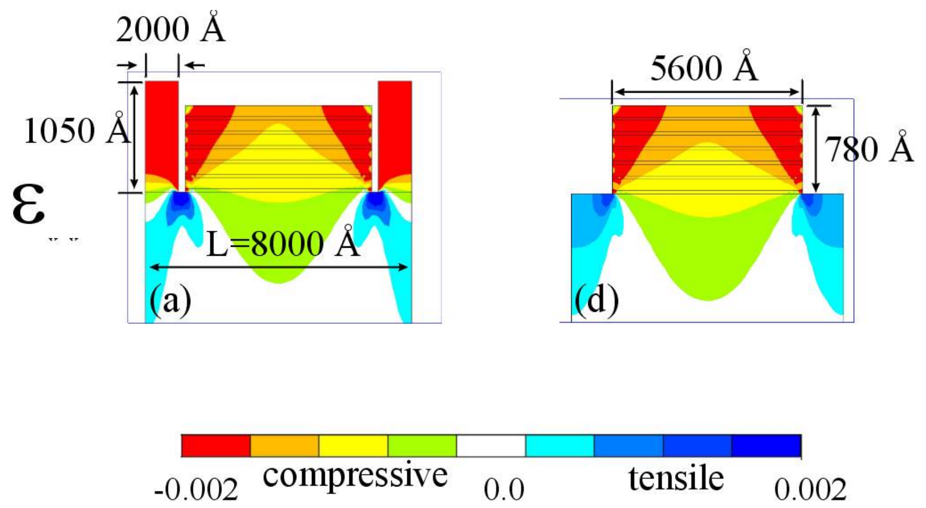

Fig. 6: Contour plots of strain tensor component ε_{xx} obtained from finite element calculations for a Si/SiGe wire sample (Fig.1b) with the mask (a) and after removal of the shadow mask (b).

3. Conclusion

SiGe quantum wells with finite lateral size grown by solid source MBE, using three different kinds of masks, were investigated with respect to their structural and optical properties. It turns out that the luminescence efficiency of wires grown into deep etched Si is much higher compared to those grown with oxide masks alone. This is due to the fact that defects at the interfaces are avoided. Detailed investigations of the lattice strain were performed both experimentally using x-ray diffraction techniques and theoretically by finite element calculations. The in-plane lattice strains are depth dependent and change after the patterned mask layer is removed.

Acknowledgements

This work was supported by ÖAD (Y.Zh.), and by the FWF.

References

[1] T. Köster, J. Gondermann, B. Hadam, B. Spangenberg, M. Schütze, H. G. Roskos, and H. Kurz, *J. Vac. Sci. Technol.* B 14 (1996) 698.

[2] S.C. Jain, H.E. Maes, K. Pinardi, *Thin Solid Films* 292 (1997) 218.

[2] J. Brunner, T. S. Rupp, H. Gossner, R. Ritter, I. Eisele, and G. Abstreiter, *Appl. Phys. Lett.* 64 (1994) 994.

[3] J. Brunner, P. Schittenhelm, J. Gonderman, B. Spangenberg, B. Hadam, T. Köster, H. G. Roskos, H. Kurz, H. Gossner, I. Eisele, and G. Abstreiter, *J. Cryst. Growth* 150 (1995) 1060.

[4] M. Kim, H. J. Osten, A. Wolff, C. Quick, H. P. Zeindl, J. Klatt, and D. Knoll, *J. Cryst. Growth* 167 (1996) 508.

[5] E. S. Kim, N. Usami, and Y. Shiraki, *Appl. Phys. Lett.* 72 (1998) 1617.

[6] H. Hirayama, T. Tatsumi, N. Aizaki, *Appl.Phys. Lett.* 52 (1998) 2242.

[7] Y. Zhuang, V. Holy, J. Stangl, A. A. Darhuber, P. Mikulik, S. Zerlauth, F. Schäffler, G. Bauer, N. Darowski, D. Lübbert, and U. Pietsch, J. Phys. D: Appl. Phys. 32 (1999) A224; Y.Zhuang et al. *Journal of Materials Science: Materials in Electronics* 10 (1999) 215.

[8] M. E. Keeffe, C. C. Umbach, and J. M. Blakely, *J. Phys. Chem. Solids* 55 (1994) 965.

[9] Z. L. Liau, and H. J. Zeiger, *J. Appl. Phys.* 67 (1990) 2434.

[10] M. Ozdemir, and A. Zangwill, *J. Vac. Sci. Technol.* A 10 (1992) 684.

[11] N. Darowski, K. Paschke, U. Pietsch, K. Wang, A. Forchel, D. Lübbert and T. Baumbach, *Physica* B 248 (1998) 104.

Self-organized Growth of SiGe and SiGeC Quantum Dots and Wires

J. Stangl, T. Roch, V. Holý, G. Bauer

Institut für Halbleiter-und Festkörperphysik, Johannes Kepler Universität A-4040 Linz, Austria

O.G. Schmidt, C. Lange, K. Eberl

Max-Planck-Institut für Festkörperforschung, D- 70569 Stuttgart, Germany

J. Zhu, K. Brunner, G. Abstreiter

Walter Schottky Institut, TU München, D- 85748 Garching, Germany

The lateral ordering, the size and shape of SiGe and SiGeC self-organized nanostructures, which were grown by molecular beam epitaxy, was investigated by grazing incidence small angle x-ray scattering and by atomic force microscopy.

1. Introduction

SiGe nanostructures can be realized by lateral patterning using lithography and etching or by self-organized growth. The latter method has the advantage that surface layer defects introduced by the fabrication procedure can be avoided. Its disadvantage is related to the rather broad size distribution. The FWHM of this size distribution can be diminished by depositing the self-organized nanostructures on suitable templates. This will also improve the lateral ordering. In this work Si/SiGe multilayers with high Ge contents, deposited on vicinal (miscut) Si substrates, which exhibit step-bunching, were used as templates for the subsequent growth of Ge rich islands and for wires oriented along the direction of steps. In order to achieve sufficiently small islands which exhibit three dimensional quantization effects, carbon induced islands have to be grown, which exhibit typical sizes of about 3 to 15 nm, accompanied by a much higher island density. Moreover, these carbon induced quantum GeC dots embedded in Si exhibit the *most intense* photoluminescence compared to all other Si based heterostructures.

2. Experimental

For improving the lateral ordering of Ge rich islands and wires on Si, we have investigated two samples of similar nominal structure, using atomic force microscopy (AFM), x-ray diffraction (XRD), and grazing incidence small angle x-ray scattering (GISAXS). Sample R826 is a 20 period $Si_{0.55}Ge_{0.44}$/Si multilayer grown by molecular beam epitaxy on (001) oriented Si substrate with a miscut of 2° towards [100] direction. Each multilayer sequence consists of 2.5 nm SiGe and 10 nm Si spacer layer. Sample R888 with the same nominal structure was grown on the vicinal (001) Si substrate with a miscut of 3.5° inclined towards [100] direction.

Furthermore we investigated buried C induced Ge quantum dot multilayers grown on (001) Si by molecular beam epitaxy. Using grazing incidence small angle x-ray scattering (GISAXS) we determined the shape, the mean radius, height, and dot distance. The dot distribution is isotropic within the (001) interfaces, and no vertical correlation of the dot positions along [001] growth direction was found.

The investigated SiGeC sample was grown by solid source molecular beam epitaxy (MBE). After deposition of 0.2 ML C, 2.4 ML Ge were deposited and subsequently a Si spacer layer of 9.6 nm. This stacking sequence was repeated 50 times. After growth the sample was annealed for ~25 min at 600 °C. Since the size of the CGe dots and their distances are of the order of about 10 and ~30 nm, respectively, the corresponding distribution of scattered intensity in reciprocal space is very broad. Therefore the conventional coplanar scattering geometry cannot be used, and we have performed measurements in noncoplanar GISAXS geometry at Troïka II beamline at the ESRF.

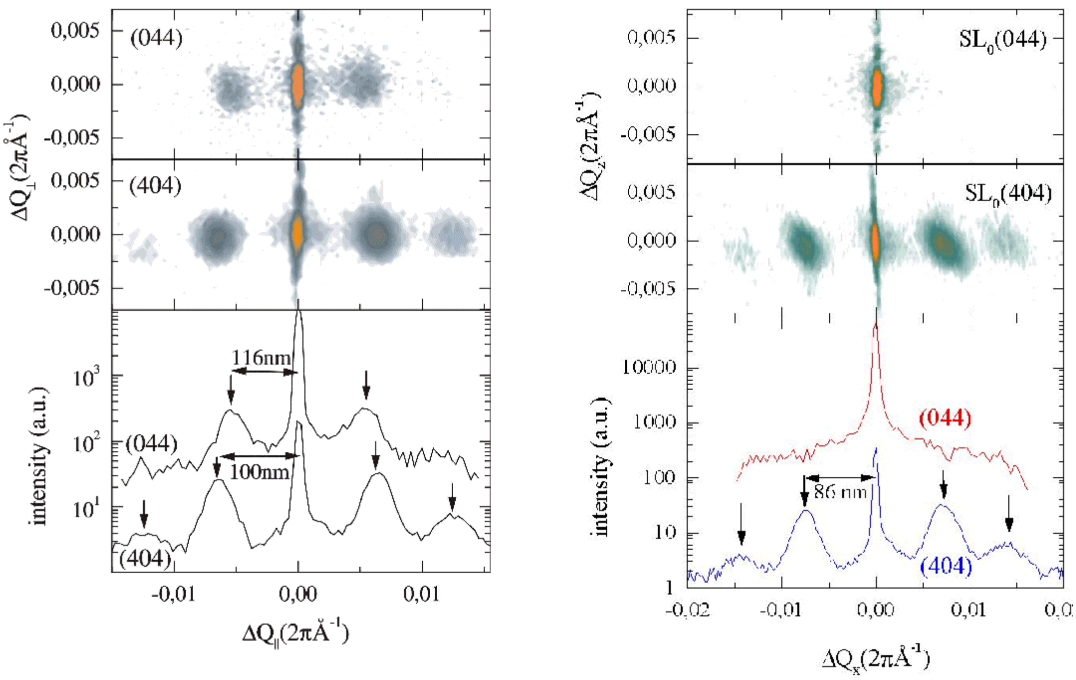

R826 R888

Fig. 1: Reciprocal space maps of samples R826 and R888 in two azimuths around (044) and (404) reflections, along steps and perpendicularly to them, respectively. The lower panels display the intensities integrated along $Q_\| = 0.005$ Å with the average dot and wire distances indicated.

In Fig.1 x-ray diffraction reciprocal maps are shown for the Ge rich island sample (R826) and for the Ge wire sample (R888) around the (044) and the (404) reflection, around the zero-th order superlattice satellite, corresponding to the azimuth along the steps and perpendicular to them, respectively. Diffusely scattered maxima for sample R826 show the correlation of dots position, which is significantly better in the direction perpendicular to the steps. For sample R888, the subsidiary maxima along Qx are missing. This indicates, that not ordered islands are present, but rather wires oriented along [010] direction, corresponding to the direction parallel to the steps. In the island multilayer R826, steps formed due to the bunching process lead to an alignment of buried dots along steps. The dots distances perpendicular to the step edges are very regular correlated by the step width, whereas the dot distances along the step edges show a significantly higher spread. In the R888 sample self-organized Ge-rich wires also at the buried interfaces are laterally ordered and oriented along the direction of the steps.

AFM area scans of the topmost surface (Fig. 2 (a), (b)) show clearly the presence of self-organized islands on the surface R826 and wires on the R888 sample surface. The average wire height is about 1 nm, whereas in the sample R826 the island height is about 4 nm. Autocorrelation spectra (Fig. 2 (c), (d)) can give an estimate on the size and shape of the coherent island domain (R826).

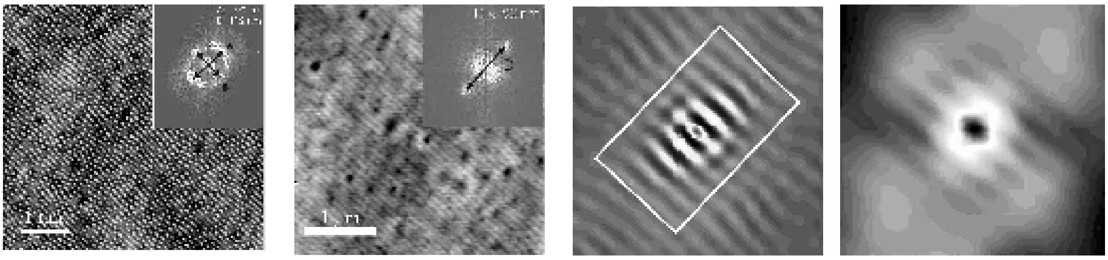

(a) R826 (b) R888 (c) R826 (d) R888

Fig. 2: AFM scans of the samples R826 (a) and R888 (b). The 2D power spectra (inset) show the mean distance of the wires. Autocorrelation spectra of samples R888 (d) and R826 (c) with the coherent dot domain (white line) 2x4, using a cutoff peak height of 10% of the central maximum.

The GISAXS spectra measured on the sample R826 at different azimuths are shown in Fig. 3 as a two-dimensional (2D) reciprocal space map. The 2D GISAXS data, which reflect the different ordering of the islands along the [100] and [010] directions for the buried island layers, agree very well with the surface morphology obtained by AFM. Hence in the azimuth parallel to the step edges the correlation of islands positions is significantly worse than perpendicular to the step edges.

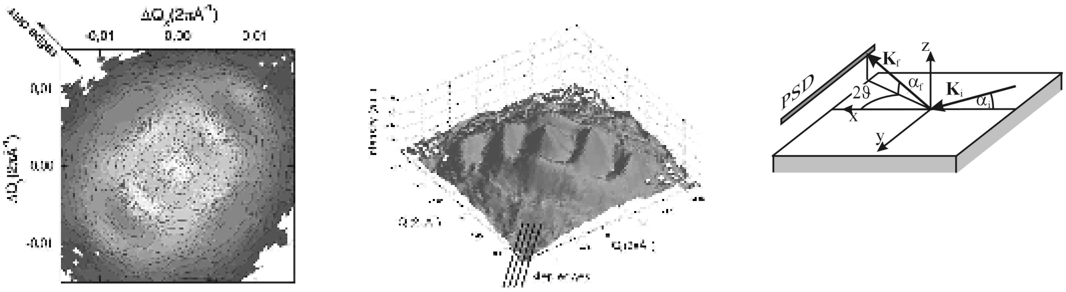

Fig. 3: GISAXS 2D map of the sample R826. The inset (right) shows the GISAXS measurement geometry, for incidence angle $\alpha_i = 1.1°$ and exit angle $\alpha_f = 0.6°$.

The GISAXS data for the GeC dots have been evaluated using an approach known from small-angle scattering [1]. The Fourier transformation of the measured intensity curve is shown in Fig. 4 (a). The maximum of $I^{FT}(r)$ at 30 nm corresponds to the mean distance between the dots. The region where $I^{FT}(r)$ is negative corresponds to a zone around each of the dots where the probability of finding a neighboring dot is *smaller* than that of a completely uncorrelated dot distribution. A good correspondence to the experimental data was found for a lens-like shape with a dot radius of R = (5.7 ± 0.3) nm and a height of about h = (1.7 ± 0.3) nm. These values agree reasonably well with AFM investigations of a single, uncapped CGe dot layer (see Fig. 4 (b)). From TEM investigations of the multilayer sample it is quite difficult to determine the exact dot dimensions due to the particularly large strain contrast in the CGe system. We found neither vertically nor laterally ordered dot distribution.

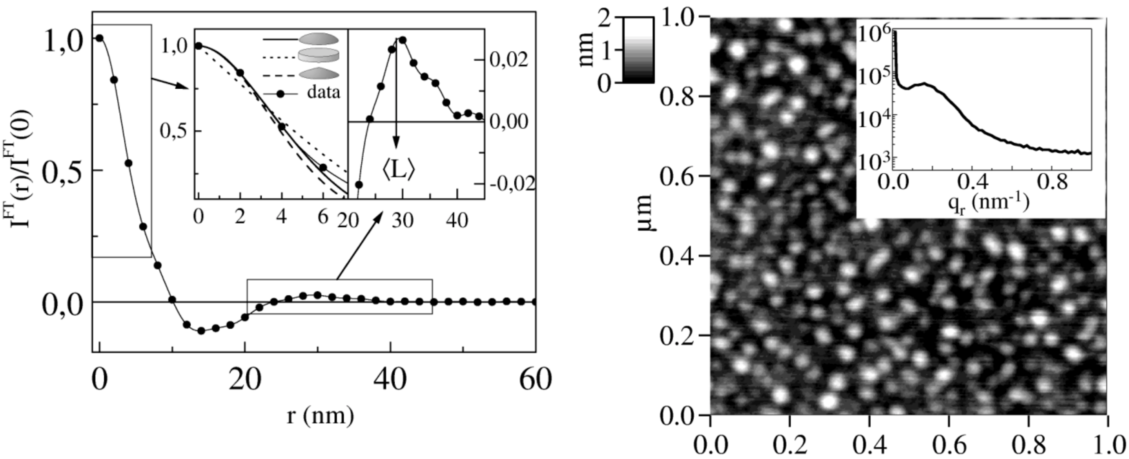

(a) (b)

Fig. 4: (a) Fourier transformation $I^{FT}(r)$ of the measured intensity for $\phi = 0$ (points). The insets show the best fit to the central peak for different dot shapes (left), and an enlargement of the peak around r = 30 nm, corresponding to the mean dot distance $\langle L \rangle$ (right). (b) AFM image of a single CGe dot layer with 0.2 ML C and 3 ML Ge. The insert displays its 2D Fourier transform, integrated along the polar angle. The peak around q_r = 0.2 nm^{-1} corresponds to the mean dot distance.

3. Conclusion

The structural properties of Si-based nanostructures were investigated by atomic force microscopy as well as by x-ray scattering techniques. The C induced Ge dots embedded in Si are promising for Si-based light emitting devices in the near infrared region.

Acknowledgements

This work was supported by the FWF and the BMWV, Vienna.

References

[1] J. Stangl, V. Holy, P. Mikulik, G. Bauer, I. Kegel, T.H. Metzger, O.G. Schmidt, C. Lange, K. Eberl, *Appl.Phys.Lett.* **74**, 3785 - 3787 (1999).

[2] K. Eberl, O. G. Schmidt, S. Schieker, N.Y. Jin-Philipp, And F. Philipp, *Solid State Electronics* **42**, 1593 (1998).

Scanning Tunneling Microscopy Investigations of Surface Undulations in Lattice-Mismatched Heteroepitaxy

G. Springholz and K. Wiesauer
Institut für Halbleiter- und Festkörperphysik, Johannes Kepler Universität, A-4040 Linz, Austria

The surface structure of relaxed IV-VI heteroepitaxial layers is studied using scanning tunneling microscopy. For bilayer structures consisting of highly relaxed EuTe layers covered by thick PbTe buffer layers, huge surface undulations with amplitudes as large as 50 Å are observed. These undulations are completely decoupled from the surface step structure and can be observed even for large cap thicknesses. The deconvolution of the surface profiles shows that the surface undulations are purely caused by the nonuniform misfit dislocation network at the EuTe/PbTe interface.

1. Introduction

Strained-layer heteroepitaxy is of considerable importance for semiconductor devices, offering more degrees of freedom in design and fabrication of modulated heterostructures and superlattices. In such structures, strain-engineering can be utilized as an additional method for adjustment of the electronic properties [1]. This is usually accomplished by predeposition of highly relaxed buffer layers as “virtual substrates” prior to the active layers. However, the strain relaxation often results in pronounced surface undulations of the buffer surface [2] – [8], such as the so-called “cross hatch” surface pattern on InGaAs [2] or SiGe [3] , [5] – [8] buffers. The origin of these undulations has remained a controversial issue. While some groups have proposed nonuniform growth due to localized dislocation strain fields [3], [7], [8], other groups have favored glide steps and lattice deformations [4] – [6]. Up to now, most studies have not been able to distinguish between these effects. In the present work, the evolution of the surface structure of highly relaxed IV-VI epitaxial layers was studied using scanning tunneling microscopy. These materials have been used extensively for the fabrication of mid-infrared diode lasers [9]. To circumvent the problems associated with the interdependence of strain relaxation and epitaxial growth, we have designed a bilayer structure, where first a highly lattice-mismatched layer is deposited to produce a dense network of misfit dislocations, followed by a nearly pseudomorphic second layer. In this two-step process, the dislocation formation within the first layer is completely decoupled from the growth of the subsequent layer.

2. Experimental

The bilayer EuTe/PbTe samples were grown by molecular beam epitaxy on 3 μm PbTe buffer layers predeposited on (111) BaF_2 substrates. Both compounds crystallize in the rock salt crystal structure and their lattice-mismatch is 2.1%. First thick PbTe buffers were deposited on the substrate, which yields high quality epitaxial layers with very smooth surfaces [10]. Onto these buffers, EuTe layers with thicknesses exceeding the critical thickness were grown in order to form a network of misfit dislocations with well defined dislocation density. Although the critical thickness for misfit dislocation formation is 18 monolayers (ML) for the EuTe/PbTe case [4], significant strain relaxation does not occur before 40 ML when dislocation multiplication sets in. The highly dislocated layers were overgrown by PbTe cap layers with thicknesses varying from 0.1 to 3 μm. For the study of the evolution of surface morphology, the samples were rapidly cooled and transferred to an UHV-STM chamber for surface imaging. The strain state of the layers and corresponding overall misfit dislocation densities were determined by high x-resolution x-ray diffraction. To access the large scale surface morphology, the samples with thick cap layers were also studied by AFM under ambient conditions.

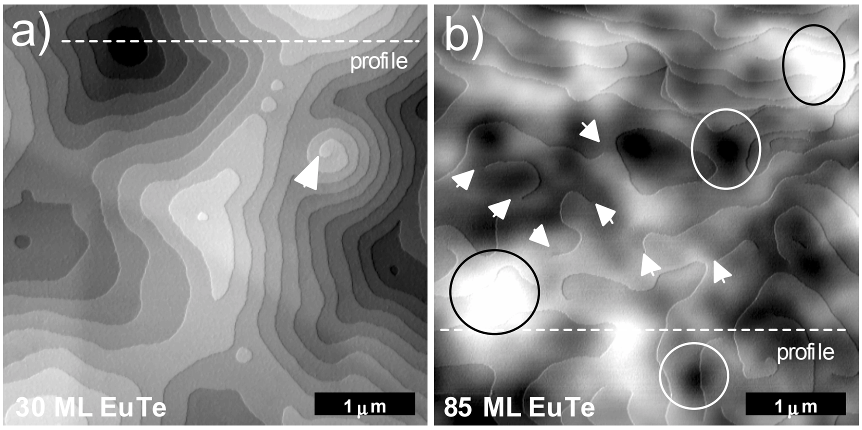

Fig. 1: STM surface images of two PbTe/EuTe bilayer samples with an EuTe layer thickness of (a) 35 ML and (b) 85 ML, but with identical 1000Å PbTe cap thickness. The arrows indicate the penetration points of threading dislocations and the surface profiles along the dashed lines are shown in Fig. 2. The strong surface contrast observed for the highly relaxed sample (b) and indicated by the circles arises from large scale surface undulations that are not correlated with the monolayer step structure.

3. Results

The STM images of two bilayer samples with different EuTe layer thicknesses but identical 1000 Å PbTe cap thickness are shown in Fig. 1. The first sample with an EuTe thickness of d_{EuTe} =30 ML is a nearly pseudomorphic structure with a negligible number of misfit dislocations (relaxed strain of less than 0.01% from x-ray diffraction). As shown in Fig. 1 (a), the surface of this sample exhibits an evenly spaced terrace structure that is essentially identical to that of the underlying PbTe buffer layer [10], with occasional threading dislocations (see arrow) that remain from the growth on the lattice-mismatched BaF_2 substrates. The measured threading dislocation density is about 10^7 cm^{-2} in this sample, which is typical also for the PbTe buffer layers [10].

In contrast, the STM image of the highly relaxed sample (Fig. 2 (b)) with d_{EuTe} = 85 ML (six times the critical thickness) reveals a completely different surface structure. The highly irregular surface steps consists of many short segments terminated by threading dislocations. In fact, the threading dislocation density of 10^9 cm^{-2} in this sample is a factor of 100 larger than that of the PbTe buffer layers. This is a clear indication for the formation of misfit dislocations at the EuTe/PbTe interfaces, with a corresponding increase of the threading dislocation density due to dislocation nucleation and multiplication processes.

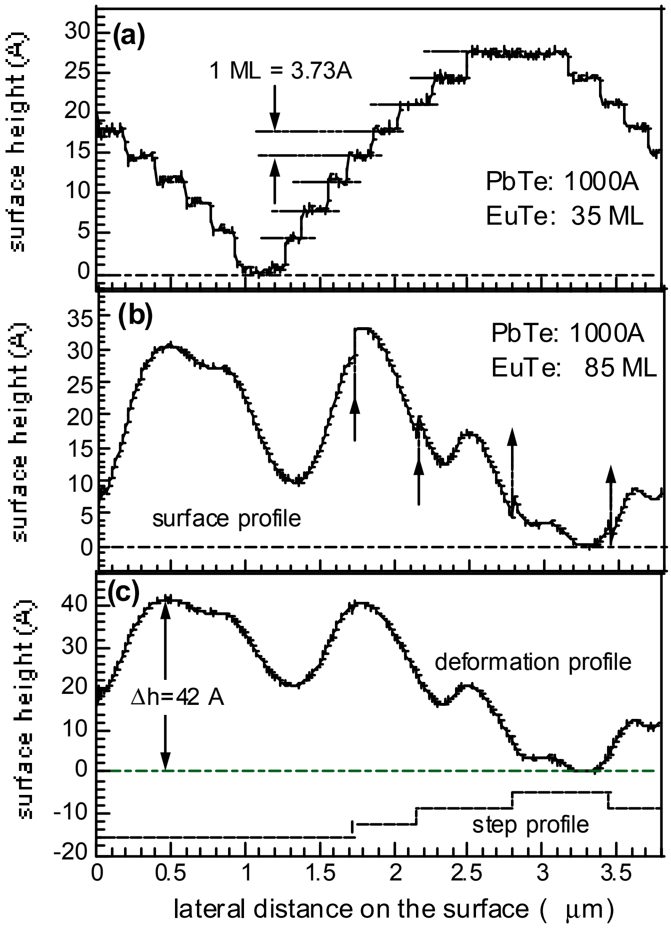

Fig. 2: Measured scanning tunneling microscopy surface profiles along the dashed lines in Fig. 1: (a) pseudomorphic structure with d_{EuTe}=30 ML, and (b) relaxed sample with d_{EuTe} = 85 ML. (c) shows the deconvoluted deformation profile (full line) and the step profile (dashed line) derived from the measured profile (b).

Even more, however, a very strong black and white contrast appears in the STM images, as is indicated by the circles in Fig. 1 (b). The corresponding local depressions and elevations of the surface of up to 50 Å by far exceed the changes in surface height due to the monolayer steps, and their lateral extent is typically between 0.5 and 1 µm. Apparently, these large scale surface undulations are not correlated to any steps on the surface, but appear on the flat terraces as well as across single monolayer steps that separate adjacent terraces. Therefore, they cannot be related to growth effects but must arise from large inhomogeneous strain fields within the misfit dislocation networks at the buried heterointerfaces.

The completely different surface structure of the two samples is even more evident from the comparison of the STM surface profiles measured along the dashed lines in Fig. 1.

Whereas for the pseudomorphic structure (Fig. 2 (a)), the surface profile consists only of a train of monolayer surface steps with 3.73 Å step height, the profile of the highly relaxed sample (Fig. 2 (b)) exhibits large scale *continuos* undulations superimposed on the surface steps. Since the individual surface steps in the STM profiles are well resolved, this surface profile can be deconvoluted into two contributions: one from the usual surface step structure (arrows in Fig. 2 (b)), and one from continuos wave-like deformations of the epitaxial surface. Figure 2 (c) shows the deconvoluted step and deformation profiles (dashed and full lines, respectively), clearly indicating that the contribution of the lattice-deformation by far exceeds that of the usual surface steps. Thus, most part of the observed surface morphology is not related to growth features.

The origin of the large-scale surface undulations can be explained as follows. As shown by our previous STM work [11], each *individual* subsurface misfit dislocation gives rise to a local deformation of the surface with an amplitude of the order of the dislocation Burgers vector (4.4 Å). The width of the deformation profile increases linearly with layer thickness, but its amplitude remains constant. Consequently, the factor ten larger surface undulation observed in the present samples must arise from the constructive overlap of the deformation fields of many individual misfit dislocations concentrated at certain areas of the interface. For a *regular* network of misfit dislocations, the surface displacements from evenly distributed dislocations would cancel out completely as soon as the depth of the dislocations is about three times larger than the dislocation spacing because the width of the individual deformation profiles is equal to the dislocation depth [11]. For *irregular* dislocation networks this is not necessarily the case. Considering a period of the surface undulations of the order of 1 µm, the existence of bunches of up to 10 individual dislocations explains the observed large scale surface undulations. Such bunches of dislocations are indeed consistent with the measured average dislocation densities of 75 μm^{-1} in our samples.

4. Conclusions

In conclusion, we have shown that the large lattice distortions in highly dislocated lattice-mismatched heteroepitaxial layers give rise to large scale continuous undulations of the epitaxial surface. We do not find any indication that the corresponding inhomogeneous elastic strain fields influence the growth processes on the surface. This general conclusion should apply also for most other strained-layer heteroepitaxial systems.

References

[1] see e.g., F. Schäffler, *Semicond. Sci. Technol.* 12, 1515 (1997).

[2] K. H. Chang, R. Gibala, D. J. Srolovitz, P. K. Bhattacharya, J. F. Mansfield, J. *Appl. Phys.* 67, 4093 (1990).

[3] J. W. P. Hsu, E. A. Fitzgerald, Y. H. Xie, P. J. Silverman, and M. J. Cardillo, Appl. *Phys. Lett.* 61, 1293 (1992).

[4] N. Frank, G. Springholz, and G. Bauer, *Phys. Rev. Lett*. 73, 2236 (1994).

[5] M. A. Lutz, R. M. Feenstra, F. K. LeGoues, P. M. Mooney, and J. O. Chu, *Appl. Phys. Lett.* 66, 724 (1995).

[6] H. Li, G. Springholz, F. Schäffler, G.Bauer, *J. Vac. Sci. Technol.* B16, 1610(1998).

[7] C. Mou and J. W. P. Hsu, *Phys. Rev.* B 53, R7610 (1997).

[8] T. Pinnington, C. Lavoie, T. Tiedje, B. Haveman, *Phys. Rev. Lett.* 79, 1698 (1997).

[9] D. L. Partin, *IEEE J. Quantum Electron.* 24, 1716 (1988).

[10] G. Springholz, A. Y. Ueta, N. Frank, G. Bauer, *Appl. Phys. Lett*. 69, 2822 (1996).

[11] G. Springholz, *Appl. Surf. Sci.* 112,12(1997)¸and *Appl. Phys. Lett.* 75, 3099 (1999).

Self-organized Hexagonal Lateral Ordering of Self-Assembled Quantum Dots in PbSe/$Pb_{1-x}Eu_xTe$ Superlattices

M. Pinczolits, G. Springholz, and G. Bauer
Institut für Halbleiter- und Festkörperphysik, Johannes Kepler Universität, A-4040 Linz, Austria

Lateral ordering and size homogenization of self-organized PbSe quantum dots in strain-symmetrized PbSe/PbEuTe superlattices was studied. From the investigation of the dot structure of superlattices with the number of periods varying from 1 to 100, it is shown that a nearly perfect lateral hexagonal PbSe dot lattice is formed already after a few periods. Because the ordering mechanism is based on the non-vertical alignment of the PbSe dots in the stack, the in-plane spacing of the dots as well as the dot sizes remain constant within each PbSe layer throughout the whole superlattice growth. Therefore, extremely homogenous three-dimensionally ordered quantum-dot arrays are formed.

1. Introduction

The spontaneous formation of three dimensional (3D) islands in strained-layer heteroepitaxy has recently evolved as a novel technique for the fabrication of self-assembled quantum dots [1], [2]. Such defect-free islands embedded in a higher band gap matrix material have proven to exhibit excellent electronic properties due to the effective quantum confinement of the charged carriers in all three directions. For practical device applications, however, the considerable variations of size and shapes within the large ensemble of quantum dots has remained a critical issue. In multilayers of self-assembled quantum dots, the vertical interaction of dots via their elastic strain fields may lead to a gradual improvement in size homogeneity, as well as to a more uniform lateral island spacing [3], [4]. This self-organization is a result of the overlap of the localized strain fields of neighboring buried islands, with a preferred nucleation of the subsequent islands on the surface where the elastic energy exhibits a local minimum. For self-assembled SiGe/Si [3] or InAs/GaAs [5] quantum dot superlattices, it has been found that in spite of the lateral ordering tendency between the vertical columns of self-assembled dots, a substantial increase of the island size as well as lateral island separation occurs during superlattice growth. Thus, the overall size homogeneity of the quantum dots in multilayers is not necessarily improved.

2. Experimental

In the present work we have studied the evolution of lateral ordering of self-assembled quantum dots in PbSe/PbEuTe superlattices. In these structures, the layer thicknesses and the composition of the PbEuTe spacer layers were adjusted to achieve a full strain-symmetrization of the superlattice stack with respect to the PbTe buffer layer. This allows the fabrication of superlattices with an arbitrary number of periods without changes in the strain status of the layers and without risk of misfit dislocation formation.

The samples were grown by molecular beam epitaxy on fully relaxed PbTe buffer layers predeposited on (111) oriented BaF_2 substrates. For all samples, the superlattice stack consisted of 5 monolayers (ML) PbSe alternating with 470 Å of PbEuTe, using growth rates of 0.08 ML/s and 3.5 Å/s, respectively, and a substrate temperature of 360 °C. To study the evolution of lateral ordering, samples with superlattice periods from N = 1 to 100 were prepared, where the last PbSe quantum dot layer was left uncapped for further analysis. After growth, the samples were rapidly cooled to room temperature to freeze-in the epitaxial surface morphology and the surface structure was imaged by atomic force microscopy (AFM) directly after removal of the samples from the MBE system. AFM measurements were carried out using an AutoProbe CP AFM and sharpened Micro- and Ultralevers of Park Scientific Instruments. Special image processing software was used for real space statistic analysis of the dot size distributions on the one hand, and for frequency space analysis of the degree of lateral ordering using Fast Fourier Transformation and Autocorrelation function analysis.

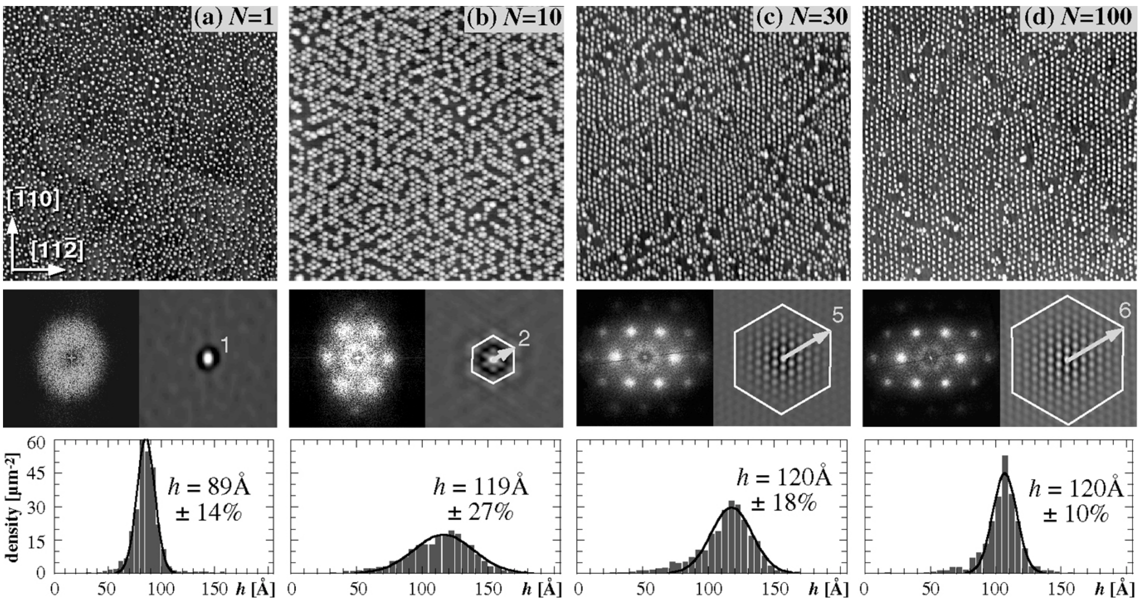

Fig. 1: Top: 3 x 3 μm^2 AFM images of (a) a single PbSe quantum dot layer and of the last dot layer of PbSe/PbEuTe dot superlattices with periods of 10 (b), 30 (c), and 100 (d). Center panel: FFT power spectra (left side) and auto correlation spectra (1x1) μm^2, right side). Lower panel: Height histograms of the PbSe dots determined from the AFM images. Abscissae indicate the dot height, the ordinates the areal dot density, and the full lines are Gaussian fits of the histograms.

A crucial aspect of our work was the adjustment of the ternary composition of the PbEuTe spacer layers, in order to achieve a full strain-symmetrization between the tensively strained PbSe layers and the compressively strained PbEuTe layers. In such a case, the in-plane lattice-constant of the free standing superlattice stack matches the lattice constant of the PbTe buffer layer, and therefore, an arbitrary number of superlattice periods can be deposited without misfit dislocation formation. Since the PbSe dot layers are under tensile strain (mismatch of –5.54 % with respect to PbTe), strain-symmetrization can be achieved only by using a spacer material that has a lattice-constant larger than PbTe. This is the case for the ternary PbEuTe, for which the lattice-constant increases with increasing Eu content. Strain-symmetrization is then achieved by equating the strain-thickness product of the two superlattice layers, as shown in detail in Ref. [6].

3. Results

Figure 1 shows a series of AFM images of the last uncapped PbSe dot layer of samples consisting of N = 1, 10, 30 and 100 SL periods. For the single layer (Fig. 1 (a)), the PbSe islands are distributed randomly on the surface without any preferred lateral correlation direction. With increasing number of SL periods, a rapidly progressing ordering of the dots occurs. Already after 10 periods, the dots are preferentially aligned in single and double rows along the <–110> directions (Fig. 1 (b)). With further increasing number of bilayers, larger and larger ordered regions are formed (see Fig. 1 (c) and (d)). For samples with N > 30, the perfect hexagonal arrangement is disrupted only by single point defects, such as missing dots, dots at interstitial positions, or occasionally, by additionally inserted dot rows (”dislocations”). The development of the lateral ordering was determined by Fourier transformation (FFT) as well as auto correlation (AC) analysis of the AFM images as shown in the center panel of Fig. 1. The FFT power spectrum of the N = 1 single dot layer AFM image exhibits a broad ring around the frequency origin. By fitting cuts through the ring in several directions with Gaussians, we obtain a mean peak position of about 12.5 μm^{-1} corresponding to an average dot distance of 800 Å. The width (FWHM) of this ring of ± 47% indicates a substantial variation of the lateral dot separation. This width is essentially independent of the surface direction, i.e., no preferred lateral alignment of the islands exists in any surface direction. In addition, the AC spectrum of the AFM image (see Fig. 1) does not exhibit any structure outside of the central maximum, indicating the lack of any lateral correlation of the dot positions.

In contrast, the FFT power spectrum of the 10 bilayer sample (Fig. 1 (b)) clearly shows six pronounced side maxima, corresponding to a mean spacing of the dot rows of 590 Å. Six side maxima appear also in the AC spectrum, which indicates that the next nearest neighbors of the dots are aligned along the <–110> directions, with a preferred dot-dot distance of 680 Å within the rows. Apart from the six side maxima, the FFT power spectrum also exhibits a well defined ring at a spatial frequency of one third of the side peaks, and this ring also exhibits a hexagonal symmetry. From a closer inspection, it is found to be due to the “missing rows” in the dot arrangement because on average every third dot row is missing (Fig. 1 (b)). For the 30- and 100-period superlattices, the peaks in the FFT spectra drastically sharpen, and many higher order satellite peaks are observed (Fig. 1(c) and (d), respectively). As shown in Fig. 2 (b), the relative FWHM of the satellite peaks, mainly reflecting the variation of the mean dot-dot distance, narrows from about ± 47% for the single layer to ± 6% for the 100-period superlattice, i.e., the dot-dot spacing during superlattice growth becomes increasingly well defined. In addition, the AC spectra reveal the formation of large perfectly ordered dot domains, with a correlation of the dot position over up to ten nearest neighboring dots. The corresponding domain sizes are indicated by the hexagons in the AC images of Fig. 2.

To gain information on the influence of ordering on the dot size variation, we analyzed the evolution of the island height distribution as a function of the SL periods.

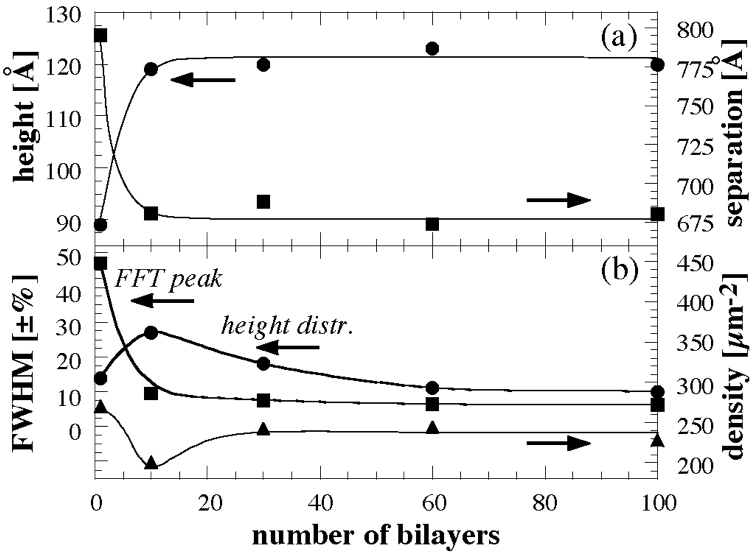

Fig. 2: Dot parameters plotted as a function of the number of the number SL periods: (a) Average dot height (dots) and average lateral dot separation in the <–110> directions determined from the separation of the satellite Fourier peaks (squares). (b) FWHM of the satellite FFT peaks and of the dot height distributions (dots and squares, respectively), and areal density of the PbSe dots (triangles).

The lowest panel in Fig. 2 shows the Gaussian-fitted height histograms of the PbSe dots determined from the statistical evaluation of several 2x2 μm^2 AFM images with a minimum of 750 single PbSe dots for each sample. The obtained average island heights and the height variations are plotted in Fig. 2 (a) and 2 (b), respectively, versus number of SL periods. For the single PbSe dot layer, at 5 ML coverage the average island height is 89 Å with a variation of ± 14%. In spite of the fact that lateral ordering sets in already after the first few SL periods, the dot height distribution at first actually broadens to ± 27% after 10 SL periods, and only thereafter decreases to reach a value of ± 10% for N = 100. A complementary transient behavior is observed for the areal dot density (see Fig. 2 (b)), which at first decreases up to 10 bilayers and then gradually increases again for higher N. With respect to the island shapes, we find no indication that the ordering process influences the dot shape.

4. Conclusions

The evolution of lateral ordering in self-organized PbSe/PbEuTe quantum dot superlattices was studied. Due to strain symmetrization, dot superlattices with large number of superlattice periods could be prepared without strain relaxation by misfit dislocation formation. From atomic force investigations it was demonstrated that remarkably homogenous 3D ordered arrays of PbSe dots are obtained. In comparison to other dot superlattice systems, the in-plane spacing of the dots, the dot sizes, and the material distribution between the wetting layer and the islands remain essentially constant throughout the whole SL growth. This yields a significant improvement of the size homogeneity of the quantum dots, which is of crucial importance for any device applications.

References

[1] D. Leonard, M. Krishnamurty, C. M. Reaves, S. P. Denbaar, and P. Petroff, Appl. Phys. Lett. 63, 3203 (1993).

[2] J.M. Moison , F. Houzay, F. Barthe, L. Leprince, E. Andre, and O. Vatel, Appl. Phys. Lett. 64, 196 (1994).

[3] J. Tersoff, C. Teichert, and M.G. Lagally, Phys. Rev. Lett. 76, 1675 (1996).

[4] G. Springholz, Holy, M. Pinczolits, and G. Bauer, Science 282, 734 (1998).

[5] G. S. Solomon, S. Komarov, J. S. Harris, and Y. Yamamoto, J. Cryst. Growth 175/176, 707 (1997).

[6] M. Pinczolits, G. Springholz and G. Bauer, Phys. Rev. B 60, 11524 (1999).

Light Emission from Er-Doped Si Diodes

W. Jantsch, G. Kocher, L. Palmetshofer, H. Przybylinska, M. Stepikhova and H. Preier

Institut für Halbleiter- und Festkörperphysik, Johannes Kepler Universität, A-4040-Linz, Austria

Depending on the incorporation and annealing conditions and the oxygen content, erbium produces a big variety of different centers in silicon and silicon related materials. Isolated centers can be excited by electron-hole pair recombination produced by forward bias in a diode with surprisingly high quantum efficiency below 100 K, but they are strongly quenched at higher temperatures. Another type of spectrum – with a much higher line width (~20 nm) and weak thermal quenching up to 370 K – is obtained after annealing at temperatures above 950 °C. This type of spectrum is identified as being due to Er in $SiO_{2-\delta}$ precipitates. Such centers have much smaller quantum efficiencies for forward bias excitation than for reverse bias. We present a study on the optimization of LED structures based on this type of centers for room temperature operation.

1. Introduction

Silicon is the by far most widely used material in microelectronics: More than 95% of the electronic devices are fabricated from it. There is only one area in which Si cannot be used so far, namely that of light generation, because of fundamental physical reasons [1]. On the other hand there is large interest in the integration of Si-based optoelectronics into Si technology for a substantial number of different applications like inexpensive displays, data communication on very different scales ranging from optical interconnects within a chip, *e.g.*, within a microprocessor as a replacement of one of the metallic interconnect planes or within a smart power electronics chip where galvanic separation of the intelligent and the high power parts are necessary. Optical communication is the main component of high performance long distance communication lines already and will be even more so in the foreseeable future where every household will be connected by an optical fiber for TV programs, internet, etc. Also for the control of complex systems, like cars or factories, the conventional wiring of sensors and actuators will be reduced to a power supply line and an optical bus, the latter steering each device via an intelligent optoelectonic device.

In recent years several concepts have been developed and investigated in order to obtain room temperature light emission from Si [1], [2]. Many of the concepts are based on the destruction of translation invariance by structurization on nm scale, like in porous Si, or a-Si, or quantum dot formation. These concepts, some of which appear very promising, suffer still from one drawback: In order to achieve emission at a particular wavelength, the dimensions must be kept very precisely which up to now is not possible. An alternative that has been proposed for the optical communication at 1.5 µm is based on optical transitions within the 4f shell of Er in various hosts including Si [3], [4]. Recently, the achievement of light emitting diodes working at 1.54 µm has been reported [4]. In this report, we describe our progress in improving the output of such devices.

2. Luminescence excitation and quenching

We introduce Er into Si by ion implantation at energies of 300 keV and above. Because of the resulting lattice damage the samples are annealed after implantation at temperatures above 900 °C. If the implanted dose exceeds the amorphization limit, a two stage annealing procedure is chosen were the amorphous layer is recrystallized by annealing at 600 °C prior to the 900 °C step. Additional oxygen doping has been proven to have several beneficial effects and as an optimum ratio, we found a factor of 10 times higher O than Er dose where the O implantation is done at an energy that provides overlap with the Er profile. Figure 1 shows typical photoluminescence spectra taken at 77 K for two identically prepared samples, one annealed at 900 °C, the other at 950 °C. The 900 °C sample shows the typical spectra of isolated Er-O complexes which are well defined in their geometrical arrangement and thus they show sharp lines originating from a well defined crystal field [5]. The 950 °C sample, in contrast, shows a rather wide spectrum, indicative of inhomogeneous broadening. This type of spectrum has been identified by us as that of Er in $SiO_{2-\delta}$ precipitates [6]. Such precipitates are formed in oxygen rich material at annealing temperatures above 950 °C.

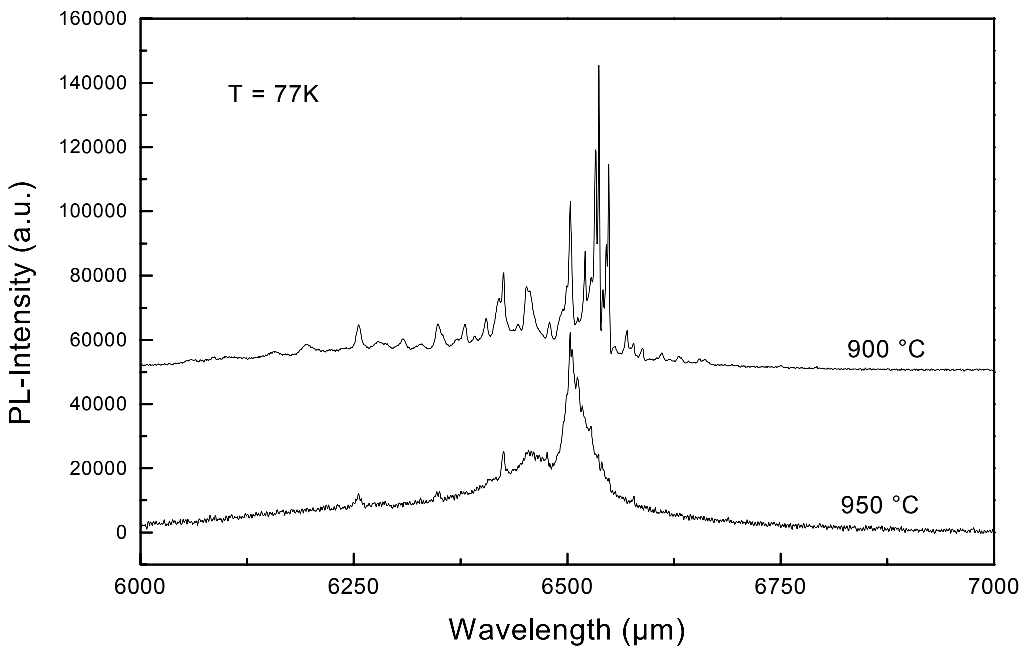

Fig. 1: Photoluminescence spectra of two Er and O implanted samples, one annealed at 900 °C, and one at 950 °C.

The two types of spectra show quite different quenching behavior: the isolated centers exhibit strong quenching already at 150 K whereas the precipitates can be observed up to 300 K. In photo-excitation, electron-hole pairs are excited and these are bound at some oxygen related defect level that acts as a “co-activator”. Finally the energy is transferred from the excited co-activator to the Er 4f shell where it causes the Er excitation. Finally, the Er relaxes to its ground state emitting a photon in the 1.5 µm band. The same type of mechanism is envisioned also for the forward bias excitation in a light emitting diode built from Si:Er. In Fig. 2, the quenching behavior is shown for photo- and electro-luminescence, the latter of diodes described below.

In Fig. 2 the temperature dependent luminescence intensity is given The quenching of the photoluminescence is ascribed to two processes: (i) back-transfer of the Er excitation to the coactivator and (ii) Auger transfer to free carriers [4]. Both processes are effective in forward biased diodes but they can be suppressed under reverse bias excitation as can be seen in Fig. 2. There the excitation is achieved by hot electrons transferring their kinetic energy to the Er 4f shell. Under reverse bias, the free carriers concentration is much lower in the junction and therefore the Auger process is ineffective. The back-transfer process is also suppressed, most likely because of smaller coupling of the 4f shell to coactivators (which are not needed here anyway) [6].

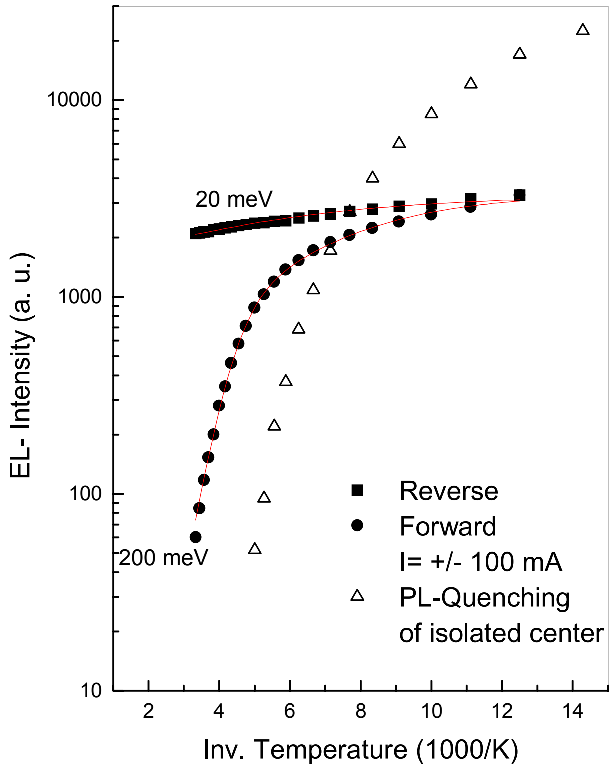

Fig. 2: Luminescence intensities of Si:Er for the isolated centers (triangles, photo- and forward bias give the same results) and for precipitates with forward bias (dots) and reverse bias (squares) excitation.

The quenching behavior shown in Fig. 2 clearly shows that room temperature emission can be achieved only on diodes containing precipitates under reverse bias excitation. Therefore we have concentrated in the following on the optimization of the precipitate luminescence excited by hot electrons.

3. LED design

There are two quantities to be optimized: (i) the size distribution of the precipitates and (ii) the volume in the diode in which precipitates are met by hot electrons. The first aim can be achieved by variation of the implantation doses and energies, the annealing procedures. Figure 3 shows typical results demonstrating that pre-annealing is of minor importance.

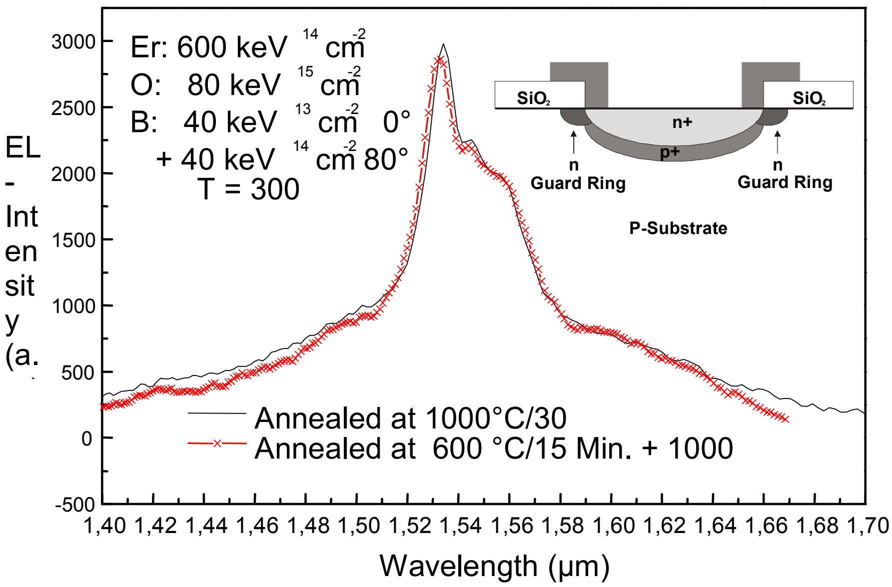

Fig. 3: Electroluminescence of two diodes operated at 300 K under reverse bias. The diodes were produced by different annealing procedures. The inset shows the diode structure schematically.

Finally, in order to optimize the excitation volume in the p-n junction we tried to design diodes for avalanche rather than tunneling breakdown. This can be achieved by a smaller doping gradient. The latter requires, however, careful design of the implantation profiles (Er is electrically active to some extent as a donor) and of the diode structure. In order to avoid breakdown at the edges, a guard ring design was used that improved both the I-V characteristics and the 1.5 µm emission at room temperature (see inset of Fig.3).

Acknowledgements

Work supported by the *Fonds zur Förderung der Wissenschaftlichen Forschung*.

References

[1] E.A. Fitzgerald and L.C. Kimerling, MRS Bulletin **23**, 39 (1998)

[2] P. M. Fauchet, J. of Luminescence 80, 53 (1999)

[3] H. Ennen, G. Pomrenke, A. Axmann, K. Eisele, W. Haydl, and J. Schneider, *Appl. Phys. Lett.* 46, 381 (1985)

[4] S. Coffa, G. Franzo, and F. Priolo, *MRS Bulletin* 23, 25 (1998)

[5] H. Przybylinska, W. Jantsch, Yu. Suprun-Belevitch, M. Stepikhova, L. Palmetshofer, G. Hendorfer, A. Kozanecki, R.J. Wilson and B.J. Sealy, *Phys Rev.* B 54, 2532 (1996)

[6] W. Jantsch, S. Lanzerstorfer, L. Palmetshofer, M. Stepikhova, H. Preier, *J. Luminescence* 80, 9 (1999)

[7] J. Stimmer, A. Reittinger, J.F. Nützel, H. Holzbrecher, Ch. Buchal and G. Abstreiter, *Appl. Phys. Lett.* 68, 23 (1996)

IV-VI Semiconductor Based Microcavities and Vertical Cavity Surface Emitting Lasers for the 4 – 6 µm Wavelength Range

W. Heiss, G. Springholz, T. Schwarzl

Microelectronics Institute, Johannes Kepler University Linz, A-4040 Linz, Austria

We have grown IV-VI semiconductor-based mid-infrared microcavities with very high quality factors by molecular-beam epitaxy. The used PbTe/EuTe Bragg mirrors with three to five periods exhibit reflectivities in excess of 99.7%. In a first order microcavity a very narrow Fabry-Perot resonance is observed with a full width at half maximum of 78 µeV. This corresponds to an ultra high effective finesse of 1700. Furthermore, we have demonstrated for the first time vertical laser emission in the 4 – 6 µm wavelength range from an optically pumped lead-salt microcavity.

1. Introduction

Microcavities consisting of high reflectivity Bragg interference mirrors have attracted tremendous interest during the last few years due to their unique physical properties and high potential for device applications. High quality microcavities with mirror reflectivities above 99 % are a prerequisite for vertical cavity surface emitting diode lasers (VCSELs). Other applications, for which moderate reflectivities are sufficient, include resonant cavity light emitting diodes and Fabry-Perot filters and modulators. Microcavities also exhibit interesting physical properties based on quantum optical effects, like cavity polaritons. Up to now the only semiconductors used for the fabrication of microcavity structures are III-V and II-VI compounds. In our present work we have explored the possibilities for fabrication of micro-cavities from IV-VI semiconductors for optoelectronic device applications in the mid infrared.

Laser devices for the mid infrared (MIR) range (2 – 30 µm) are of high interest due to the various gas absorption lines in this region permitting sensitive gas spectroscopy. The typical semiconductors used for that purpose are the lead salts (IV-VI semiconductors). These IV-VI lasers are all edge emitting devices. Thus, we explored the feasibility of surface emitting lead salt lasers in adopting the concept of microcavity lasers and demonstrated for the first time IV-VI vertical cavity surface emitting lasers (VCSELs) at 4.8 and 6.1 µm with high finesse PbEuTe/EuTe microcavity structures [1,2].

2. Microcavities with ultra high finesse

The IV-VI microcavities were fabricated by molecular beam epitaxy on (111) oriented BaF_2 substrates using PbTe and EuTe for the quarter wavelength layers in the Bragg mirrors, and PbTe as cavity material. The advantage of this combination of materials is the very high refractive index contrast of 90 % between the PbTe and EuTe layers. The design of the microcavity structures was based on theoretical calculations using the transfer matrix method, with the dispersion of the refractive indices of the layer materials determined by FTIR transmission measurements. The optical characterization of the multilayer samples was performed with FTIR transmission measurements.

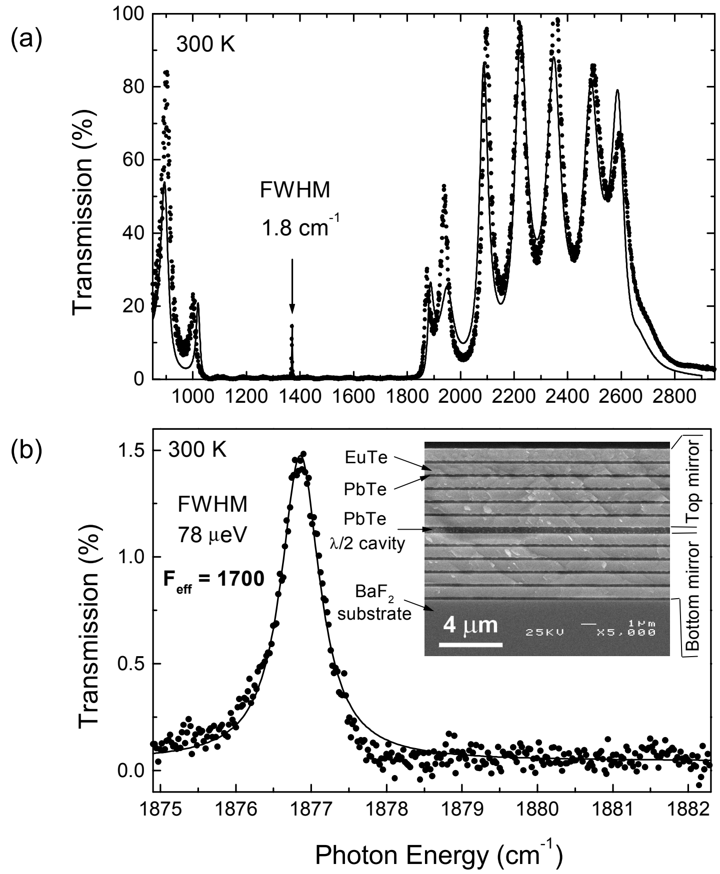

Fig. 1: FTIR transmission spectrum at 300 K of (λ/2) PbTe/EuTe microcavities with (a) a four pair bottom Bragg mirror and a three pair top mirror, and (b) five layer pair bottom and top Bragg mirror. The dots represent the measured data and the solid line the theoretical transmission spectrum calculated by the transfer matrix method. For (b) the peak was fitted with a Lorentzian, which yields a peak width of 0.63 cm^{-1} and an effective finesse of 1700. The inset shows a scanning electron micrograph of the selectively etched cleavage edge of the microcavity structure (b) with an additional (λ/4) EuTe top layer.

Figure 1 (a) shows the FTIR transmission spectrum at room temperature of a microcavity structure designed for an operation wavelength of 7.3 µm. It consists of four PbTe/EuTe Bragg mirror pairs at the bottom and three mirror pairs at the top of the sample, with a half wavelength PbTe cavity in between. The transmission spectrum exhibits a very wide stop centered around the cavity resonance at 1370 cm^{-1} (λ = 7.3 µm). Outside of the stop band Fabry-Perot interference appear with a transmission cut off at 2600 cm^{-1} due to the absorption edge of PbTe. The full width at half maximum (FWHM) of the cavity peak is only 1.8 cm^{-1}, providing evidence for the high quality of the microcavity. The FTIR spectrum around the cavity resonance for a microcavity with *five* PbTe/EuTe quarter wavelength layers as top and bottom mirrors is shown in Fig. 1 (b). The Lorentzian shaped sharp resonance at ν_r =1877 cm^{-1} (λ_r = 5.32 µm) exhibits a

FWHM of only 0.63 cm^{-1}, which corresponds to a cavity quality factor or finesse of 2980. Taking into account the finite penetration of the light into the Bragg mirrors with an effective cavity length of 1.74 for the given refractive index contrast, an *effective* cavity finesse of 1700 can be deduced [3]. This represents by far the highest finesse for any mid-infrared Fabry-Perot cavity reported so far, and even exceeds the best effective finesse value of GaAs/AlAs microcavities.

3. Vertical emitting mid-infrared laser structures

In the following, the fabrication of IV-VI semiconductor vertical cavity surface emitting lasers for the 4 – 6 µm range is demonstrated. The samples were grown by molecular beam epitaxy on (111) oriented BaF_2 substrates and consist of two distributed Bragg reflectors with λ/2 or 2λ microcavities in between. PbTe quantum wells (QWs) are inserted at the antinode positions of the cavity as laser active layers. For one set of samples (A), the Bragg mirrors consisted of PbEuTe layers with alternating Eu concentration [2] and with 18 and 24 periods for the upper and lower mirrors. For the second set of samples (B), the mirrors consisted of $Pb_{0.95}Eu_{0.05}Te$ alternating with EuTe layers. In this case, due to the very high refractive index contrast of over 80 % only three layer pairs are required to obtain ultra-high cavity finesses [1]. The VCSELs were optically pumped with pulsed laser excitation. Strongly forward directed stimulated emission was found at 6.07 µm for samples (A) at 25 K with a line width of 11 nm (370 µeV).

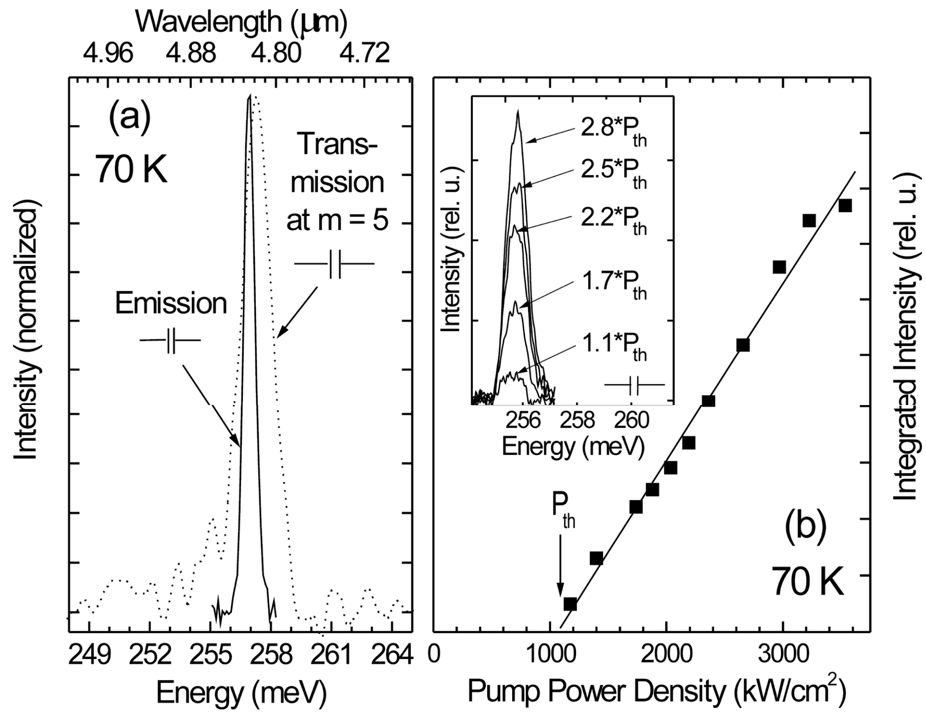

Fig. 2: (a) VCSEL emission spectrum (solid line) and corresponding cavity resonance peak (dashed line) from FTIR measurements at 70 K. The stimulated emission was induced by optical pumping with a $Nd:YV0_4$ laser.
(b) Integrated emission intensity at 4.82 µm versus pump power. The insert shows the emission spectra at various pump powers. The spectral resolution of the measurements is marked by –| |– .

The other VCSEL structure (B) emitted at 4.82 μm at temperatures between 35 K and 85 K (see Fig. 2) with an estimated threshold power density of about 5 kW/cm^2 and an emission line width of only 4 nm (210 μeV). The line widths linearly decrease with increasing pump power, as expected for laser emission. Both emission wavelengths agree with the microcavity resonances, and a pronounced spectral narrowing with respect to the cavity mode is observed. From a detailed analysis of the emission behavior, we find clear evidence that the maximum operation temperature is not due to intrinsic effects but is related to the detuning between the cavity mode and the spontaneous emission of the active material arising from the strong temperature dependence of the PbTe band gap. Therefore, much higher operation temperatures are expected for cavities with resonances matching the spontaneous emission at higher temperatures.

4. Summary

We have demonstrated the fabrication of ultra-high-finesse IV-VI microcavities for the mid-infrared spectral region using high-reflectivity PbTe/EuTe Bragg mirrors. Due to the high refractive index contrast between the materials, only three to five layer pairs are required for reflectivities over 99.7 %. Transmission measurements show one sharp resonance in the center of the mirror stop-band. From the full width at half maximum of the resonance peak, an effective finesse of 1700 was found.

In addition, we demonstrated an optically pumped mid-infrared vertical cavity surface emitting quantum well laser based on IV-VI compounds. Because no cleavage is required for facet formation, these devices can be grown on readily available BaF_2 substrates, which provide major advantages over conventional lasers on lead salt substrates. As a consequence, vertical emitting lasers could lead to higher operation temperatures and lower threshold currents for mid-infrared IV-VI lasers, which opens promising perspectives for device applications.

References

[1] G. Springholz, T. Schwarzl, M. Aigle, H. Pascher, and W. Heiß, 4.8 μm vertical emitting PbTe quantum well lasers based on high finesse EuTe/PbEuTe microcavities, *Appl. Phys. Lett*. **76**, 1807 (2000)

[2] T. Schwarzl, W. Heiß, G. Springholz, M. Aigle, H. Pascher, 6 μm vertical cavity surface emitting laser based on IV-VI semiconductor compounds, *Electronics Letters* **36***,* 323 (2000)

[3] T. Schwarzl, W. Heiß and G. Springholz, Ultra-high-finesse IV-VI microcavities for the mid infrared, *Appl. Phys. Lett.*, **75**, 1246, (1999)

Reflection Difference Spectroscopy on II- VI Semiconductors; a Tool to Investigate Surface Processes In Situ During Growth

K. Hingerl, W. Hilber, R. E. Balderas-Navarro, A. Bonanni, H. Sitter and D. Stifter

(1) Johannes Kepler Universität Linz, Institut für Halbleiter- und Festkörperphysik, Altenbergerstr. 69, A-4040 Linz
(2) Profactor GmbH, Wehrgrabengasse 5, A-4400 Steyr

In this contribution the last year's work on Reflection Difference Spectroscopy is described in order to understand the physical and chemical processes occurring at the surface of the growing II-VI materials in situ in an molecular beam epitaxy chamber during epitaxial growth. The main focus in the last year was laid onto the investigation of dichroism in the epilayer due to surface stress or a surface electric field.

1. Introduction

As the materials and structures of semiconductor technology become more complex, interest in developing real time process monitoring techniques during crystal growth is rapidly increasing. Optical Probes are best suited to be applied simultaneously with crystal growth, because they are noninvasive and nondestructive. A technique currently strongly used is *Reflectance Difference Spectroscopy* (RDS), which can monitor in situ surface processes in real time under UHV (MBE, ALE) as well as under atmospheric pressure (CBE, OMCVD) conditions.

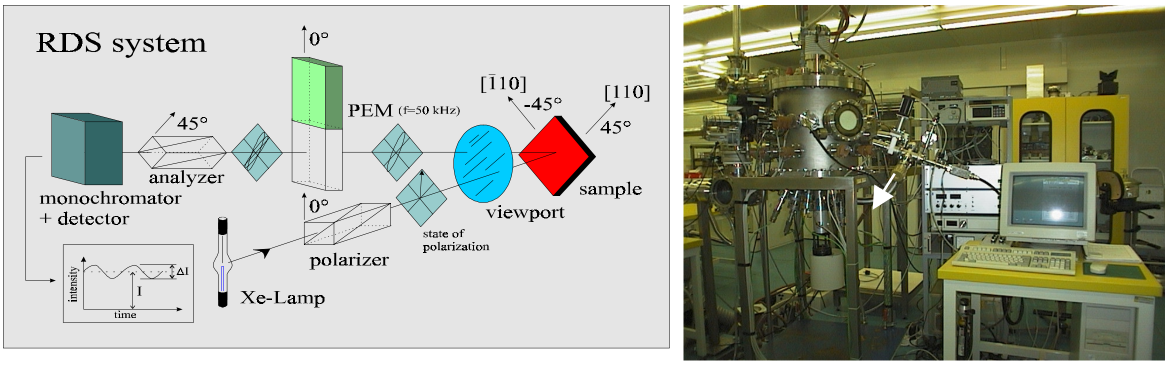

(a) (b)

Fig. 1: (a): The alignment of the optical components of the RDS system; (b): A photo of the experimental setup of the UHV MBE chamber with the attached RDS in the cleanroom at Linz University (arrow).

The measured signal is the difference between the near normal incidence reflectances of light linearly polarized along the two principal axes investigated as a function of time, photon energy, and/or surface condition. For cubic materials the uninteresting bulk reflection cancels in subtraction, leaving the signal from the lower symmetry surface. However, there are also identified sources for bulk anisotropy for zincblende (001) surfaces which break the 4-fold rotational symmetry. We mention spontaneous ordering, the linear electro-optic effect, dislocations, and quantum confinement.

Within the last years the understanding of information delivered by RDS and of kinetic RD data has grown considerably, however full exploitation of the power of these optical techniques needs further investigations, particularly when heteroepitaxial systems are concerned. Therefore, since the beginning of the work in February 1997, the major effort was directed onto these topics in II-VI semiconductors:

a) *In situ* Determination of In Plane Stress and Strain Anisotropy in ZnSe/ZnTe/CdTe (001) Layers on GaAs.
b) *In situ* Observation of Doping Efficiency and Doping Processes during crystal growth.
c) *In situ* investigation of the growth mode of Mn and MnTe layers in CdTe.
d) Reflectance difference spectroscopy of Mn intra-ion transitions in p-doped diluted magnetic semiconductors.

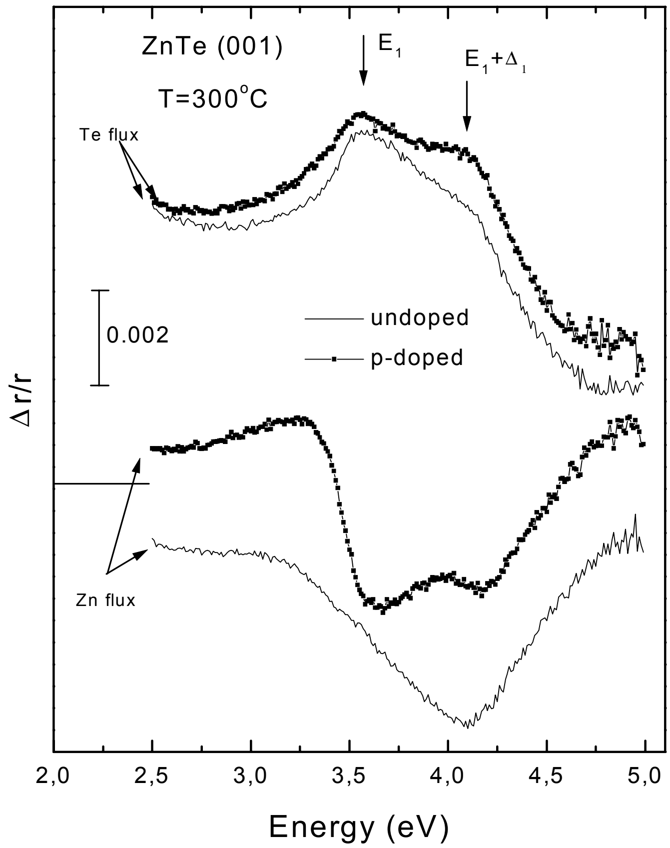

Fig. 2: Changes of the RDS spectra with and without doping. It can be seen that the broad surface related structures centered around 3.5 eV for Te surface termination and around 4.2 eV for Zn Termination are superimposed by sharper bulk related peaks when the samples are doped.

2. Results

2.1 Anisotropic in-plane strain

Is there an anisotropic in-plane strain occurring due to dimerization for II-VI compounds? Furthermore we tried to find a theoretical description connecting the symmetry of the wave-functions and the polarization dependence of the optical transition matrix elements with the measured spectra (Bikus and Pir Hamiltonian) [6], [10].

2.2 Linear electro-optic effect

The linear electro-optic effect (LEO), i.e., the change of the dielectric function, respectively, of the refractive index with applied electric fields, can be used for monitoring the doping concentration. Because the Fermi level in the bulk material changes with the activated dopant concentration, and at the surface a pinning of the Fermi level occurs, there is a built-in field and a depletion zone.[2], [4].

We have used reflectance difference (RD) spectroscopy (uv – visible energy range) during the growth and doping process of CdTe (001) and ZnTe (001) layers by molecular beam epitaxy (MBE). The MBE chamber is equipped with an electron cyclotron resonance cell to generate N plasma and a $ZnCl_2$ effusion cell for the p and n-type doping, respectively. After the first stages of the growth and prior doping, different spectral features were found as we changed from Cd(Zn) to Te stabilized conditions due to surface anisotropy. However, as the doping of the growing layer further increased, the RD spectra of both surfaces showed resonances around E_1 and $E_1 + \Delta_1$ interband transitions due to the linear electro-optic (LEO) effect. Although RD spectra exhibit similar line shapes dominated by surface transitions, differences due to the LEO can be isolated. Figure 2 above shows the changes of the RDS spectra with and without doping. It can be seen that the broad surface related structures centered around 3.5 eV for Te surface termination and around 4.2 eV for Zn Termination are superimposed by sharper bulk related peaks when the samples are doped.

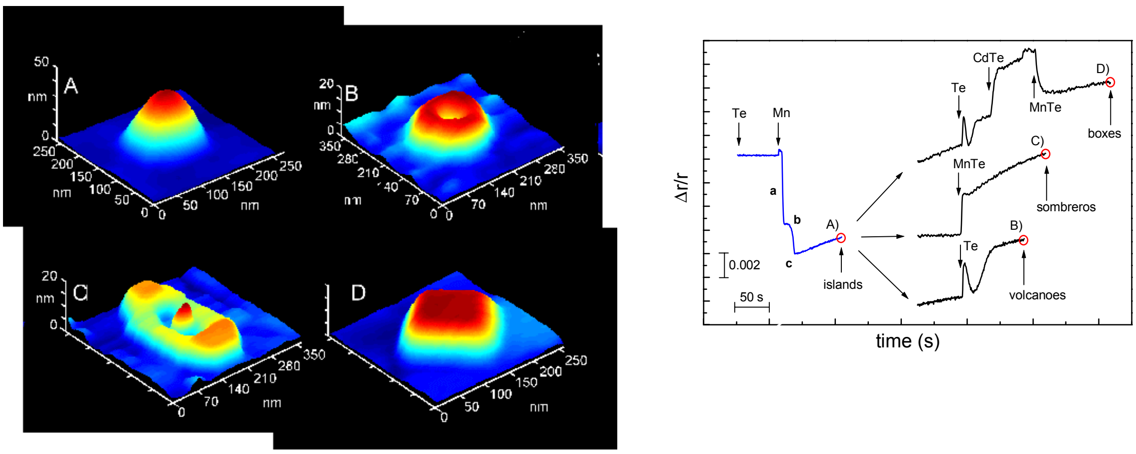

Fig. 3: On the left side the topography of the different dots, measured with AFM ex situ is shown; on the right side the RDS transients, leading to the different sizes are shown. The shutter sequence is displayed in the inset.

2.3 Self-assembling Mn-based nanostructures on CdTe

Another major topic were self-assembling Mn-based nanostructures on CdTe, where the reproducibility of size and shape for epitaxially grown self-assembling Mn-based nanostructures was achieved by tracing the formation process via reflectance difference spectroscopy. Pure Mn crystallites were at first fabricated on a semiconductor surface and in a second stage a variety of queer, strain-induced island morphologies was obtained with the deposition of semiconducting materials on the magnetic precursors. The exact control pursued, the possibility of shape tuning and the size range, let foresee forthcoming studies and applications in the field of confinement in low dimensions [1], [8].

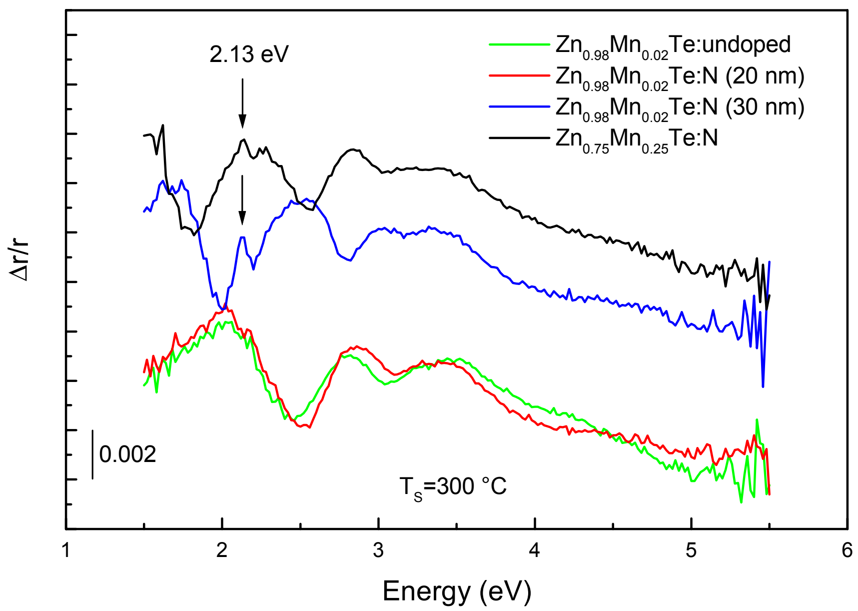

Fig. 4: Four RDS spectra of doped and undoped $Zn_{1-x}Mn_xTe$. It can be seen that at 2.13 eV an extra peak is occurring, which is ascribed to intra Mn transitions due to the symmetry breaking of the electric field.

2.4 Reflectance difference spectroscopy of Mn intra-ion transitions in p-doped diluted magnetic semiconductors

By performing in-situ reflectance difference spectroscopy (RDS) during and upon the epitaxial growth of the diluted magnetic semiconductor ZnMnTe heavily p-doped with N, it was possible to observe below and in the band gap region features occurring from intra-Mn d-level transitions. Since Mn on substitutional Zn sites is in a cubic environment and RDS measures the difference between the reflectances of light polarized along the two in-plane eigenstates, these transitions are detectable because of the breaking of the C4 rotational symmetry. In undoped materials the spectroscopic window for observation may open only for high values of magnetic ions concentration, whereas in doped crystals it was possible to detect the transitions at growth temperature and at Mn concentrations as low as 2% [5].

Acknowledgements

Funding: ÖAW (APART), FWF, ÖAD, EC- Competitive and Sustainable Growth

Collaborations

- Joint Research Center for Atom Technology (JRCAT) ,Tsukuba 305-8562, Japan;
- Institute for Materials Research, Tohoku University, Sendai 980-8577, Japan;
- Defense Research Agency, UK,

References

[1] A. Bonanni, H. Seyringer, H. Sitter, D. Stifter and K. Hingerl: "Control of morphology changes of self-assembled Mn-based nanostructures overgrown with mismatched maetrial", Appl. Phys. Lett. **74**, 3732, (1999)

[2] D.Stifter, A.Bonanni, M.Garcia-Rocha, M.Schmid, K.Hingerl, H.Sitter: "In situ reflectance difference spectroscopy:Nitrogen-plasma doping of MBE grown ZnTe layers", J.Cryst.Growth **201,** 132 (1999)

[3] A.Bonanni, D.Stifter, K.Hingerl, H.Seyringer, H.Sitter: "In-situ characterisation of the growth dynamics in MBE of Mn-based II-VI compounds: self-organised Mn structures on CdTe", J. Cryst. Growth.**201,** 707 (1999)

[4] D.Stifter, M. Schmid and K.Hingerl, A.Bonanni, m. Garcia Rocha and H.Sitter: In situ reflectance difference spectroscopy of II-VI compounds: A real time study of N plasma doping during molecular beam epitaxy", Jour. Vac. Sci. & Techn. **B17,** 1697 (1999)

[5] A. Bonanni, K. Hingerl, H. Sitter, D. Stifter: Reflectance Difference Spectroscopy of Mn Intra Ion Transitions in p- doped diluted magnetic semiconductors", phys. Stat.sol. **215,** 47 (1999)

[6] T. Hanada, T. Yasuda, A. Ohtake, K. Hingerl, S. Miwa, K. Arai, and T. Yao: "In Situ Observation of Strain Induced Optical Anisotropy of $ZnS_{1-x}Se_x$/GaAs(110) during Molecular Beam Epitaxy", Phys Rev. **B60,** (8909) (1999)

[7] D. Stifter, K. Hingerl, H. Sitter: "Zerstörungsfreie Messung dünner Schichten mit polarisationsoptischen Methoden", e&i, ÖVE, **116**, 315, (1999)

[8] A.Bonanni, G. Prechtl, W.Heiss, F. Schinagl, S. Holl, H. Krenn , H.Sitter, D.Stifter and K.Hingerl: "Reflectance Difference Spectroscopy and magneto-optical analysis of digital magnetic heterostructures", Jour. Vac. Sci. & Techn. **B17,** 1722(1999)

[9] K. E Miller, K. Hingerl, C. Brabec, A. J. Heeger, and N. S. Sariciftci: "Reflectance Anisotropy Spectroscopy of Oriented Films of Semiconducting Polymers", submitted to J. Chem. Phys.

[10] R. E. Balderas-Navarro, K. Hingerl, W. Hilber, D. Stifter, A. Bonanni, and H. Sitter: "In situ reflectance-difference spectroscopy of doped CdTe and ZnTe grown by molecular beam epitaxy", submitted to J. Jour. Vac. Sci. & Techn..

A Comparative Study of Iron Films on II-VI and III-V-Semiconductors

K. Bierleutgeb, H. Sitter, H. Krenn, and H. Seyringer

Institut für Halbleiter- und Festkörperphysik, J. Kepler Universität Linz, 4040 Linz

The incorporation of magnetic layers in semiconductor heterostructures is an increasingly active area of study. Especially the growth of ferromagnetic iron is an attractive field of investigation. A UHV chamber has been attached to an MBE system to study the growth of iron films on GaAs as well as on II-VI-semiconductors. Since interfacial effects are expected to play an important role in thin-film heterostructures resulting in a broad range of magnetic properties depending on film thickness and deposition conditions, we performed a comparative study of iron on III-V and on II-VI semiconductors. The obtained films are characterized by superconducting quantum interference device to determine the magnetic properties.

1. Introduction

The study of transition metal overlayers on semiconductor substrates is an attractive field of investigation. There is great interest in the catalytic, electronic, and magnetic properties of these materials in thin film form. Properties of thin films often differ significantly from those of the bulk due to surface and interface effects, which may dominate the overall behavior of these films.

The motivation for installing a UHV-chamber for iron thin film growth includes the investigation of the effect of magnetic fields onto dilute magnetic semiconductors such as unusual magneto-optic and magneto-transport properties. Besides we plan to grow hybrid ferromagnetic / semiconductor structures offering devices like magnetic memory elements, spin polarized current injection devices etc. [1].

We report about the first steps we have taken: A UHV-chamber, which has been designed to grow ferromagnetic bcc α-iron on the prototype materials GaAs or II-VI semiconductors like ZnSe, was attached to the existing MBE chamber. While GaAs and ZnSe possess a fcc zincblende structure, α-iron is bcc and the lattice parameters differ by a factor very close to two. We expect that at the Fe/GaAs interface interdiffusion will take place leading to the formation of FeAs compounds. The Fe/ZnSe interface is less reactive than the Fe/GaAs interface [2].

2. Experimental

A UHV-chamber for the growth of epitaxial iron films was attached to our existing MBE-system via a UHV tunnel, which also has access to an Auger electron spectrometer. In the MBE-system, which has been described elsewhere [3], we can grow II-VI-compound semiconductors (Zn,Cd)(Se,Te). A reflection high energy electron diffraction (RHEED) and a reflectance difference spectroscopy (RDS) system are installed in the

MBE chamber allowing to make *in situ* investigations in UHV without the effects of oxidation.

3d-transition metals (Fe, Co, Ni, …) have a relatively low vapor pressure and therefore require source temperatures in excess of 1100 °C to achieve deposition rates commonly employed in surface studies [4]. Therefore we chose a rod-fed electron beam source, which allows clean and controlled deposition of high-temperature materials at relatively low rates. With this method the heat load onto the source material is minimized.

Via the UHV tunnel it is possible to transfer the samples from the iron evaporation chamber to the MBE system to perform investigations of the surface structure by RHEED. We plan to attach a spectroscopic ellipsometer directly to the iron-chamber, which will allow us to make in-situ characterization during growth.

Iron films were either deposited directly onto (100) GaAs substrates or on ZnSe epilayers grown previously on GaAs in the MBE system.

Prior to growth the (100) GaAs substrates were heated up to 720 °C and kept at that temperature for a few seconds to remove the oxide till a streaky RHEED-pattern could be observed. When growing a ZnSe epilayer we used a Zn and a Se effusion cell with beam equivalent pressures of $0.2*10^{-8}$ mbar and $0.9*10^{-7}$ mbar respectively. ZnSe was grown in atomic layer epitaxy (ALE) mode yielding a growth rate of 10 Å/min at a substrate temperature of 300 °C. The thickness of the ZnSe epilayer was chosen to be 500 Å, which is below the critical thickness at which dislocations start to form. At that thickness the ZnSe is still pseudomorphic to the GaAs substrate [2].

Then the sample was cooled down to 100 – 150 °C before being transferred to the iron-chamber through the UHV tunnel. There the sample was heated up to 165 °C again. During iron growth the flux monitor current observed was around 2900 nA. This yielded in an growth rate of approximately 9 Å/min.

After growth of iron the sample was transferred back to the MBE-system to perform RHEED measurements. Then the samples were exposed to air and could oxidize.

Figure 1 shows the RHEED patterns taken at different steps of growth: After growing iron directly onto the GaAs substrates (Fig. 1 (a) – (b)) the RHEED-pattern indicates a flat surface although the iron-surface does not approach the flatness of the GaAs substrate. When inserting a ZnSe epilayer (Fig. 1 (a) – (c) – (d)) we see that the ZnSe epilayer heals surface roughness of the GaAs substrate resulting in a more streaky pattern. The RHEED pattern in Fig. 1 (d) was taken along the [110] direction after growth of iron. The iron surface with a ZnSe epilayer even seems to be smoother than the surface of iron directly on GaAs as the RHEED streaks are more pronounced.

From RHEED we see that iron grows in registry with the (001) GaAs / (001) ZnSe surface such that [100] Fe || [100] GaAs / [100] ZnSe. The streaks in the RHEED-pattern of iron have twice the distance than the streaks of GaAs / ZnSe. This factor of 2 in the reciprocal lattice gives a factor of 0.5 for the lattice constant as expected.

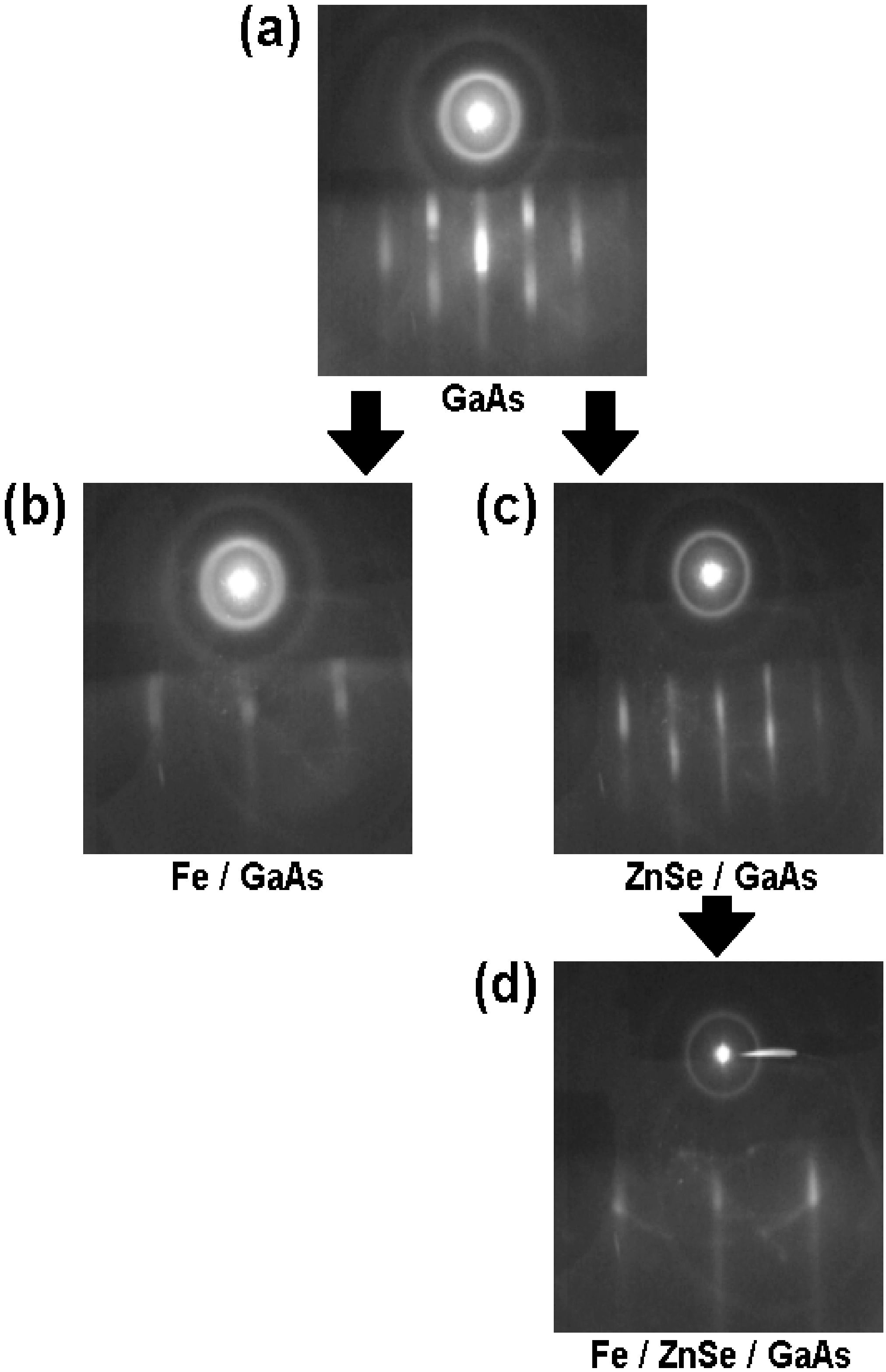

Fig 1: RHEED-patterns taken along the (110)-direction. (a) GaAs after deoxidation, (b) Fe after growth direct on GaAs, (c) ZnSe layers after growth, (d) Fe after growth on ZnSe epilayers.

We took AFM images (topography in contact mode) of the iron surface to study the mode of film growth. From literature we expected a three-dimensional growth mode for iron on GaAs while a predominantly layer-by-layer growth can be expected for iron on ZnSe [5]. While the surface of iron on GaAs is completely island-like, the growth of iron on a ZnSe epilayer is not completely layer-by-layer, but we can see larger smooth regions between remaining islands. As the ZnSe epilayer also was not completely flat, we can interpret the islands in the Fe surface as a reproduction of the ZnSe surface roughness.

Superconducting Quantum Interference Device measurements are currently undertaken. The curves of magnetization versus applied magnetic field show a pronounced rectangular hysteresis indicating a single domain behavior, which proofs the excellent internal structure of the iron films. This was observed for iron films both on GaAs as well as on ZnSe epilayers.

3. Conclusion

A new UHV chamber has been installed to grow iron films on II-VI- and on III-V-semiconductors. The use of electron beam evaporation allows clean deposition at relatively low growth rates and minimizes the heat load onto the source material.

We were successful in growing high-quality epitaxial iron films with an excellent internal structure directly on GaAs and on ZnSe epilayers. Although growth on ZnSe is not completely layer-by-layer-like, we see significant differences in comparison to growth on GaAs both in RHEED-patterns and in AFM-images.

Acknowledgements

This work was supported by the Fonds zur Förderung der Wissenschaftlichen Forschung.

References

[1] G. A. Prinz, "Science and Technology of Nanostructured Magnetic Materials", *Plenum Press New York*, 1991, p. 41

[2] B. T. Jonker and G. A. Prinz, *J. Appl. Phys.* 69 (1991) 2938

[3] W. Faschinger and H. Sitter, *J. Cryst. Growth* 99 (1990) 566

[4] B. T. Jonker, *J. Vac. Sci. Technol.* A 8 (1990) 3883

[5] B. T. Jonker, G. A. Prinz, and Y. U. Idzerda, *J. Vac. Sci. Technol.* B 9 (1991) 2437

Optical Characterization of CdTe/CdMgTe Quantum Wells Containing Single (Sub)Monolayers MnTe

W. Heiss, G. Prechtl, W. Jantsch

Microelectronics Institute, Johannes Kepler University Linz, A-4040 Linz, Austria

We perform photoluminescence (PL), polarization dependent PL excitation, and magneto-optical Kerr rotation experiments on II-VI quantum wells containing ultra narrow MnTe layers. From a comparison of the change of the optical transition energies upon rapid thermal annealing with model calculations we determine the actual width of the MnTe barriers. We find the barrier width to be very close to its nominal values. In addition, for a single monolayer MnTe we detect the antiferromagnetic-paramagnetic phase transition at a critical temperature of 50 K by a kink in the temperature dependence of the inverse Zeeman splitting. Furthermore, we have used the Zeeman splitting induced by a quarter monolayer MnTe inserted in a nonmagnetic quantum well at various positions to map the probability density of free holes in growth direction.

1. Introduction

Zincblende (ZB) MnTe is a prototype of a fcc Heisenberg system with strongly dominating antiferromagnetic nearest-neighbor interactions. While bulk grown crystals of MnTe exhibit the hexagonal NiAs crystal structure [1], by non-equilibrium growth techniques like molecular beam epitaxy (MBE) single crystals of MnTe can be synthesized also in the ZB phase [2]. In previous works, mainly epilayers of ZB MnTe [3], [4] and superlattices containing MnTe layers with a thickness of *several* monolayers (MLs) [4], [5] were investigated. Recently, new heterostructures have been developed in which fractional MLs of magnetic ions are introduced digitally within a semiconductor quantum well [6]. These structures are of special interest due to the possibility to tailor the spin splitting in addition to the electronic eigenstates [6]. Therefore, we investigate the magneto-optical properties of single ZB MnTe layers with a thickness corresponding to a coverage of *one*-or *one half* or *one quarter* of a ML, embedded in non-magnetic quantum wells. In particular, we investigate (a) the migration of the Mn ions in such structures, leading to a broadening of the MnTe barriers [7], and (b), the antiferromagnetic – paramagnetic phase transition of a single monolayer MnTe [8]. Furthermore, we apply a quarter ML MnTe to map out the probability density of free carriers in a square quantum well [9].

2. Samples and Experimental Details

Our samples are CdTe quantum wells with various width embedded between $Cd_{1-x}Mg_xTe$ barriers. All samples contain a single MnTe (sub)monolayer at various positions. The growth of the samples was performed at the Institute of Physics, Polish

Academy of Sciences in Warsaw (Poland). The samples are grown by molecular beam epitaxy (MBE) either on (001)-oriented $Cd_{0.96}Zn_{0.04}Te$ substrates ore on GaAs substrates. The growth rate was chosen to be very slow (8 s/ML) in order to control the Mn incorporation precisely and to get long enough growth times as compared to the opening and closing times of the shutters. Each interface was smoothed by performing growth interruptions under Te excess. The two-dimensional growth was monitored by RHEED oscillations.

Similar as in diluted magnetic semiconductors, in our quantum well samples, the exciton spin (Zeeman) splitting is strongly enhanced by spin-spin exchange interactions between the d electrons of the Mn^{2+} ions and the s-like conduction-band and p-like valence band electrons in the quantum well. With applied field, all e_1-hh_1 transitions, one with positive (σ^+) and the other with negative helicity (σ^-), can be observed. The energy difference between these transitions ΔE is directly proportional to the magnetization M [10]. Therefore, M can be measured directly by magneto optical spectroscopy.

All measurements were performed in Faraday configuration. We performed polarization dependent photoluminescence (PL) and PL excitation (PLE) experiments in magnetic fields up to 6 T. Furthermore, the magneto-optical Kerr rotation was measured by the use of a photoelastic modulator. For excitation a tunable Coherent CR 599 dye laser was used, operating in the wavelength range between 620 nm and 800 nm.

3. Results and Discussions

To estimate the actual barrier width of a nominal 1 ML thick MnTe barrier we have performed rapid thermal annealing experiments. The annealing step results in diffusion of the Mn out of the barriers. For small Mn diffusion lengths, the PL transition shifts to the blue due to the broadening of the MnTe barrier while for larger diffusion lengths the PL shifts to the red, because the barrier height decrease. Furthermore, the Zeeman splitting increases significantly upon annealing, since the number of antiferromagnetically coupled Mn ions in the barrier decreases while the number of paramagnetic background ions in the quantum well increases. In particular, in a quantum well sample containing a single ML MnTe we find a 14 meV blue shift of the PL transition upon annealing and an increase of the spin splitting from 23 meV to 60 meV at 6 T. In contrast, for a similar sample containing a MnTe barrier with a nominal width equivalent to one half ML, we find a 3 meV red shift upon 15 s rapid thermal annealing at 440 °C. From a comparison of these experimental observations with band structure calculations assuming Gaussian shaped MnTe barriers we obtain the actual barrier width before and after annealing. The width of the Mn distribution after annealing corresponds to a diffusion length of 1.5 nm. From this value a diffusion coefficient of 1.5×10^{-15} cm^2/s can be obtained, in good agreement with results given in the literature for the same annealing conditions [11]. Before annealing, the deduced width of the Mn distribution corresponds to a barrier width of 1.25 MLs. In addition, an absolute upper limit for this value of 1.65 MLs can be obtained.

For a quantum well sample containing a MnTe barrier with the nominal thickness of one ML we have studied the temperature dependence of the inverse Zeeman splitting $1/\Delta E$ in detail. At low temperatures, $1/\Delta E$ increases linearly with increasing T. At a critical temperature of 50 K a kink is observed and for higher temperatures $1/\Delta E$ rises linearly again, but with a smaller gradient. The temperature dependence of the Zeeman splitting can be fitted by the use of a Brillouin function and two phenomenological quantities, the effective manganese concentration x_e and an antiferromagnetic temperature T_{AF}. Up to 50 K, a good fit of the temperature dependence of $1/\Delta E$ can be obtained using a constant value for $T_{AF} = 23$ K and $x_e = 0.9$ %. For higher temperatures, above the kink, a good fit can be obtained only by increasing both of these parameters. This sudden increase of x_e at $T_{critical} = 50$ K indicates a phase transition of the antiferromagnetically coupled magnetic ions in the MnTe ML. The value of x_e obtained for the temperature range below $T_{critical}$ is much smaller than the value obtained by averaging the total number of magnetic ions present in a single MnTe ML over the whole CdTe quantum well ($x_{av} = 6$ %). This indicates that the enhanced Zeeman splitting observed below $T_{critical}$ is caused mainly by the isolated Mn ions migrated from the antiferromagnetically coupled MnTe layer into the CdTe quantum well by diffusion.

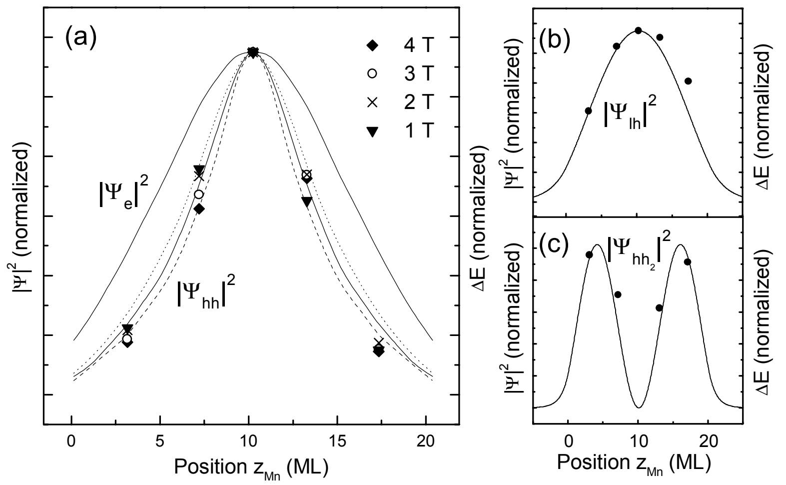

Fig. 1: (a) Probability density (PD) of the heavy hole ground state calculated for various valence band offsets (0.25 (dashed), 0.33 (solid) and 0.45 (dotted)) and of the electron ground state (valence band offset 0.33). The symbols display the experimentally observed interband Zeeman splitting of the e_1-hh_1 transition. (b) PD of the light hole ground state compared with the Zeeman splitting of the e_1-lh_1 transition. (c) As (b) but for the first excited heavy hole state hh_1.

Furthermore, we have investigated the Zeeman splitting in a series of five 20 ML wide quantum well structures (S1 to S5), where each sample contains a narrow MnTe barrier with a Mn content equivalent to ¼ ML coverage. In sample S1 the MnTe layer is inserted after the 3rd ML of CdTe, while in S2 to S5 the magnetic probes are embedded after the 7th, 10th, 13th, and 17th ML of CdTe, respectively. Assuming the sp-d exchange interaction to be strongly localized, it can be shown that the Zeeman splitting in this set of samples is proportional to the probability density of free carriers as function on the position of the magnetic probe in the well [9]. This is demonstrated in Fig. 1, where the probability density of the electrons and the holes calculated for different valence band offsets is compared to the experimental Zeeman splitting. This comparison shows that the measured values correspond to the probability density of the holes and not of the electrons, which is in contrast to all previous experiments [12] – [14]. Furthermore, Fig. 1 shows the probability density of the light holes in (b) and of the first excited heavy hole state in (c), in good agreement with the experimental data.

4. Summary

We characterize CdTe/CdMgTe quantum wells containing fractional MnTe monolayers by magneto-optical spectroscopy. In particular, we perform photoluminescence (PL), polarization dependent PL excitation, and magneto-optical Kerr rotation experiments. By comparing the change of the PL transition energies upon rapid thermal annealing with results of band structure calculations we determine the actual width of the MnTe barriers. We find for a nominal one monolayer thick MnTe barrier a broadening of the barrier width by Mn migration of only 0.25 monolayers. In this sample the antiferromagnetic-paramagnetic phase transition is detected by optical spectroscopy at a critical temperature of 50 K. In addition, we have demonstrated that the Zeeman splitting induced by a quarter monolayer MnTe inserted in a nonmagnetic quantum well at various positions can be used to map the probability density of free holes in growth direction.

References

[1] J.W. Allen, G. Lucovsky, and J.C. Mikkelsen, Jr., *Solid State Commun.* **24**, 367 (1977)

[2] S.M. Drubin, J. Han, Sungki O, M. Kobayashi, D.R. Menke, R.L. Gunshor, Q. Fu, N. Pelekanos, A.V. Nurmikko, D. Li, J. Gonsalves, and N. Otsuka, *Appl. Phys. Lett.* **55**, 2087 (1989)

[3] K. Ando, K. Takahashi, T. Okuda, and M. Umehara, *Phys. Rev.* **B 46**, 12289 (1992)

[4] T.M. Giebultowicz, P. Klosowski, N. Samarth, H. Luo, J.K. Furdyna, and J.J. Rhyne, *Phys. Rev.* **B 48**, 12817 (1993)

[5] M. Pohlt, W. Herbst, H. Pascher, W. Faschinger, and G. Bauer, *Phys. Rev.* **B 57**, 9988 (1998)

[6] S. A. Crooker, D. A. Tulchinsky, J. Levy, D. D. Awshalom, R. Garcia, N. Samarth, *Phys. Rev. Lett.* **75**, 505 (1995)

[7] G. Prechtl, W. Heiss, S. Mackowski, A. Bonanni, G. Karczewski, H. Sitter, W. Jantsch, *Sem. Sci. Technol.* (in print)

[8] G. Prechtl, W. Heiss, A. Bonanni, H. Sitter, W. Jantsch, S. Mackowski, G. Karczewski, *Physica E* (in print)

[9] G. Prechtl, W. Heiss, A. Bonanni, W. Jantsch, S. Mackowski, E. Janik, G. Karczewski, *Phys. Rev. B* (in print)

[10] D. U. Bartholomew, J. K. Furdyna, A. K. Ramdas, *Phys. Rev. B*. **43**, 6943 (1986)

[11] D. Tönnies, G. Bacher, A. Forchel, A. Waag, G. Landwehr, *Appl. Phys. Lett.* **64**, 766 (1994)

[12] P. H. Beton, J. Wang, N. Mori, L. Eaves, P. C. Main, T. J. Foster, M. Henini, *Phys. Rev. Lett.* **75**, 1996 (1995)

[13] J. Y. Marzin, J. M. Gerard, *Phys. Rev. Lett.* **62**, 2172 (1989)

[14] G. Salis, B. Graf, K. Ensslin, K. Campman, K. Maranowski, A. C. Gossard, *Phys. Rev. Lett.* **79**, 5106 (1997)

Appendix

The Society's Managing Committee and Address

President:

Univ.Prof. Dr. Erich GORNIK (up to December 31st, 1999)
TU Wien, Institut für Festkörperelektronik

Univ.Prof. Dr. Günther BAUER (from January 1st, 2000)
Universität Linz, Institut für Halbleiter- und Festkörperphysik

First Vice-President:

Mag. Miron PASSWEG (up to December 31st, 1999)
Bundesarbeitskammer

Dipl.-Ing. Gerhard KRAINZ (from January 1st, 2000)
Wirtschaftskammer Österreich

Second Vice-President:

Univ.Prof. Dr. Günther BAUER (up to December 31st, 1999)
Universität Linz, Institut für Halbleiterphysik

Univ.Prof. Dr. Erich GORNIK (from January 1st, 2000)
TU Wien, Institut für Festkörperelektronik

Board:

Dr. Wolfgang ATTWENGER (up to December 31st, 1999)
ÖFZ Seibersdorf

Univ.-Prof. Dr. Emmerich BERTAGNOLLI (from January 1st, 2000)
TU Wien, Institut für Festkörperelektronik

Univ.Prof. Dr. Wolfgang FALLMANN
TU Wien, Institut für Industrielle Elektronik und Materialwissenschaften

Univ.Prof. Dr. Helmut HEINRICH
Universität Linz, Institut für Halbleiter- und Festkörperphysik

Dipl.-Ing. Gerhard KRAINZ (up to December 31st, 1999)
Wirtschaftskammer Österreich

Univ.Prof. Dr. Hans LEOPOLD
TU Graz, Institut für Elektronik

Univ.Prof. Dr. Fritz PASCHKE
TU Wien, Institut für Industrielle Elektronik und Materialwissenschaften

Mag. Miron PASSWEG (from January 1st, 2000)
Bundesarbeitskammer

Dr. Robert SCHAWARZ
TU Wien, Institut für Industrielle Elektronik und Materialwissenschaften

Univ.Prof. Dr. Arnold SCHMIDT
TU Wien, Institut für Photonik

Univ.Prof. Dr. Siegfried SELBERHERR
TU Wien, Institut für Mikroelektronik

Rainer URANSCHEK (from January 1st, 2000)
Forschungs- und Prüfzentrum Arsenal GmbH

Secretary-General:

A.o. Univ.Prof. Dr. Karl RIEDLING
TU Wien, Institut für Industrielle Elektronik und Materialwissenschaften

Administration:

Claudia BENEDELA

Address:

Gesellschaft für Mikroelektronik
c/o Technische Universität Wien
Institut für Industrielle Elektronik und Materialwissenschaften
Gußhausstraße 27-29/366, A-1040 Wien

Phone: +43-1-588 01-36657

Fax: +43-1-588 01-36699

Mail: gme@iaee.tuwien.ac.at

WWW: http://www.iaee.tuwien.ac.at/gme/